Best Tips of the Month

Over 150+ Pages of Technical Content

John M. Campbell & Company

Best of John M. Campbell & Company Tip of the Month

Table of Contents

For more information on upcoming John M. Campbell courses, please visit www.jmcampbell.com.

Quick Determination of the Methanol Injection Rate for Natural-Gas Hydrate Inhibition

By: Dr. Mahmood Moshfeghian

The formation of hydrates in processing facilities and pipelines has been a problem to the natural gas industry. Whether the problem occurs in transportation or processing, hydrate formation can cause shutdowns and even destruction of valuable equipment. Because of these devastating and often costly consequences of hydrate formation, methods have been applied to prevent hydrate development in gas streams. The conditions that tend to promote hydrate formation include: low temperature, high pressure, and a gas at or below its water dew point temperature with "free" water present. The formation of hydrates can be prevented by using any of the following techniques; (a) adjusting the temperature above and pressure below the hydrate formation condition, which may not be practically possible due to economical and/or operational reasons, (b) dehydrating a gas stream with solid desiccant or glycol dehydration to prevent a free water phase, and (c) impeding hydrate formation in the free water phase by injection of an inhibitor. The most common inhibitors are methanol (MeOH), monoethylene glycol (MEG) and diethylene glycol (DEG). Typically, methanol is used in a non-regenerable system while MEG and DEG are used in regenerable processes. With the use of inhibitors, the injected inhibitor may distribute into three possible phases: (a) the vapor hydrocarbon phase, (b) the liquid hydrocarbon phase and (c) the aqueous phase in which the hydrate inhibition occurs and the inhibitor has an effect on hydrate formation inhibition. Therefore, calculating the inhibitor concentration in aqueous phase is important.

Several models have been developed for prediction of hydrate formation condition in the presence of an inhibitor. Hammerschmidt [1], Nielsen and Bucklin [2], Carroll [3] and Moshfeghian-Maddox [4] correlations are used to predict concentration of inhibitors in an aqueous solution and for lowering the hydrate formation temperature. Portability and simplicity are advantages of these correlations since they are applicable even with a simple calculator and the results are in good agreement with the experimental data [1-4]. It is to be noted that simulation packages such as ProMax® [5], HYSYS® [6] and GCAP [7] are available for predicting the effect of inhibitors on hydrate formation.

The injection rate is a function of feed gas temperature (FGT), pressure (FGP), relative density (SG), hydrate formation temperature depression (HFTD), and lean solution concentration. Recently, Moshfeghian and Taraf [8-10] proposed a shortcut/graphical method to predict the required MEG or MeOH weight percent and flowrate for a desired depression in hydrate temperature of natural gas mixtures.

In this tip of the month (TOTM), we will demonstrate how the diagrams presented by Moshfeghian and Taraf [10] can be used to determine the concentration of MeOH in the rich solution and the required total injection rate for a desired hydrate formation temperature.

Figures 1-4 are applicable for any wet natural gas mixture with specific gravity of 0.6. Note that the right hand y-axis represents the total injection rate of MeOH which may distribute into gas phase, liquid hydrocarbon phase and rich solution phase. In order to extend the

application of these charts to gas mixtures with other specific gravities, two correction factors W_1 and W_2 should be used. These correction factors are used to correct the inhibitor concentration in the rich solution for other relative densities (0.65-0.80) which are shown in Figure 5. W_1 is the correction factor due to the difference of inhibitor concentration in the rich solution in different hydrate formation temperature depression. This factor is applicable for gas with specific gravities greater than 0.6. W_2 is the correction factor due to the difference in inhibitor concentration in the rich solution due to the difference in gas specific gravities. To determine W_2, the *S*-factor is defined as follow:

$$S = \frac{(Specific\ Gravity - 0.65)}{0.05}$$

By calculating the *S*-factor, W_2 can be easily read from Figure 5. This correction factor is applicable for gas with specific gravities of 0.65 and greater.

Using W_1 and W_2, the obtained weight percent from Figures 1-4 (Wt_{fig}) is corrected as follows:

$$\Delta W = W_1 + W_2$$

$$Wt_r = Wt_{fig} - \Delta W$$

The obtained flow rate from charts (Figures 1-4) should be corrected further using flow rate correction factor (FLC) presented in Figure 6. The correction factor can be applied as follow:

$$FlowRate = FlowRate_{fig} + F \times FLC$$

$$F = \frac{(Specific\ Gravity - 0.60)}{0.05}$$

Considering the above correction factors, the charts are applicable for natural wet gases with specific gravities of 0.6-0.8 saturated, at temperature of 20, 30, 40 and 50 oC and pressures of 3, 5, 7 and 9 MPa.

As mentioned earlier, the inhibitor in the aqueous phase (rich solution) has an effect on hydrate formation inhibition and it is independent of the inhibitor weight percent in the lean solution. The same hydrate temperature depression is achieved when there is a similar inhibitor weight percent in the rich solution. However, the injection rate is a function of both lean and rich stream concentration.

Therefore, a simple material balance gives the following equation:

$$Rate_{Lean-NewSolution} = \frac{wt\%_{Rich-Chart} \times Rate_{Lean-Chart}}{wt\%_{Lean-NewSolution} - wt\%_{Rich-Chart}} \left(\frac{wt\%_{Lean-Chart}}{wt\%_{Rich-Chart}} - 1 \right)$$

Where:

$Rate_{Lean-NewSolution}$ = required injection rate for new lean concentration
$wt\%_{Lean-NewSolution}$ = concentration of inhibitor in the new lean solution
$wt\%_{Rich-Chart}$ = required concentration in the rich solution
$Rate_{Lean-Chart}$ = required injection rate
$wt\%_{Lean-Chart}$ = specified lean concentration (100 wt% for MeOH)

Case Study

To demonstrate the application of the proposed charts, example 6.6 in Volume 1 of "Gas Conditioning and Processing," [11] is considered. In this example it is stated that 3.5×10^6 Sm^3/d of natural gas leaves an offshore platform at 40 ^oC and 8000 kPa. The hydrate temperature of the gas is 17 ^oC. The gas arrives onshore at 5 ^oC and 6500 kPa. The associated condensate production is 60 $m^3/10^6$ Sm^3. The amount of methanol required to prevent hydrate formation in the pipeline is to be estimated.

It should be noted that in this example the composition (or relative density) of natural gas is not given; therefore, to demonstrate the use of these charts a relative density of 0.6 is assumed. The feed gas pressure is 8 MPa so a linear interpolation between 7MPa (Figure 3) and 9 MPa (Figure 4) is applied.

The summary of known data is:

FGT = 40 ^oC; HFT = 17 ^oC, FGP = 8 MPa, SG = 0.60, Inhibitor = 100 Wt % MeOH

Minimum Flowing Temperature (MFT) = 5 ^oC

HFTD = HFT – MFT = 17 – 5 = 12 ^oC

Due to the uncertainties involved in all inhibitor injection calculation methods, a safety factor is normally applied to the hydrate formation temperature depression. For example, this case has the HFTD set to the minimum flowing temperature. In practical situations, a design factor such as 5 deg ^oF (2.8 ^oC) below the minimum flowing temperature is used to ensure any errors in the estimation method are covered, and also to ensure that the minimum temperature includes any upset process condition.

As an example, the location of HFTD, required weight percent and injection rate of MeOH for pressure of 9 MPa for this example are shown in Figure 4. The results are tabulated in Table 1, and a comparison between the results of this work and those based on the Hammerschmidt [11] equation, ProMax [5], HYSYS [6], and GCAP [7] is shown in Table 2. As can be seen from Table 2, the agreement between the graphical method and ProMax is quite good. The methanol injection rates as estimated by HYSYS are significantly lower than the other methods, and caution should be applied if one is using HYSYS for inhibitor injection estimates. It is likely that the differences in the natural gas water dew point predictions are

the result of this discrepancy. Also note for modeling methanol liquid systems in process simulators, a polar equation of state package for the vapor phase and a polar model for the liquid phases must be selected to obtain accurate results.

Conclusions

For determination of required methanol concentrations in the aqueous phase (rich solution) and its flowrate for a desired depression in hydrate formation temperature of a wet natural gas mixture, reference charts proposed by Moshfeghian and Taraf [10] can be used. These charts were generated for pressures 3, 5, 7, and 9 MPa based on ProMax and are generated for a natural gas mixture with relative density of 0.6 but are extended to gases with relative densities up to 0.8 by using two correction factors. A simple equation was also proposed to extend the charts' usage to other lean MeOH concentrations.

The results obtained by these charts are compared with the results of the other methods for a practical case and good agreement is found. It is also suggested that linear interpolation can be used for pressures between 3, 5, 7, and 9 MPa.

.

REFERENCES

1. Hammerschmidt, E.G., "Formation of gas hydrates in natural gas transmission lines", Ind. & Eng. Chem., Vol: 26, p. 851, 1943.
2. Nielsen, R. B. and R.W. Bucklin, "Why not use methanol for hydrate control", Hydrocarbon Processing, Vol: 62, No. 4, P 71, April 1983.
3. Carroll, J., "Natural Gas Hydrates, A Guide for Engineers", Gulf Professional Publishing, 2003.
4. Moshfeghian, M. and R. N. Maddox, "Method predicts hydrates for high-pressure gas stream", Oil and Gas J., August 1993.
5. **ProMax®**, Bryan Research & Engineering Inc, Version 2.0, Bryan, Texas, 2007
6. **HYSYS®** v 2006, Aspen Technology Inc., Cambridge, Massachusetts, 2006
7. **GCAP®**, 8th Ed., Facilities Analysis Software, John M. Campbell & Co., Norman, Oklahoma, 2009.
8. Moshfeghian, M. and Taraf, R., "New method yields MEG injection rate". Oil and Gas J., September 2008.
9. Moshfeghian, M. and Taraf, R., "A new shortcut/graphical method to determine the required MEG injection rate for natural gas hydrate inhibition," 87th Annual Gas Processor Association Convention March 2-5, in Grapevine, Texas, (2008).
10. Moshfeghian, M. and Taraf, R., "Generalized Graphical Method to Determine the Required MEG and Methanol Injection Rate for Natural-Gas Hydrate Inhibition," 88th Annual Gas Processor Association Convention March 8-11, in San Antonio, Texas, (2009).
11. Campbell, J. M., "Gas Conditioning and Processing", Vol. 1, The Basic Principles, 7th Ed., Second Printing, J. M. Campbell and Company, Norman, Oklahoma, 1994.

Table 1. Results for example 6.6 of Volume 1 of "Gas Conditioning and processing" [11]

	Required Weight % in Rich Solution	Required Injection Rate ($kg/10^6\ Sm^3$)
@ 7 MPa Pressure Using Figure 6 and 10	23.7	694.5
@ 9 MPa Pressure Using Figure 7 and 11	23.4	635.1
@ 8 MPa Pressure Using Linear Interpolation	23.5	664.8

Table 2. Results Comparison

Method	Required Wt % in Rich Solution	Required Injection Rate (kg/day)
Hammerschmidt Equation [1, 11]	23.0	2330
ProMax [5]	24.4	2391
HYSYS [6]	24.0	2091
GCAP [7]	22.8	2105
This Work	23.5	2327

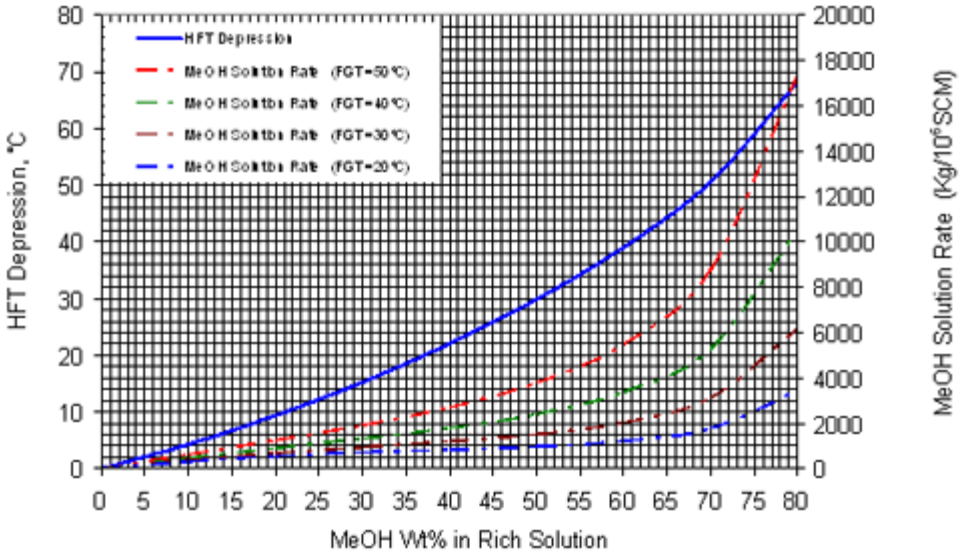

Figure 1. HFT depression and MeOH solution Rate Vs
MeOH wt% in Rich Solution @ 3 MPa using 100 Wt% MeOH Lean Solution

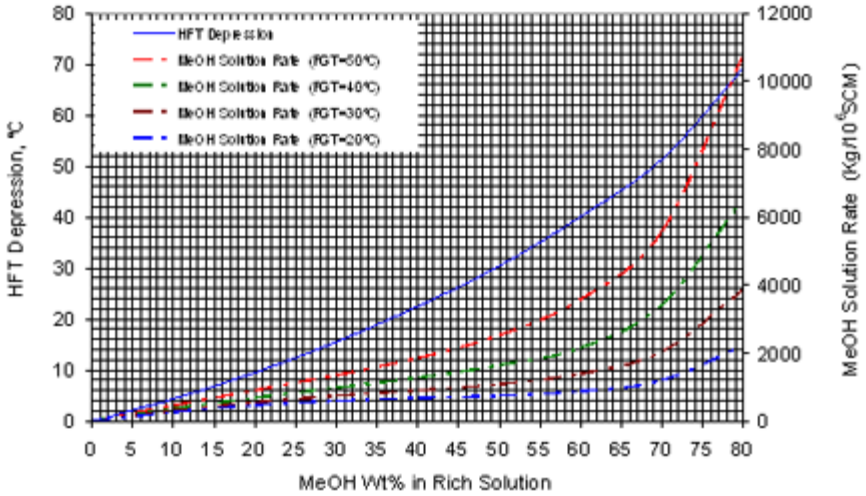

Figure 2. HFT depression and MeOH solution Rate Vs
MeOH wt% in Rich Solution @ 5 MPa using 100 Wt% MeOH Lean Solution

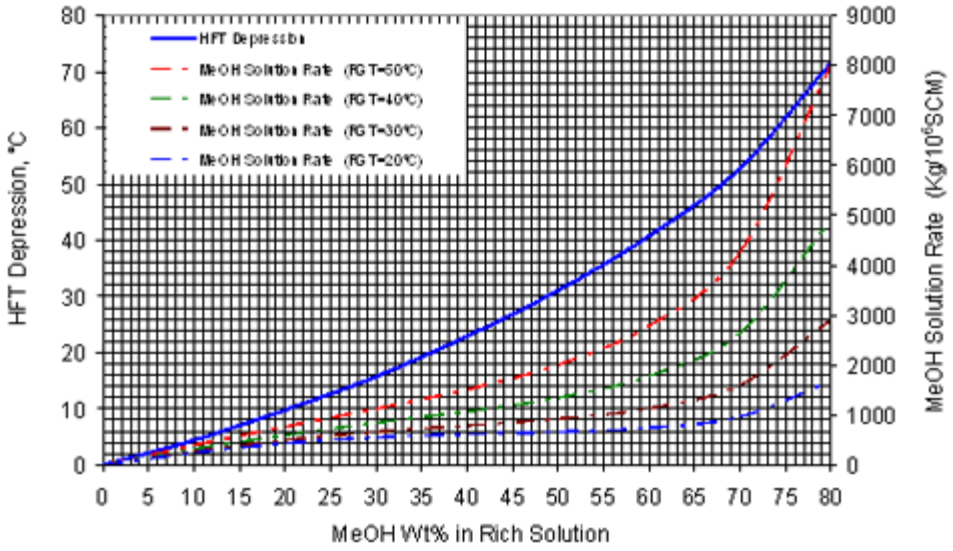

Figure 3. HFT depression and MeOH solution Rate Vs
MeOH wt% in Rich Solution @ 7 MPa using 100 Wt% MeOH Lean Solution

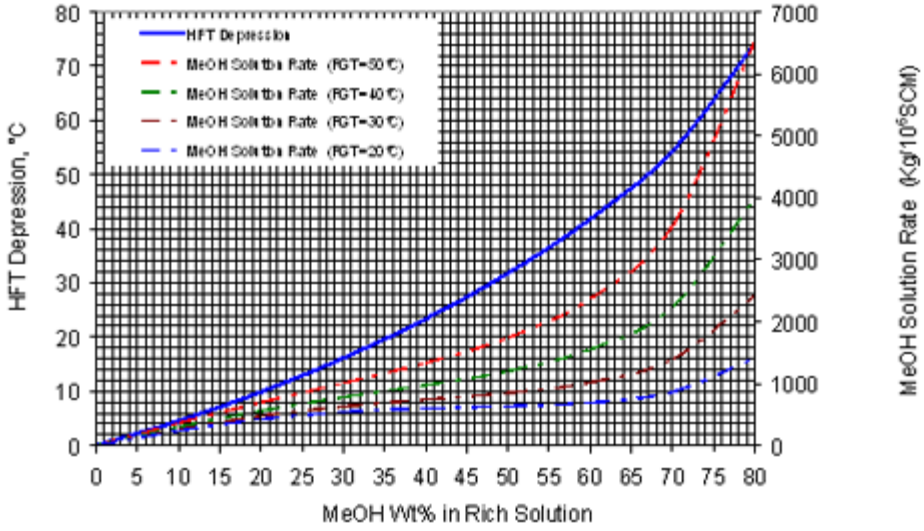

Figure 4. HFT depression and MeOH solution Rate Vs
MeOH wt% in Rich Solution @ 9 MPa using 100 Wt% MeOH Lean Solution

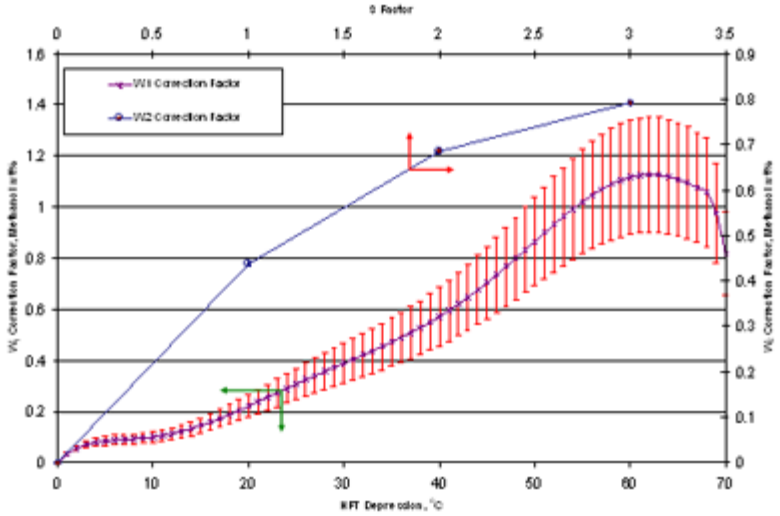

Figure 5. Methanol weight percent correction Factors (W_1 and W_2) as a function of HFT depression and S factor, respectively

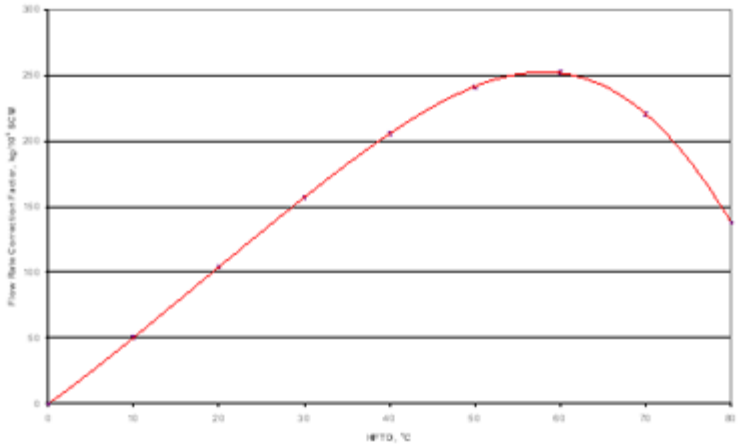

Figure 6. Methanol flow rate correction factor (FLC) as a function of HFT depression

Three Simple Things to Improve Process Safety Management

by Clyde Young

In this Tip of the Month, we look at how to deal with some of the challenges of managing process safety. This TOTM is an excerpt of a paper presented by JMC Instructor/Consultant, Clyde Young at the 2008 **Mary K. O'Connor Process Safety Symposium**.

"Process safety practices and formal safety management systems have been in place in some companies for many years. Process Safety Management (PSM) is widely credited for reductions in major accident risk and in improved chemical industry performance. Nevertheless, many organizations continue to be challenged by inadequate management system performance, resource pressures, and stagnant process safety results."

Meeting the challenges of a PSM system and insuring that the risk associated with our business is addressed can be challenging. This is one of the reasons that the **Center for Chemical Process Safety (CCPS)** published their "Guidelines for Risk Based Process Safety" in 2007. This book is being used as a reference for the PetroSkills HSE course, Risk Based Process Safety Management. During delivery of this course over the last couple of years, participants have agreed that one of the challenges facing them at the local level is that some elements of the PSM system they work with are somewhat complicated and are focused on trying to achieve consistency throughout an organization. While the concept of having consistency throughout an organization is an excellent goal, issues at the local level sometimes make this difficult to accomplish.

It is at the plant and process level that catastrophic incidents occur. It is at this level where resources are sometimes stretched thin and the risk is increased. What can be done at the plant and process level to simplify things and insure that hazards are identified, addressed and the consequences are reduced?

It is important to know that all processes in the oil and gas industry are designed to run according to specified parameters. Based on specific criteria, processes are designed to run at a specific flow rate, at specified pressures, temperatures and levels. This should be considered "normal". Unless some kind of batch operation is being dealt with, processes in the oil and gas business are generally designed to run at "normal" for extended lengths of time.

There are four characteristics of an effective management system. These are:

- formality,
- flexibility,
- accountability and
- control

A formalized management system uses procedures, policies, and guidelines to direct personnel to the correct actions and the best resources to manage the process. A flexible system has mechanisms in place to react to conditions if they change. It is not possible to foresee the future, but it is possible to know what to do, in a formalized way when a situation requires action. In order for a system to

work, people must be held accountable to perform the tasks that are required. A system with accountability insures that there is no question about who is to do what. Add these characteristics together, and the system becomes controlled.

To meet the requirements of an effective PSM system, Process Safety Information (PSI) is required, which essentially documents how the process has been designed and built. Conducting the required Process Hazard Analysis (PHA) study identifies hazards and operability problems that may be built into the process. Well developed operating procedures directs how the process will be run during "normal" and what will be done to bring the process back to "normal" if there are deviations. Providing training to personnel insures that those most exposed to the hazards and operability problems are competent to keep the process within the range of "normal" and return it if it deviates. Mechanical integrity programs keep the equipment in the process from running to failure. All of the above elements and others are basically used to define and maintain "normal" operations.

In his book, "Managing the Risks of Organizational Accidents," James Reason talks about active and latent failures in his Swiss cheese model of defenses. Active failures include errors, omissions, and violations. Active failures have a direct and immediate effect on the process. Latent failures include poor design, gaps in supervision, unworkable procedures, and lack of training. These latent failures are always there, may exist for years and can increase the likelihood of active failures.

Process safety management systems are in place to manage the risk associated with the processes we operate. To manage the risk, it has to be identified, reduced or eliminated. Incidents have to be responded to and the consequences of such incidents have to be rectified. Knowing that latent failures exist in all processes and systems, identifying these latent conditions is a key element of identifying risk.

The first of the three simple things to improve process safety management is geared toward identifying risk and especially latent conditions. Implementing an effective near miss/incident reporting system should help identify latent failures in our processes.

Many organizations have already implemented a near miss/incident reporting program of some kind. Some of these programs work very well. In some cases, the program's start well but reporting begins to taper off after a while. This can happen because of perceived time constraints or management response that is inadequate or inappropriate.

Whether the theory of H.W. Heinrich's safety pyramid is to be believed, it would still seem reasonable that if there is a major incident, there were indications that the latent failures were starting to line up, so that the likelihood of an active failure is increased.

Why do near miss/incident reporting systems fail to produce the results desired when they are first implemented? Some reasons include:

- "It's inconvenient to fill out a "near-miss form." It's less stressful to just forget it happened."
- Near-miss experiences are typically private affairs, and there's no way to hold people accountable for them.
- Organizational influences have an impact on near-miss reporting.
- Slogans like "all injuries are preventable". Employees think to themselves, "If all injuries are preventable and I almost got injured, I sure don't want anyone to think I'm so careless."

While these reasons may well have an influence on the success of a near miss/incident reporting system, consider that people have a difficult time deciding if something is a near miss or an incident. There are many different definitions of a "near miss". Incidents are sometimes categorized into tiers or levels and the reporting requirements for each tier are different. Why can't issues be simplified to ensure that all important information is collected and analyzed?

To simplify things, let's change the definition of a near miss/incident to:

"Anything unusual that occurs."

Think about the concept that all processes are designed to operate as "normal". Any operator will tell you that a running process has a certain sound, vibration, feel and even a smell that is "normal". An effective operator can tell something is not quite right almost immediately. The operator may not know exactly what isn't right, but any changes to the "normal" are noticed. All operators and all supervisors of operations need to know anything unusual that occurs. The problem is that sometimes these things are passed along verbally or in operator logs and there is no formalized process in place to investigate further. Remember, latent failures need to be identified before they become active failures.

If a near miss/incident is defined as anything unusual that occurs, it becomes very simple to determine if something needs to be reported. A strange sound or change in the feel of the process will lead to an investigation. All near miss/incident reports must be investigated. The investigation can be very simple or it can be very detailed and thorough. It just depends on what has been reported. A strange sound may only require someone to observe and write a brief description of what is found. A failed pump seal may require a more thorough investigation that includes an audit of the facility's mechanical integrity program.

It is also important to communicate the findings of these investigations so that the latent failures are identified and eliminated or reduced. Receiving no feedback about a report that is filed is one way to insure that personnel will stop reporting things. Assigning blame and disciplining personnel is a sure way to drive near misses and incidents underground and insure that nothing is reported. The focus should be on what happened rather than who did what.

This formalized process doesn't have to go on forever. At some point, personnel will begin to understand that all unusual things need to be examined and perhaps even investigated. The organizations culture will begin to move toward the generative culture where issues dealing with risk and safety are actively sought. At this point, the organization can step back and take another look at the near miss/incident reporting program and modify it as necessary.

[1] *Guidelines For Risk Based Process Safety, page ii,* American Institute of Chemical Engineers, Center for Chemical Process Safety

Three Simple Things to Improve Process Safety Management

by Clyde Young

In this Tip of the Month, we look at how to deal with some of the challenges of managing process safety. This TOTM is an excerpt of a paper presented by JMC Instructor/Consultant, Clyde Young at the 2008 **Mary K. O'Connor Process Safety Symposium**. This TOTM continues where the February 2009, TOTM left off.

Processes are designed to run in a "normal" mode. No process is really stagnant and throughout the life cycle of a process, changes will be made. When defining "normal", some tolerance should be built in to allow a range of operating conditions for operators to work within. When changes to operating parameters, or the equipment in the process are required, these must be evaluated and approved. Any effective process safety management system will contain an element to deal with Management of Change (MOC). Experience conducting training, audits and process hazard analysis studies indicate that identifying what changes require evaluation using the MOC process can be confusing at times. Some organizations only evaluate technical changes to the process and equipment and ignore or forget about managing changes to the PSM system or personnel changes within the organization.

Insuring that PHAs are consistent with the process through the revalidation process is less time consuming and more likely to yield effective results if the facility's MOC program is rigorously followed. If this cannot be assured, then the only choice may be a complete redo of the PHAs. This could be very expensive and resource intensive.

To alleviate confusion and especially to insure that all personnel within an organization understand and will follow the MOC program requires practice. As more MOCs are developed and approved, all personnel become more competent at evaluating change and meeting the requirements of the program. Ever since the US Occupational Safety and Health Administration (OSHA) implemented the PSM standard in 1992, one of the hottest debate topics witnessed in plant offices is about replacement in kind. OSHA and CCPS define a replacement in kind as meeting the design specification of the original. This is a workable definition, but can cause some confusion when personnel are not well versed in PSM and risk management.

The second simple thing which can be done to improve process safety management systems is to do away with the concept of replacement in kind. Again, this does not have to be and probably can't be accomplished throughout an organization; this can certainly be implemented at the process and plant level for a specified period of time. The purpose of this change would be to end the debates and more importantly allow personnel an opportunity to practice and become competent at all the issues associated with performing changes.

A real life example illustrates this:

A Waukesha 7042 engine is scheduled for overhaul. Three options are considered:

- overhaul in place by company personnel,
- overhaul in place with contract personnel

- removal of engine and ship to contractor for overhaul.

The most economical choice was found to be, swap the engine with another 7042 engine. The only difference is the serial number. This was determined to be a replacement in kind, and by definition it is. However, the older 7042 engine was "grandfathered" under the facility's air discharge permit from the environmental regulatory body. As soon as a new engine, with a different serial number was installed, the "grandfathering' of the older engine was invalid and a new air permit had to be issued. To meet the requirements of the new permit, air/fuel ratio controllers and catalytic converters were required. This change cost the company approximately $70,000 above the highest priced option that was analyzed. This change also increased the workload on maintenance and operations staff, which could affect other areas of operations.

During audits, there have been several instances where plant personnel try to stretch the replacement in kind exemption so that changes to the process are not evaluated with the MOC process. The most frequent reasoning for this is that the MOC process is too cumbersome and takes too long. In the end, the MOC process is being bypassed and potential hazards may not be addressed appropriately.

The MOC process to, evaluate personnel changes, is used by some organizations, but generally it occurs for changes at the supervisory level. But consider that no two people are the same. Both have different skill sets and it is important to dig a bit deeper into the "design specification of the original" to determine what the real impact of personnel changes might be. Especially consider the reassignment or replacement of operations and maintenance personnel. Identifying gaps in their technical competencies should be an important part of the MOC evaluation. The evaluation can be a powerful tool for performance management and identification of training opportunities for development.

In the end, doing away with the replacement in kind exemption within a facility's MOC process can increase the process safety competencies of all personnel. Process safety competency is one of the elements of the CCPS Risk Based Safety Management guidelines. Increased competency leads to a change in the culture and hopefully a safer process. Within the world of adult learning, it is recognized that learners must be given the opportunity to apply lessons to the job or the training may be lost. Considerable time and effort may be spent providing training to personnel on the procedures for managing change, but how often are they given the opportunity to put this training into practice within the working environment?

Three Simple Things to Improve Process Safety Management

by Clyde Young

In this Tip of the Month, we look at how to deal with some of the challenges of managing process safety. This TOTM is an excerpt of a paper presented by JMC Instructor/Consultant, Clyde Young at the 2008 **Mary K. O'Connor Process Safety Symposium**. This TOTM continues where the February 2009, TOTM left off.

When there are newspaper accounts of process incidents that have occurred, there is usually a statement along the lines of, "It just happened with no warning." There are warning signs for every incident. Latent failures exist in all processes and eventually lead to active failures when circumstances align. Personnel must be taught how to see and react to these warning signs.

Throughout the lifecycle of a process, many tasks are performed. Even when a process is running in "normal" mode, operators perform routine tasks and maintenance to keep the process at "normal". Now and then, the process is shut down for maintenance and then started again. Every time a task is performed there is the possibility that a latent condition may expose itself and lead to an active failure. Many organizations have implemented a requirement that all job tasks be analyzed through a process known as Job Task Analysis (JTA), Job Safety Analysis (JSA), or Job Hazard Analysis (JHA). There are many titles and acronyms for this process, but all have one common theme. Analyze the task to be performed, identify hazards and mitigate those hazards. Sadly, these analyses become routine and the documentation associated with them becomes nothing more than a checklist that needs to be filled out and turned in. This is sometimes known as "pencil whipping" the form.

Performing a job hazard analysis is not difficult, but does need to be a formalized process that controls or eliminates the hazards identified. This is the third simple thing we can do to improve our process safety management systems.

Review the checklist below:

1. **PROCEDURES**

- **What are the procedures for the task?**
- **What is unclear about the procedures?**
- **What order will we use these procedures?**
- **What permits are needed for hazard controls?**

2. **EQUIPMENT AND TOOLS**

- **What are the right tools for the job?**
- **What is the correct way to use them?**
- **What is the condition of each tool?**

3. **POSITIONS OF PEOPLE**

- **What could we be struck by?**
- **What could we strike ourselves against?**
- **What can we get caught in/on/between?**
- **What are potential trip/fall hazards?**
- **What are potential hand/finger pinch points?**
- **What extreme temperatures will we be in/around?**
- **What are the risks of inhaling, absorbing, swallowing hazardous substances?**
- **What are the noise levels?**
- **What electrical current/energized system could we come in contact with?**
- **What would be a cause for overexerting ourselves?**

4. **PERSONAL PROTECTIVE EQUIPMENT (PPE)**

- **What is the proper PPE?**

Hard hat, glasses/goggles, ear plugs, gloves, steel toe boots, respiratory system, fire retardant clothing

5. **CHANGING THE COURSE OF WORK**

- **What would cause us to have to stop or rearrange the job?**
- **What would cause us to change our tools or equipment?**
- **What would cause us to have to change our position?**
- **What would cause us to have to change our PPE?**

YOU HAVE THE RIGHT AND
THE OBLIGATION TO

STOP UNSAFE ACTS

The above checklist is being used by a major oil and gas production company and has become a key element of how they do things. In other words, it is part of their culture. Contractors working for this company have begun using the checklist to analyze the tasks they perform.

The procedure for using the checklist is simple. All personnel assigned to perform a task will gather for a meeting. Each person has a copy of this checklist and one person will be assigned to document the findings of the meeting. A leader is assigned and the leader begins asking the questions, in the order written. The group answers each question and all the answers are documented. This is vital because if the process is not documented, it did not happen. Each group member follows along with the checklist and it is their responsibility to insure that the leader does not skip a question or that any member does not fail to answer a question.

Consider the first question, “What are the procedures for the task?” Answering this question will require that the appropriate procedures are gathered. The second question, “What is unclear about the procedures?” will insure that all personnel have reviewed the procedures. If there is no written procedure, then one must be created.

As the checklist is reviewed and each question answered and documented, a thorough review of the job will be conducted and any hazards or issues identified will be mitigated or addressed. In the end, all personnel will become more competent at identifying and mitigating hazards. Latent failures may be exposed and the job can proceed safely.

Some may say, "Wait a minute here. Conducting JHAs is usually considered a personnel safety issue and we know that having a good personnel safety record does not indicate effective process safety." This is true, but one of the elements of risk based process safety is safe work practices. On many occasions, process incidents begin with routine job tasks that are not performed correctly. Using the JHA checklist according to a formalized procedure yields several benefits. Personnel performing the jobs have the necessary procedures for performing the task. The procedures are reviewed to insure accuracy. Procedures are identified for development. Training issues are identified for personnel who do not understand the procedures or task. Hazards that are not readily apparent are identified and mitigated before the job. Latent failures are identified and addressed. Deviations from "normal" can be predicted and addressed early in a project or task. Even if an organization has implemented a global JHA process, local management can use this JHA checklist to enhance the organization's process.

Performing a JHA with this checklist may be a bit time consuming at first. As personnel become more familiar with and practice the process, the time required will be reduced. The analysis of each job will take as long as necessary to do a thorough review. Even though production pressures are always part of every job, whatever time is required to do an effective analysis will be worth it.

The three simple things presented in this paper are meant to be implemented at the process/plant level, not at the global level of an organization. Implementing them at the process and plant level is much like a pilot project and the process of implementation can be more easily fine-tuned. Effective process safety management system implementation and maintenance can be difficult and time consuming. These simple things can be modified as personnel become more competent and thus make management of process safety more efficient and effective.

The Center for Chemical Process Safety (CCPS) book, "Guidelines for Risk Based Process Safety", concludes with the following [1]:

> *"Standing still, congratulating ourselves on the successes of the past 20 years, and celebrating accidents that did not occur because of all of our hard work, will not prevent the next accident. Improvement will always be necessary. We must choose between moving forward, standing still, or slipping backward. We need not debate which direction to choose, only embrace the opportunity for each company to make a risk informed decision regarding which forward path leads more directly to the ultimate goal of a safe, effective, and economically competitive operation."*

Too often it is heard that the reason something is done a certain way is because it's always been done that way. That does not mean the way things are done is correct or efficient. These three simple things may seem onerous at first, but they do not have to be permanent changes. They only need to be implemented long enough to insure personnel are competent and efficient at process

safety. This is especially important when it is considered that over the next 10 years it is estimated that the oil and gas industry will be required to replace everyone who was hired in the early 1980's.

The next generation of workers in our industry needs to be given every opportunity to become competent at process safety.

REFERENCE

1. Center for Chemical Process Safety (CCPS) , "Guidelines for Risk Based Process Safety", **http://www.wiley.com/WileyCDA/WileyTitle/productCd-0470165693.html**

How Sensitive Are Crude Oil Pumping Requirements to Viscosity?

By Dr. Mahmood Moshfeghian

During the life cycle of a crude oil pipeline the properties of transported oil change, because in gathering systems the produced oils come from different wells. New wells may be added or some wells may go out of production for maintenance and repair. Production rates during the life of wells vary, too. In addition the properties of crude oil change during production. Due to seasonal variation, the average line temperature may also change. As it is shown in the proceeding sections, viscosity of crude oil is a strong function of API gravity and temperature.

In the March 2009 tip of the month (TOTM), procedures for calculation of friction losses in oil and gas pipelines were presented. The sensitivity of friction pressure drop with the wall roughness factor was also demonstrated.

In this TOTM, we will study crude oil °API and the pipeline average temperature and how they effect the pumping requirement. For a case study, we will consider a 160.9 km (100 miles) pipeline with an outside diameter of 406.4 mm (16 in) carrying crude oil with a flow rate of 0.313 m3/s (170,000 bbl/day). The pipeline design pressure is 8.963 MPa (1300 psia) with a maximum operating pressure of 8.067 MPa (1170 psia). The wall thickness was estimated to be 6.12 mm (0.24 in). The wall roughness is 51 microns (0.002 in) or a relative roughness (ε/D) of 0.00013. The procedures outlined in the March 2009 TOTM were used to calculate the line pressure drop due to friction. Then assuming 75 % pumping efficiency, the required pumping power was calculated. Since the objective was to study the effect °API and the line average temperature have on the pumping power requirement, we will ignore elevation change. The change in pumping power requirements due to changes in crude oil °API and line average temperature for this case study will be demonstrated.

Case Study 1: Effect of Line Average Temperature (Seasonal Variation)

To study the effect of the line average temperature on the pumping power requirement, an in house computer program called OP&P (Oil Production and Processing) was used to perform the calculations as outlined in the March 2009 TOTM. For a 35 °API crude oil in the pipeline described in the preceding section, the required pumping power was calculated for the line average temperature ranging from 21.1 to 37.8 °C (70 to 100 °F). For each case, the required pumping power was compared with an arbitrary base case (85 °F or 29.4 °C) and the percentage change in the pumping power requirement was calculated, accordingly. Figure 1 presents the percent change in power requirement as a function of line average temperature. There is about 5% change in the pumping power requirement for the temperature range considered.

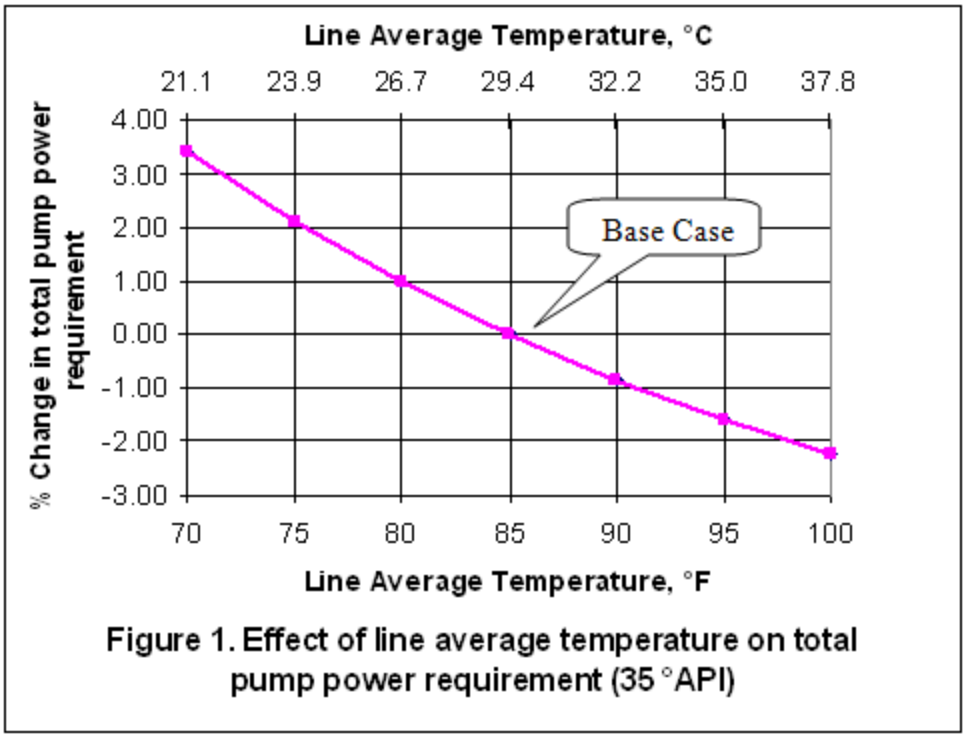

Figure 1. Effect of line average temperature on total pump power requirement (35 °API)

Note as the line average temperature increases, the power requirement decreases. This can be explained by referring to Figure 2 in which the oil viscosity decreases as the temperature increases.

Lower viscosity results in higher Reynolds (i.e. Reynolds $\mathrm{Re} = \frac{(V)(D)(\rho)}{\mu}$ is the ratio of inertia force to viscous force); therefore, the friction factor decreases (refer to the Moody friction factor diagram in the March 2009 TOTM).

Case Study 2: Effect of Variation of Crude Oil API

In this case, the effect of crude oil °API on the total pump power requirement for three different line average temperatures was studied. For each line average temperature, the crude oil °API was varied from 30 to 40 and the total pumping power requirement was calculated and compared to the base case (35 °API and average line temperature of 29.4°C=85°F).

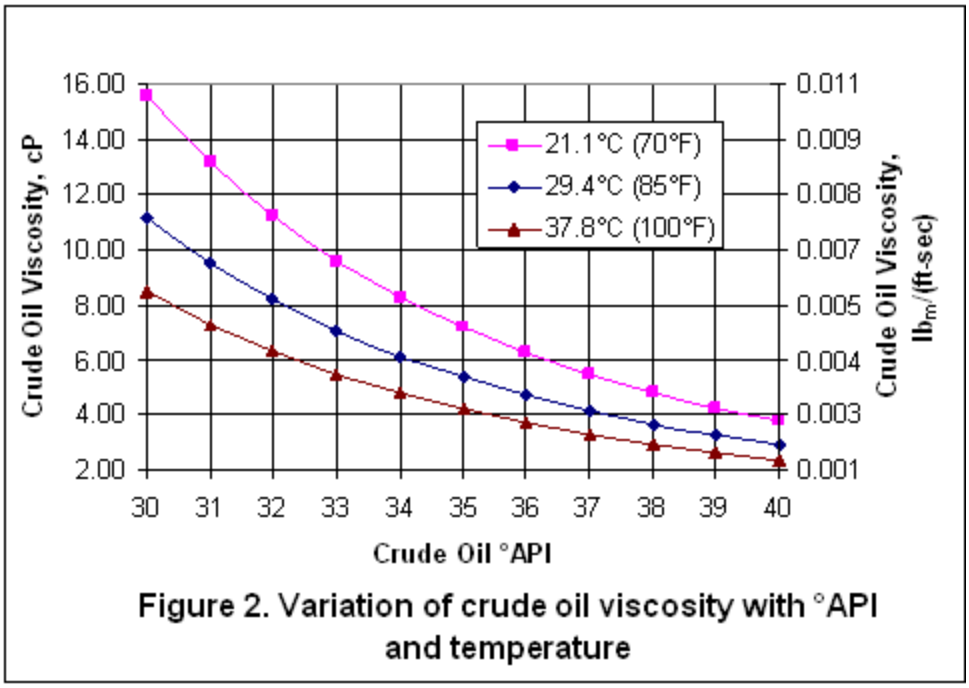

Figure 2. Variation of crude oil viscosity with °API and temperature

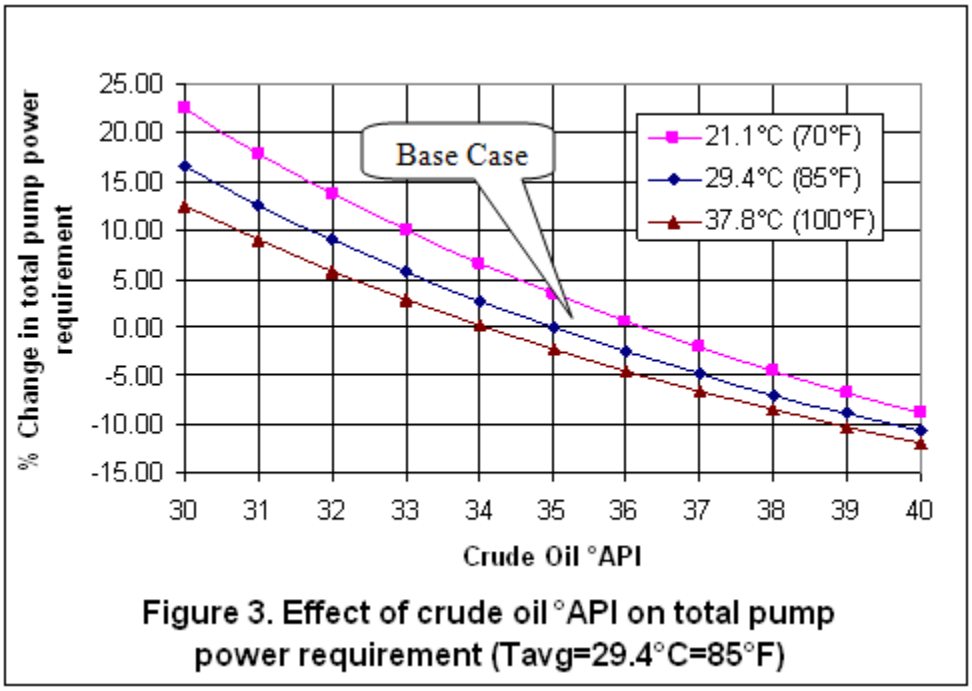

Figure 3. Effect of crude oil °API on total pump power requirement (Tavg=29.4°C=85°F)

For each case the percent change in total power requirement was calculated and is presented in Figure 3. As shown in this figure, when °API increases the total power requirement decreases. This also can be explained by referring to Figure 2 in which the crude oil viscosity decreases as ° API increases. The effect of viscosity is more pronounced at lower line average temperature (i.e. 21.1 °C or 70°F). Figure 3 also indicates that there is about 25 % change in total power requirement as °API varies from 30 to 40 °API. This is a big change and should be considered during design of crude oil pipelines.

Discussion and Conclusions

The analysis of Figure1-3 indicates that for the oil pipeline, the pumping power requirement varies as the crude oil °API changes. Increasing °API or line average temperature reduces the crude oil viscosity (see Figure 2). The reduction of viscosity results in higher Reynolds number, lower friction factor and in effect lower pumping power requirements.

In practical situations, an originating station takes crude out of storage and the midline stations taking suction from the upstream section of pipeline. In some parts of the world, the suction temperature to the originating pumps is +38 °C (+100 °F) but the temperature to the midline station is ground temperature (this assumes a buried line below the frost line) approximately 18 °C (65 °F). The originating station will always be more affected by temperature because storage will follow ambient - whereas the midline station will operate at notionally constant temperature +/- 5.5 °C (+/-10 °F) in the lower 9 °C (48 °F). For the case studied in this TOTM, the number of pumping stations varied from 2.5 to 3.2.

In light of the above discussion, a sound pipeline design should consider expected variation in crude oil °API and the line average temperature.

Important Aspects of Centrifugal Compressor Testing-Part 1

by Joe Honeywell

Every centrifugal compressor, whether it is new or has been in service for many years will most likely be tested to verify its thermodynamic performance. For a new machine the testing may be conducted in the manufacturer's facility under strict controlled conditions or in the field at actual operating conditions. Older compressors that have been placed in service after maintenance or have been operating for an extended period of time may require testing to verify the efficiency and normal operation. This TOTM will review ASME PTC-10 (also referred to as the Code) testing procedure and other topics that contribute to an accurate centrifugal compressor test results.

This two-part series will review the salient aspects of a performance test. Part 1 will review the thermodynamic performance test objectives established in the Code as well as other factors to consider in a testing procedure. While this code is primarily applicable to shop testing it can also apply to field testing. Part 2 will review the Code assumptions and basic performance relationships. It will also examine the three important principles that influence the operating conditions and ultimately influence the accuracy of the performance test. They are volume ratio, Machine Mach Number and Machine Reynolds Number.

Introduction

The purpose of a performance test is to verify that a centrifugal compressor will perform in accordance with the manufacturer's design at the operating conditions given in the specifications. It also provides a method of confirming the shape of the compressor head-flow curve, efficiency, and the maximum and minimum flow limits at various speeds. Frequently a performance test is conducted under field conditions with the specified gas and operating conditions. However, if the performance test is conducted in the shop it may not be possible to test the compressor with the specified gas because of safety concerns or testing facility limitations. Whether the test is conducted in the field or in the shop, proof of the compressor design is recommended and often necessary to demonstrate contractual obligations and mechanical integrity.

Frequently the gas composition used to confirm a compressor performance differs from the specified gas. This is often the case regardless if the test is conducted in the field or in the shop. For field tests, where the gas composition and operating conditions are set by the process, adjustments must be made in the calculations to confirm the compressor design specifications. Typically, a shop test is conducted with a carefully selected mixture of gases blended together to form a gas that has physical properties that closely resemble the specified gas. Even with a substitute gas, differences remain which influence the test results.

The original compressor design places limits on the thermodynamic performance. The most important of these limits include flow rate, power, temperature, pressure and speed. There are other design restraints which are not as commonly known but will also influence the compressor performance. Such factors are volume ratio, Mach number and Reynolds number. These limits were incorporated in the compressor design and are influenced by gas properties, operating conditions and the mechanical design. To verify the design and operating limits for a compressor, it is necessary to test the machine. For new machines, these tests are commonly performed in the manufacturer's facility; however, the testing is sometimes performed in the field. It may also be helpful to periodically test a compressor to trend the machine performance. Testing conducted during commissioning will establish a baseline of performance. Periodic field tests are often conducted to verify the overall performance and signal changes that may predict mechanical damage, internal fouling, or other deteriorating conditions.

Summary of ASME PTC-10 – Performance Test Code

The procedure presented in the Code provides a method of verifying the thermodynamic performance of centrifugal and axial compressors. This code offers two types of tests which are based on the deviation between test and specified conditions. A detail procedure is given for calculating and correcting results for differences in gas properties and test conditions. The following briefly describes the guiding principles of the Code.

- Type 1 test is conducted with the specified gas at or very near to the specified operating conditions. While the actual and test operating conditions may differ, the permissible deviations are limited. See Table 1, 2 and 3 for deviation limits of testing variables of a Type 1 test.
- Type 2 test is conducted with either the specified gas or a substitute gas. The test operating conditions will often differ significantly from the specified conditions. The operating conditions are subject to limitations based on the compressor aerodynamic design. See Table 2 and 3 for permissible deviations of operating conditions and test gas properties.
- The calculation method of a Type 1 and Type 2 test may conform to either Ideal or Real Gas laws. Physical property limitations are given in Table 3 if Ideal Gas Law methodology is used.

Table 1
Permissible Deviation from Specific Operating Conditions for Type 1 Tests

Variable	Symbol	Units	Permissible Deviation
Inlet pressure	p_i	psia	5%
Inlet temperature	T_i	°R	8%
Speed	N	rpm	2%
Molecular weight	MW	lbm/lbmole	2%
Cooling temperature difference		°R	5%
Coolant flow rate		gal/min	3%
Capacity	q_i	ft³/min	4%

GENERAL NOTES:
(a) Type 1 tests are to be conducted with the specified gas. Deviations are based on the specified values where pressures and temperatures are expressed in absolute values.
(b) The combined effect of inlet pressure, temperature and molecular weight shall not produce more than an 8% deviation in the inlet gas density.
(c) The combined effect of the deviations shall not exceed the limits of Table 2. Cooling temperature difference is defined as inlet gas temperature minus inlet cooling water temperature.
(d) See ASME PTC-10 for a description of nomenclature.

Table 2
Permissible Deviation from Specified Operating Parameters for Type 1 and 2 Tests

Parameter	Symbol	Limit of Test Values as Percent of Design Values	
		Min	Max
Specific volume ratio	v_i/v_d	95	105
Flow coefficient	ϕ	96	104
Machine Mach number Centrifugal compressors	M_m	See Part 2	
Machine Reynolds number Centrifugal compressors [Note 1]	Rem	See Part 2	

NOTE:
(1) Minimum allowable test Machine Reynolds number is 90,000.
(2) See ASME PTC-10 for a description of nomenclature.

Table 3
Limits of Departure from Ideal Gas Laws of Specified and Test Gases

Pressure Ratio	Maximum Ratio k max/k min	Allowed Range for Function X Min	Allowed Range for Function X Max	Allowed Range for Function Y Min	Allowed Range for Function Y Max
1.4	1.12	-0.344	0.279	0.925	1.071
2	1.10	-0.175	0.167	0.964	1.034
4	1.09	-0.073	0.071	0.982	1.017
8	1.08	-0.041	0.039	0.988	1.011
16	1.07	-0.031	0.033	0.991	1.008
32	1.06	-0.025	0.028	0.993	1.006

GENERAL NOTES:
(a) Where: $X = -\frac{T}{v}\left(\frac{\partial v}{\partial T}\right)_p - 1$ and $Y = \frac{p}{v}\left(\frac{\partial v}{\partial p}\right)_T$

(b) Maximum and minimum values of k shall apply to both the specified and test gas over the complete range of conditions.
(c) When these limits are exceeded by either the specified gas or the test gas at any point along the compression path real gas calculation methods shall be used for that gas. Ideal or real gas method may be used if these limits are not exceeded.
(c) See ASME PTC-10 for a description of nomenclature.

The Code also gives procedures for calculating and correcting test results for difference between the test conditions and specified conditions. It also gives recommendations for accurate testing including compressor testing schemes, instrumentation, piping configuration and test value uncertainties. The following summarizes each topic.

- Thermodynamic calculations may utilize either enthalpy, isentropic or polytropic methods. The Code provides equations and examples for determining compressor work (also referred to as head), gas and overall efficiencies, gas and shaft power, and parasitic losses.
- The Code gives a correction procedure for test gases and test operating conditions that deviated from the specified operating conditions.
- Compressor testing may be open-loop or closed-loop; however, the test results are subject to limits that may give preference to the test arrangement.
- Instrumentation methods and measurement uncertainties (refer to PTC-19 series of standards) used to test compressors are given.
- Recommendations for piping layout are also included.

Test Gas Selection

There are many gases commonly used to test compressors. They are selected based on physical properties, toxicity, flammability and environmental concerns. See Table 4 for a list of the most frequently used gases. The manufacturers will sometimes blend the various gases to match the

equivalency criteria and the test facilities limitations. Following are recommendations to consider when selecting a test gas.

- The compressor mechanical design may impose constraints on the test. Consider the machine rotor dynamics, overspeed, maximum temperature and power limitations when selecting a test gas.
- Avoid flow rate mismatch of impellers. The volume ratio equivalency is the most important parameter in selecting a test gas. This may also place limitations on the operating conditions. More on this subject in Part 2. of this series.
- The test gas molecular weight should closely match the molecular weight of the specified gas.
- The test gas k-value should closely match the specified gas to duplicate the
- Machine Mach Number. If this is not practical then the test k-value should be slightly greater to avoid possible stonewall limitations.
- Select a test gas with minimum Reynolds Number deviation from the specified gas. This will minimize the efficiency and head correction factors. This is especially important for machines with a low Machine Reynolds Number.

Table 4
Typical Test Gas Mediums [1]

Test Gas	Molecular Weight	k-Value [2]	Absolute Viscosity-cP [2]
Helium	4.003	1.667	0.0194
Nitrogen	28.014	1.401	0.0174
Air (dry)	28.959	1.401	0.0175
Carbon Dioxide	44.010	1.299	0.0145
R134a	102.0	1.124	0.0114
Natural Gas [4]	17.1 [3]	1.26 [3]	0.010 [3]
Propane	44.096	1.141	0.00789

Note:
1. From "Compressors 201" course at Turbomachinery Conference, 2009
2 Values from National Institute of Standards and Technology and Gas Processors Suppliers Association
3. Values at 60 ^{0}F (15.6 C) and 14.696 psia (101.3 kPa)
4. Gas composition and physical properties varies with local utility

Test Objectives

The following are some factors to consider as part of the performance test procedure.

- API 617 requires a minimum of five test points to be taken at the operating speed to demonstrate the surge point, stonewall, required operating point and two alternate points. The user may optionally request additional test points to verify compressor performance at alternate speeds. For example, extra data points may be needed to verify the surge line or critical process operating conditions for variable speed machines.

- The test may be performed as a Type 1 or Type 2 test. Type 1 is normally more accurate and is typically reserved when test conditions can be made to closely match the specified operating conditions. A Type 2 test is typically a shop test utilizing a substitute gas.
- If a Type 2 test is recommended, the test gas may be a pure gas such as those listed in Table 4, or a mixture of gases. The composition of the test gas should be agreed upon before testing. In addition, the composition of the test gas should be sampled before, during and after the test. Some gas mixtures tend to stratify and give erroneous results.
- The physical properties of the test gas are critical to the outcome especially if it is a mixture of selected gases. An agreement on the physical properties is recommended.
- Normally an agreement is made as to the "equation of state" used to calculate the results of the test. Not all EOS programs give the same results, nor is there industry agreement as to which method is best.
- Discuss the specific driver used in the test. Will a shop driver or the specified driver be used? Will the driver be fixed or variable speed? If it is variable speed, will it be motor, gas turbine or steam turbine?
- If a gear is part of the test, will it be manufacturer or user supplied? Is the efficiency of the gear known? Tests can be performed to verify gear efficiency.
- Will the gas be cooled with a water-cooled or air-cooled exchanger? Is there temperature limitations on the coolant used in the test?
- Is the allowable working pressure of equipment and piping systems adequate for the test? Will a pressure safety valve be needed to protect the system and is it properly sized?
- An agreement on how the input power will be measured is important. Options include, heat balance, calibrated driver, dynamometer, and torque meter. Review the specific method of measuring input power with the manufacturer.
- A piping and instrument schematic is recommended. The drawing should show details of the test loop including the placement of major equipment, number and location of instruments, and piping size. This is especially important for compressors with multiple sections, inlet sidestream, or back-to-back configuration.
- Before proceeding with a performance test a written procedure is recommended that outlines how the test will be conducted. The procedure should clearly convey the scope of the test, the responsibilities of each party, test piping and instrument arrangement, measurement methods, uncertainty limits, calibration, taking of test data and how to interpret results, and acceptance criteria.

REFERENCES

1. ASME PTC-10, "Performance test Code on Compressors and Exhausters", 1997.
2. API Standard 617, "Centrifugal compressors for Petroleum, Chemical, and Gas Services Industries", 1995.

3. Kurz, R., Brun, K, & Legrand, D.D., “Field Performance Testing of Gas Turbine
4. Driven Compressor Sets”, Proceeding of the 28th Turbomachinery Symposium, 1999.
5. Short Course “Centrifugal Compressors 201”, Colby, G.M., et al. 38th
6. Turbomachinery Symposium, 2009.
7. National Institute of Standards and Technology, Web Site for Properties of Fluids.

Variation of Properties in the Dense Phase Region; Part 1 - Pure Compounds

by Mark Bothamley and Mahmood Moshfeghian

In this tip of the month (TOTM) we will describe the dense phase of a pure compound, what it is, and how it impacts processes. We will illustrate how thermophysical properties change in the dense phase as well as in the neighboring phases. The application of dense phase in the oil and gas industry will be discussed briefly. In next month TOTM, we will discuss the dense phase behavior of multi- component systems.

When a pure compound, in gaseous or liquid state, is heated and compressed above the critical temperature and pressure, it becomes a dense, highly compressible fluid that demonstrates properties of both liquid and gas. For a pure compound, above critical pressure and critical temperature, the system is oftentimes referred to as a "dense fluid" or "super critical fluid" to distinguish it from normal vapor and liquid (see Figure 1 for carbon dioxide). Dense phase is a fourth (Solid, Liquid, Gas, Dense) phase that cannot be described by the senses. The word "fluid" refers to anything that will flow and applies equally well to gas and liquid. Pure compounds in the dense phase or supercritical fluid state normally have better dissolving ability than do the same substances in the liquid state. The dense phase has a viscosity similar to that of a gas, but a density closer to that of a liquid. Because of its unique properties, dense phase has become attractive for transportation of natural gas, enhanced oil recovery, food processing and pharmaceutical processing products.

The low viscosity of dense phase, super critical carbon dioxide (compared with familiar liquid solvents), makes it attractive for enhanced oil recovery (EOR) since it can penetrate through porous media (reservoir formation). As carbon dioxide dissolves in oil, it reduces viscosity and oil-water interfacial tension, swells the oil and can provide highly efficient displacement if miscibility is achieved. Additionally, substances disperse throughout the dense phase rapidly, due to high diffusion coefficients. Carbon dioxide is of particular interest in dense-fluid technology because it is inexpensive, non-flammable, non-toxic, and odorless. Pipelines have been built to transport natural gas in the dense phase region due to its higher density, and this also provides the added benefit of no liquids formation in the pipeline.

In the following section we will illustrate the variation of thermophysical properties in the dense phase and its neighboring phases. Methane properties have been calculated with HYSYS software for a series of temperatures and pressures. Table 1 presents, the pressures and temperatures and their paths used in this study.

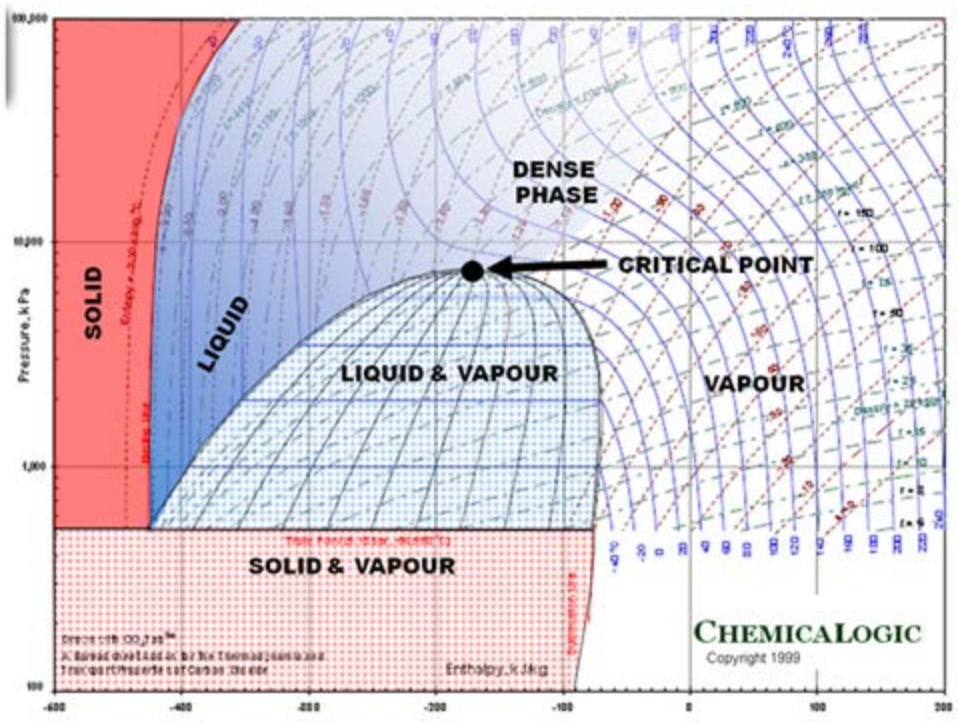

Figure 1. Pressure-enthalpy diagram for carbon dioxide identifying different phases

The calculated thermophysical properties are plotted as a function of pressure and temperature in Figures 2 to 9. The thermophysical property is shown on the left- hand side y-axis, temperature on the x-axis and pressure on the right-hand side y-axis.

Table 1. Pressure-Temperature combination and the paths chosen for methane

Point	Location	Temperature		Pressure		Path
		°C	°F	MPa(g)	Psig	
1	A	-97.7	-143.8	2.758	400	A to B: Saturated liquid to subcooled liquid
2	B	-117.8	-180.0	2.758	400	B to C: Isothermal, subcooled liquid to compressed liquid
3		-117.8	-180.0	3.447	500	
4		-117.8	-180.0	4.137	600	
5		-117.8	-180.0	4.826	700	
6	C	-117.8	-180.0	5.516	800	C to D: Isobaric, compressed liquid to dense phase (Super Critical Fluid)
7		-95.6	-140.0	5.516	800	
8		-90.0	-130.0	5.516	800	
9		-84.4	-120.0	5.516	800	
10		-78.9	-110.0	5.516	800	
11		-73.3	-100.0	5.516	800	
12	D	-62.2	-80.0	5.516	800	D to E: Isothermal, dense phase (super critical fluid) to super heated vapor (gas)
13		-62.2	-80.0	4.826	700	
14		-62.2	-80.0	4.137	600	
15		-62.2	-80.0	3.447	500	
16	E	-62.2	-80.0	2.758	400	E to F: Isobaric, super heated vapor (gas) to saturated vapor
17		-84.4	-120.0	2.758	400	
18	F	-97.7	-143.8	2.758	400	

Critical Temperature = -82.6 °C = -116.7 °F and Critical Pressure = 4.604 MPa = 667.7 Psia

Density:

Figure 2 presents the variation of density in different phases as a function of pressure and temperature. In the isobaric subcooling path of AB, liquid density increases gradually. However, in the isothermal compression of BC path, a small increase of density is observed. In the isobaric CD path, compressed liquid density decreases gradually as temperature is increased well into the dense phase region. However, as the temperature increases further in the dense phase, density reduction is accelerated. Reduction of density is further accelerated during isothermal expansion of DE. Isobaric cooling of vapor along EF path corresponds with a gradual increase in density. It can be noted the values of dense phase density are close to the liquid phase density in some areas of the dense phase region, and is overall significantly higher than the vapor phase densities.

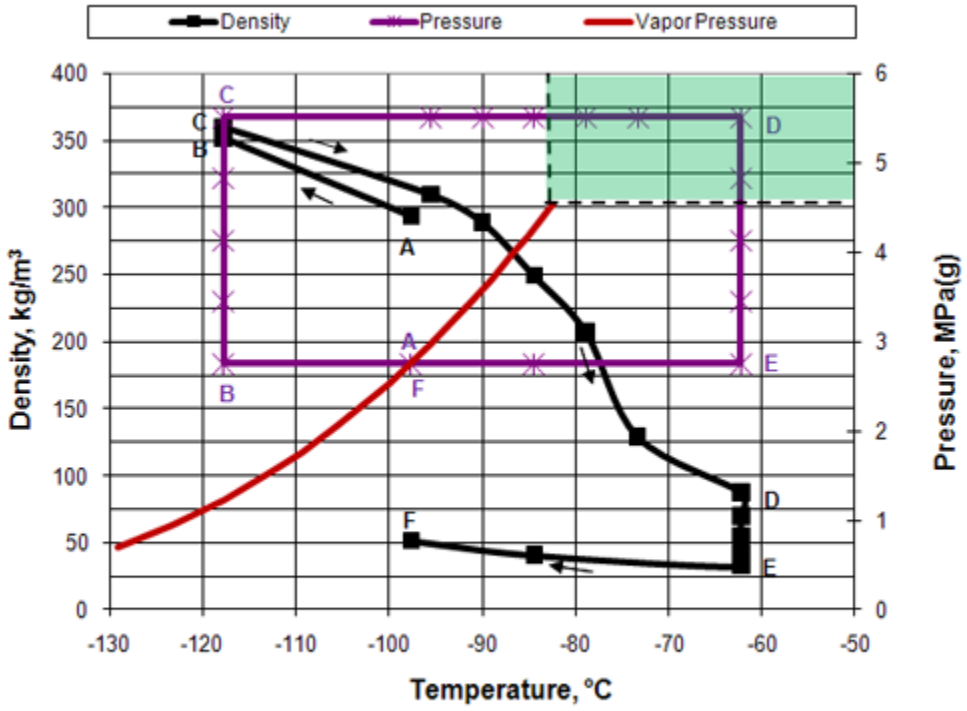

Figure 2. CH_4 density as a function of pressure and temperature

Viscosity:

Figure 3 presents the variation of viscosity in different phases as a function of pressure and temperature. In the isobaric subcooling path of AB, liquid viscosity increases rapidly. However, in the isothermal compression of BC path, a very small change of viscosity is observed. In the isobaric CD path, compressed liquid viscosity decreases linearly and sharply as temperature is increased well into the dense phase region. As the temperature increases further in the dense phase, viscosity reduction becomes gradual and approaches the gas phase values. Reduction of viscosity is quite small during isothermal expansion of DE. Isobaric cooling of vapor along EF path corresponds with no appreciable change in viscosity.

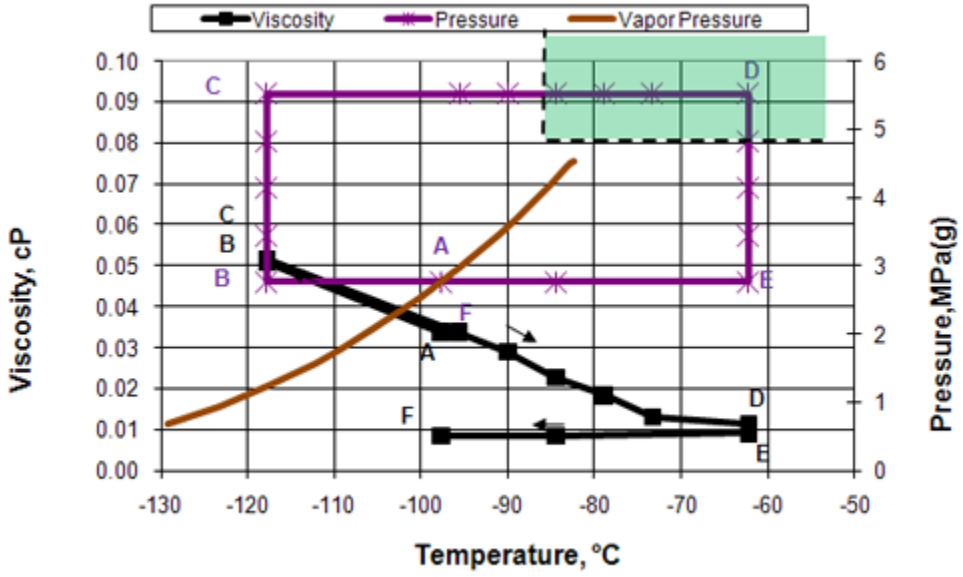

Figure 3. CH_4 viscosity as a function of presure and temperature

Compressibility Factor:

In general, the compressibility factor Z, calculated by an equation of state is not accurate for the liquid phase. Therefore, Figure 4 which presents compressibility factor as a function of pressure and temperature should be considered for qualitative study only. In the isobaric subcooling path of AB, Z remains almost constant. However, in the isothermal compression of BC path, Z increases drastically. In the isobaric CD path, Z increases gradually as temperature is increased well into the dense phase region. As the temperature increases further in the dense phase, the increase in Z is accelerated. The increase in Z is further accelerated during isothermal expansion of DE. Isobaric cooling of vapor along FF path corresponds with a gradual decrease in Z.

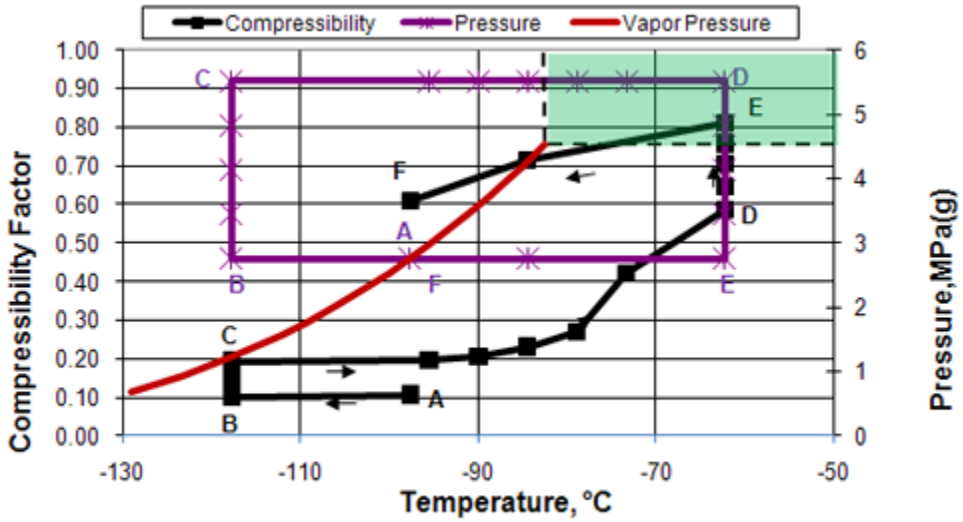

Figure 4. CH_4 compressibility factor as a function of pressure and temperature

Surface Tension:

Figure 5 shows that in the liquid phase, surface tension is a strong function of temperature but independent of pressure. Above the critical temperature, surface tension is not applicable and its value is zero.

Heat Capacity:

Generally, heat capacity is applicable in a single phase region and should not be used when there is a phase change. Figure 6 presents the variation of density in different phases as a function of pressure and temperature. In the isobaric subcooling path of AB, liquid heat capacity decreases. In the

isothermal compression of BC path, a small decrease of heat capacity is observed. In the isobaric CD path, compressed liquid heat capacity increases gradually as temperature is increased well into the dense phase region. As the temperature increases further in the dense phase, heat capacity reaches a maximum value and then starts to decrease. This is strange behavior and surprisingly high values are calculated. Similar results were obtained using ProMax software. Reduction of heat capacity is further noticed during isothermal expansion of DE. Isobaric cooling of vapor along EF path corresponds with a gradual increase in heat capacity.

Thermal Conductivity:

Figure 7 presents the variation of thermal conductivity in different phases as a function of pressure and temperature. In the isobaric subcooling path of AB, liquid thermal conductivity increases. In the isothermal compression of BC path, no change is observed. In the isobaric CD path, compressed liquid thermal conductivity decreases gradually as temperature is increased well into the dense phase region. However, as the temperature increases further in the dense phase, thermal conductivity reduction is accelerated. Reduction of thermal conductivity is further noticed during isothermal expansion of DE. Isobaric cooling of vapor along EF path corresponds with a small decrease in thermal conductivity.

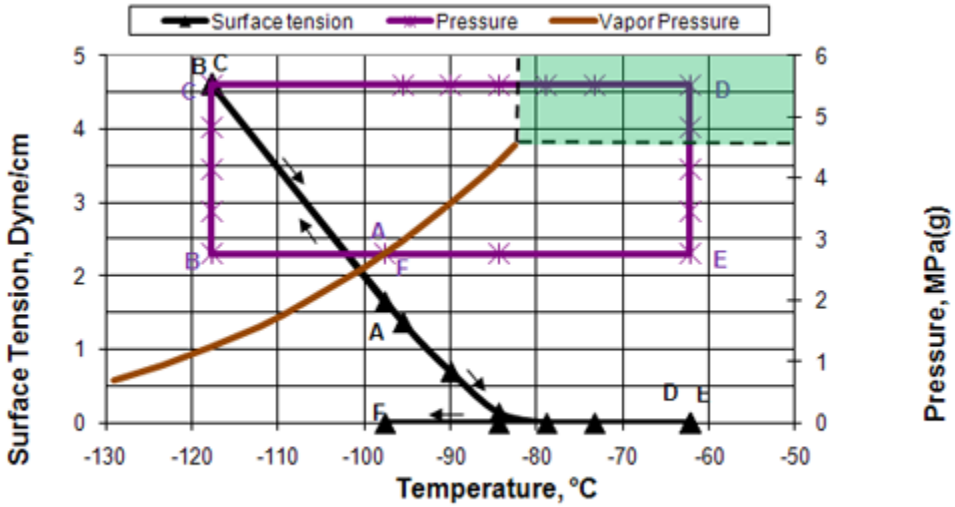

Figure 5. CH_4 Surface tension as a function of pressure and temperature

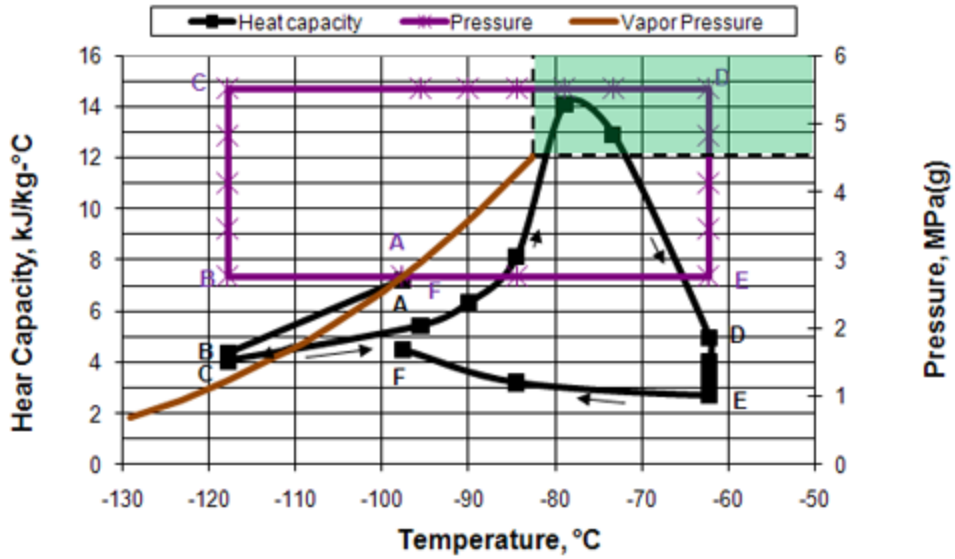

Figure 6. CH_4 Heat capacity as a function of pressure and temperature

Enthalpy and Entropy:

Figures 8 and 9 present the variation of enthalpy and entropy in different phases as a function of pressure and temperature. As shown in these figures, their qualitative variations are similar. In the isobaric subcooling path of AB, liquid enthalpy and entropy decrease. In the isothermal compression of BC path, no change is observed. During the isobaric CD path, compressed liquid enthalpy and entropy values increase gradually as temperature is increased well into the dense phase region. However, as the temperature increases further in the dense phase, the enthalpy and entropy increase becomes larger. The increase in enthalpy and entropy is further noticed during isothermal expansion of DE. Isobaric cooling of vapor along EF path corresponds with a decrease in enthalpy and entropy.

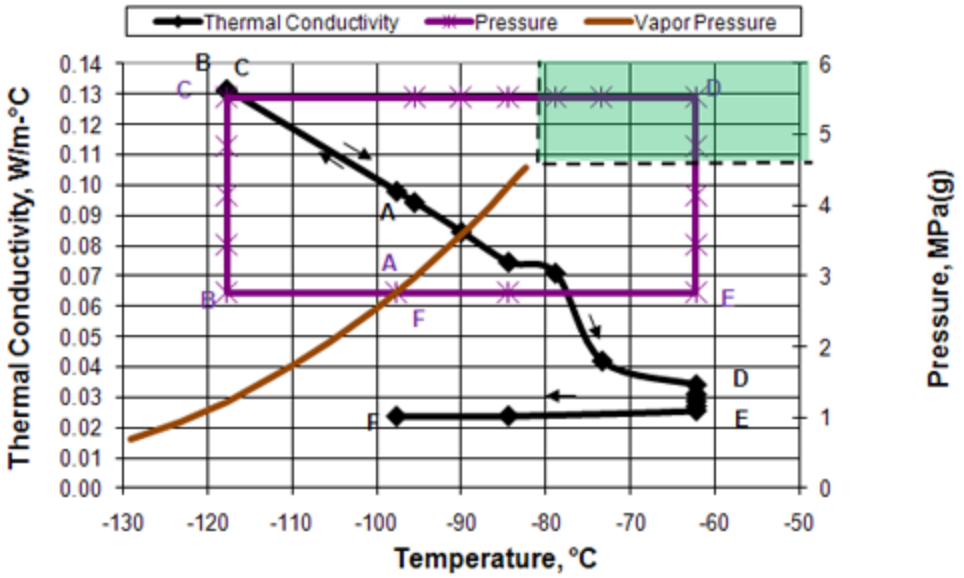

Figure 7. CH_4 Thermal conductivity as a function of pressure and temperature

Conclusions:

Dense phase behavior is unique and has special features. The thermophysical properties in this phase may vary abnormally. Care should be taken when equations of state are used to predict thermophysical properties in dense phase. Evaluation of equations of state should be performed in advance to assure their accuracy in this region. Many simulators offer the option to use liquid-based algorithms (e.g. COSTALD) for this region.

As shown in Figure 1, there is a gradual change of phase transition from gas-to- dense and dense-to-liquid phases or vice versa. Dense phase is a highly compressible fluid that demonstrates properties of both liquid and gas. The dense phase has a viscosity similar to that of a gas, but a density closer to that of a liquid. This is a favorable condition for transporting natural gas in dense phase as well as carbon dioxide injection into crude oil reservoir for enhanced oil recovery.

REFERENCE

1. ASPENone, Engineering Suite, HYSYS Version 2006, Aspen Technology, Inc., Cambridge, Massachusetts U.S.A., 2006.

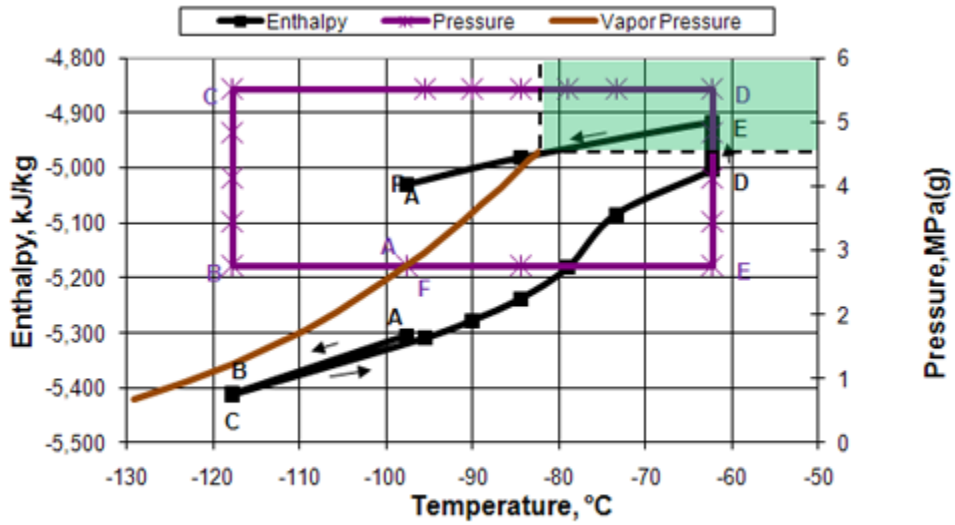

Figure 8. CH_4 Enthalpy as a function of pressure and temperature

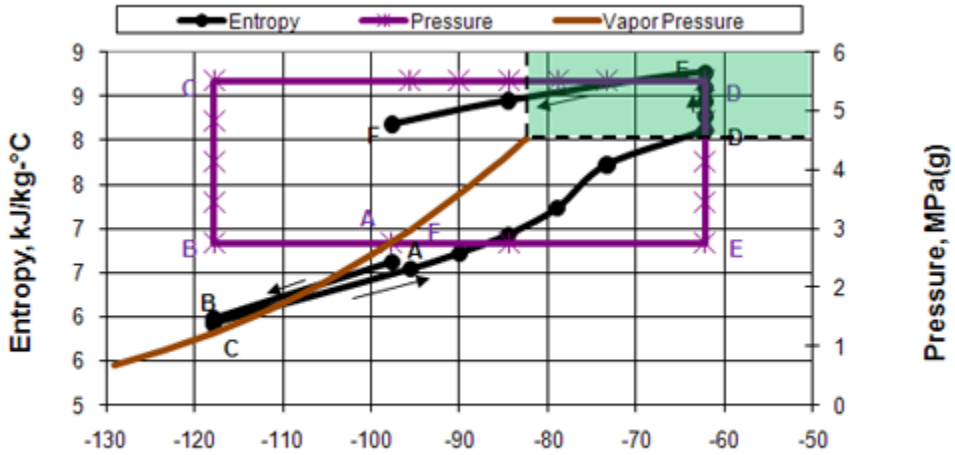

Figure 9. CH4 Entropy as a function of pressure and temperature

Should the TEG Dehydration Unit Design Be Based on the Water Dew Point or Hydrate Formation Temperature?

By Dr. Mahmood Moshfeghian

Glycol dehydration is the most common dehydration process used to meet pipeline sales specifications and field requirements (gas lift, fuel, etc.). Triethylene glycol (TEG) is the most common glycol used in absorption systems. Chapter 18, Gas Conditioning and Processing [1] presents the process flow diagram and basics of glycol units. A key parameter in sizing the TEG dehydration unit is the water dew point temperature of dry gas leaving the contactor tower. Once the dry gas water dew point temperature and contactor pressure are specified, water content charts similar to Figure 1 in reference [2] can be used to estimate the water content of lean sweet dry gas. The required lean TEG concentration is thermodynamically related to the dry gas water content which influences the operating (OPEX) and capital (CAPEX) costs. The lower dry gas water content requires a higher lean TEG concentration. This parameter sets the lean TEG concentration entering the top of contactor and the required number of trays (or height of packing) in the contactor tower.

The rich TEG solution is normally regenerated at low pressure and high temperature. Maximum concentrations achievable in an atmospheric regenerator operating at a decomposition temperature of 404 °F (206°C) is 98.7 weight %. The corresponding dry gas water dew point temperature for this lean TEG weight % and contactor temperature of 100°F (38°C) is 18°F (8°C).

If the lean glycol concentration required at the absorber to meet the dew point specification is higher than the above maximum concentrations, then some method of further increasing the glycol concentration at the regenerator must be incorporated in the unit. Virtually all of these methods involve lowering the partial pressure of the glycol solution either by pulling a vacuum on the regenerator or by introducing stripping gas into the regenerator.

For water saturated gases, the water dew point temperature is either above or at the hydrate formation temperature. However, if the gas is water under-saturated, the hydrate formation temperature will be higher than water dew point. This means at a given specified water dew point temperature, there are two water content values; the lower value will be at the hydrate formation temperature and the higher value will be at the water dew point temperature. Therefore, the designer has to choose one of these two values. Which value should be chosen? The answer to this question is “It depends”! The lower value of water content means higher lean TEG concentration and consequently higher CAPEX and OPEX.

In this TOTM we will attempt to answer the question by studying a case in which the specified water dew point temperature is below the hydrate formation temperature. For this purpose, we will discussthe water content of natural gas in equilibrium with hydrate and when the condensed water phase is liquid. The water content chart of Figure 6.1 in reference [2] is based on the assumption that the condensed water phase is a liquid. However, at temperatures below the hydrate temperature of the

gas, the "condensed" phase will be a solid (hydrate). The water content of a gas in equilibrium with a hydrate will be lower than equilibrium with a metastable liquid.

Hydrate formation is a time dependent process. The rate at which hydrate crystals form depends upon several factors including gas composition, presence of crystal nucleation sites in the liquid phase, degree of agitation, etc. During this transient "hydrate formation period" the liquid water present is termed "metastable liquid." Metastable water is liquid water which, at equilibrium, will exist as a hydrate.

Reference [3] presents experimental data showing equilibrium water contents of gases above hydrates. Data from Reference [3] are presented in Figure 6.5 of reference [2] and plotted here as rotated square in Figure 1 at 1000 Psia (6,897 kPa). For comparative purposes, the "metastable" water content of the gas (dashed line) as well as the hydrate formation temperature (solid line) calculated by ProMax [4] using the Peng-Robinson [5] equation of state are also shown. The water content of gases in the hydrate region is a strong function of composition. Figure 1 should not be applied to other gas compositions.

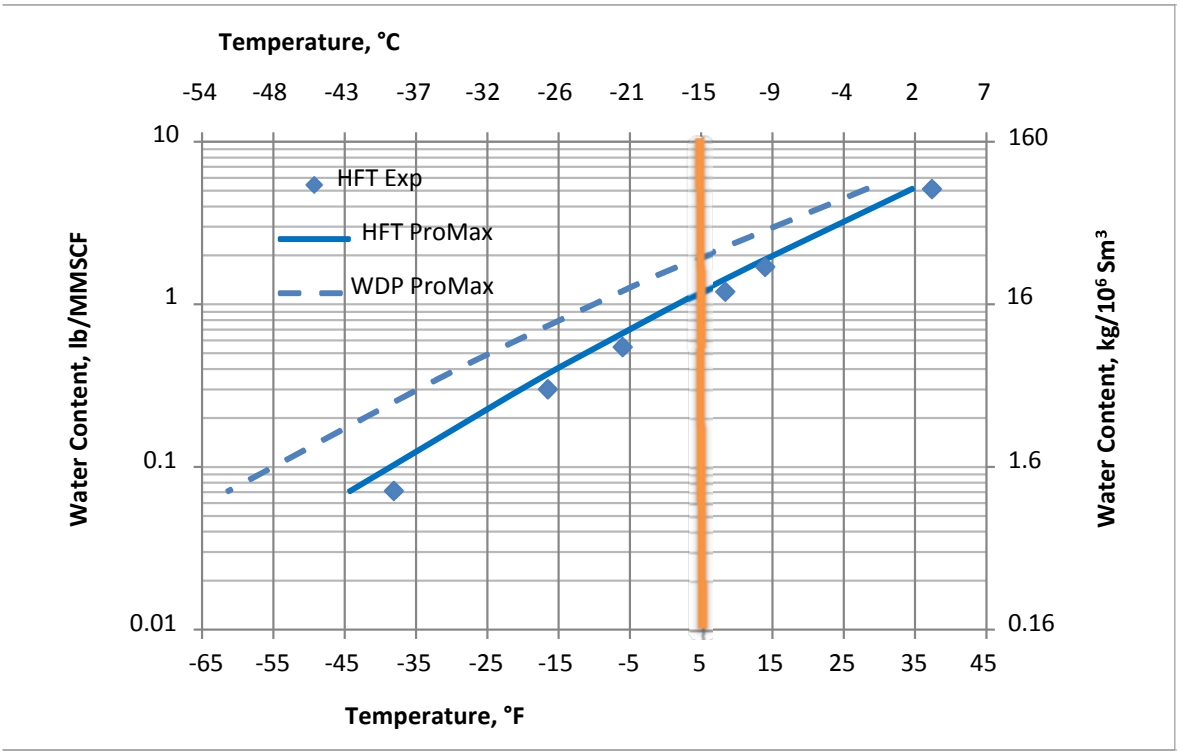

Figure 1. Water content of 94.69 mole % methane and 5.31 mole % propane - gas in equilibrium with hydrate at 1000 Psia (6,897 kPa)

Case Study:

To demonstrate, the effect of water content of a dried gas in equilibrium with hydrate on the required lean TEG concentration, let's consider the gas mixture presented in Figure 1. This gas enters a contactor tower at 1000 Psia (6,897 kPa) and 100 °F (37.8°C) with a rate of 144 MMSCFD (4.077 10^6 Sm^3/d). At this condition, the water content of the wet gas is 57.6 lb/MMSCF (922.4 kg/10^6 Sm^3). It is desired to dehydrate the gas to a water dew point temperature of 5°F (-15°C) using a TEG dehydration unit.

Results and Discussion:

According to Figure 1, at a temperature of 5°F (-15°C) the water content is 1.2 lb/MMSCF (19.2 kg/10^6 Sm^3) and 1.97 lb/MMSCF (31.5 kg/10^6 Sm^3) in equilibrium with metastable water and hydrate phase, respectively. ProMax was used to simulate this TEG dehydration unit for the case of three theoretical trays in the contactor tower. The simulation results for these two water content cases are shown in Table 1. This table clearly indicates that the required lean TEG concentrations are not the same and consequently will impact the regeneration requirements of the rich TEG solution. The difference between the lean TEG concentrations will be even more at a lower dry gas water dew point specification.
The simulation results clearly indicate that the choice of water content for a specified dry gas water dew point as the basis for design affects the required lean TEG concentration and consequently the rich TEG solution regeneration requirements.

Table 1. Comparison of simulation results for two different water content specifications

Simulation Results Using ProMax	Based on Water Dew Point Temperature of 5 °F (-15°C)	Based on Hydrate Formation Temperature of 5 °F (-15°C)
Water Dew Point Temperature , °F (°C)	5.0 (-15.0)	-6.2 (-21.2)
Hydrate Formation Temperature, °F (°C)	14.7 (-9.6)	5.0 (-15.0)
Water Content, lb/MMSCF (kg/10^6 Sm^3)	1.97 (31.5)	1.20 (19.2)
Gallon/lb of Water Removed (liter/kg of Water Removed)	3.95 (32.9)	3.90 (32.4)
Lean TEG Weight %	99.45	99.72

Conclusions:

When designing dehydration systems, particularly TEG systems to meet extremely low water dew point specifications, it is necessary to determine the water content of the dried gas in

equilibrium with a hydrate using a correlation like that presented in Figure 1. If a metastable correlation is used, one will overestimate the saturated water content of the gas at the dew point specification. This, in turn, may result in a dehydration design which is unable to meet the required water removal. Where experimental data is unavailable, utilization of an EOS-based correlation which has been tuned to empirical data can provide an estimate of water content in equilibrium with hydrates.

To meet pipeline sales specifications, it is normally acceptable to use the water content in equilibrium with the metastable phase (the dashed line in Figure 1) because the difference in the water contents is not that high. However, for extremely low water dew point specifications where there is a cryogenic process downstream, it is recommended to use the water content in equilibrium with hydrate (the solid line in Figure 1).

REFERENCES

1. Campbell, J. M., "Gas Conditioning and Processing", Vol. 2, The Equipment Module,8th Ed., Second Printing, J. M. Campbell and Company, Norman, Oklahoma, 2002
2. Campbell, J. M., "Gas Conditioning and Processing", Vol. 1, The Basic Principles, 8thEd., Second Printing, J. M. Campbell and Company, Norman, Oklahoma, 2002
3. Song, K.Y. and Kobayashi, R, “Measurement & Interpretation of the Water Content of a Methane-5.31 Mol% Propane Mixture in the Gaseous State in Equilibrium With Hydrate,” Research Report RR-50, Gas Processors Association, Tula, Oklahoma,1982
4. ProMax 3.1, Bryan Research and Engineering, Inc, Bryan, Texas, 2010.
5. Peng, D. Y. and Robinson, D. B., I. and E. C. Fund, Vol. 15, p. 59, 1976

Distribution of Sulfur-Containing Compounds in NGL Products

By: Dr. Mahmood Moshfeghian

Natural gas liquids (NGLs) consist of the hydrocarbon components in a produced gas stream that can be extracted and sold. Common NGL products are ethane (C_2H_6), propane (C_3H_8), butanes (iC_4H_{10} and nC_4H_{10}) and natural gasoline (C_{5+}). Ethane is the lightest NGL and its recovery can be justified in those areas where a ready petrochemical market and a viable transportation network exist. Ethane is mainly used as a petrochemical feedstock. Propane is used for petrochemical feedstock, and also finds wide application as a domestic and industrial fuel. Propane is frequently sold as a mixture of propane and butane called LPG (Liquefied Petroleum Gas).

The market for butanes is primarily as a petrochemical feedstock, fuel and/or for gasoline blending when vapor pressure requirements allow it. Isobutane (iC_4) is the most valuable of the NGLs. Its primary use is as refinery feedstock for manufacture of high octane blending components for motor gasoline. Normal butane can be used as a feedstock to olefin plants where it is converted to mono-olefins (ethylene and propylene) and the diolefin, butadiene as well as other by-products. The largest use for isobutane is as a gasoline blending component for octane number and vapor pressure control. Natural gasoline refers to the pentanes and heavier components in a gas stream and they are also commonly referred to as condensate or naphtha; it usually consists primarily of straight and branched chain paraffins. Natural gasoline is most commonly used as refinery feedstock, although it can also be used as a petrochemical feedstock. The details of the processes required, and the principles of their operation are discussed in Maddox and Lilly [1], and Maddox and Morgan [2]. A summary about the distribution of sulfur-containing compounds is presented on pages of 287-291 [2]. Specifically, page 290 presents the conclusions from the papers presented by Harryman and Smith [3, 4] which highlight the complexity of sulfur-containing distribution in the NGL product streams.

Raw NGL feed to an NGL fractionation (NF) plant may contain sulfur-containing compounds such as carbonyl sulfide (COS), methyl mercaptan (MeSH), ethyl mercaptan (EtSH), carbon disulfide (CS_2), isopropyl mercaptan (iC_3SH), isobutyl mercaptan (iC_4SH), etc. For the purpose of meeting NGL products specification, it is important to accurately determine the distribution and concentration of the various mercaptans during NF process.

Likins and Hix [5] evaluated the accuracy of four commercial simulation programs by comparing their predicted K-values with the experimentally measured values. They concluded that "*In this limited evaluation against laboratory VLE data, no one program can be claimed to be an outstanding winner. Although simulator D does an excellent job with one system, it poorly predicts behavior in the second system and is surpassed by simulator B. Simulator C behaves erratically in that its predictions range from excellent to horrible (dimethyl sulfide) depending on the component.*" They also simulated two different NF plants using commercial simulation programs and compared the distribution and concentration of mercaptans in different product streams with field data. Again, they concluded that none of the simulators do a good job modeling the sulfur distribution overall.

In order to improve the accuracy of commercial simulators, Alsayegh *et al.* [6] presented a

procedure to determine the binary interaction parameters between mercaptans and hydrocarbons using experimentally measured vapor-liquid equilibria (VLE).

In this tip of the month (TOTM), we will determine the distribution and concentration of different mercaptans in an NGL fractionation plant using HYSYS [7] Peng-Robinson [8] equation of state. The built-in HYSYS binary interaction parameters were used in this study. The NF plant is the same as the one described by Alsayegh *et al.* [6]. The feed composition, rate, and condition are shown in Table 1 [6] and the plant process flow diagram is shown in Figure 1 [6].

Table 1. Feed composition and condition [6]

Component	**Mole %**	**PPM(mole)**
H2S	0.0032	32.3
CO2	0.2688	
Methane	2.6450	
Ethane	25.1452	
Propane	34.1877	
i-Butane	7.2677	
n-Butane	15.7183	
i-Pentane	4.4362	
n-Pentane	4.6731	
n-Hexane	3.1329	
n-Heptane	1.0851	
n-Octane	0.6954	
n-Nonane	0.4687	
n-Decane	0.2457	
COS	0.0004	3.6
MeSH	0.0125	124.7
EtSH	0.0096	95.8
CS2	0.0012	12.5
iC3SH	0.0018	17.8
iC4SH	0.0013	13.4
Properties:		
Temperature, °C	45.8	
Pressure, kPa	2412.4	
Molar Flow, kmole/h	4488.7	

Figure 1. Process Flow diagram for NGL fractionation plant [6]

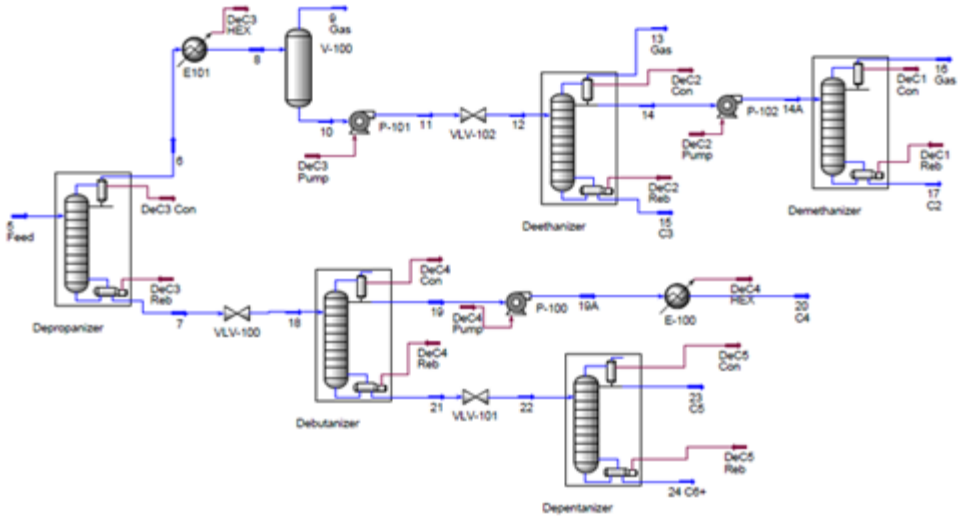

The column specifications are shown in Table 2 [6]. An overall tray efficiency of 90 percent was used for all columns. In the last column of Table 2, DV and D represent the vapor and the total rate of the overhead stream, respectively. Therefore, the D_V/D is the vapor fraction in the overhead product stream. In addition, reflux ratio (L/D) is defined as the reflux rate (L) divided by the total overhead stream rate.

Table 2. Column specification used in simulation [6]

Column	No of Trays	Feed Tray From Bottom	Distillate Rate (D) kmole/h	Reflux Ratio (L/D)	Overhead Pressure kPa	Bottom Pressure kPa	Vapor Fraction D_V/D
Depropanizer	40	25	2805.75	2.20	2256	2412	1.0000
Deethanizer	50	30	1083.70	1.60	1991	2160	0.1521
Demethanizer	24	24	131.49	1.60	2305	2317	1.0000
Debutanizer	40	22	1027.16	1.55	579	608	0.0000
Depentanizer	36	13	400.17	1.55	343	363	0.0000

Expected Product Distribution:

Figure 2, reproduced from Figure 9 of Likins and Hix paper [5], shows a descending order log scale bar-graph of the pure compounds vapor pressure for the components of interest to this study. This figure shows that COS should distribute to both the ethane and the propane streams. MeSH, with a vapor pressure close to n-butane should distribute primarily with the butanes with a small amount distributing to the pentane stream. EtSH, having a vapor pressure between butane and pentane, should distribute primarily with butane and pentant. CS_2 should distribute primarily to the pentane and the C_6 streams with only minor distribution to the butane stream. The heavier sulfur compounds should end up almost entirely in the C_6 stream.

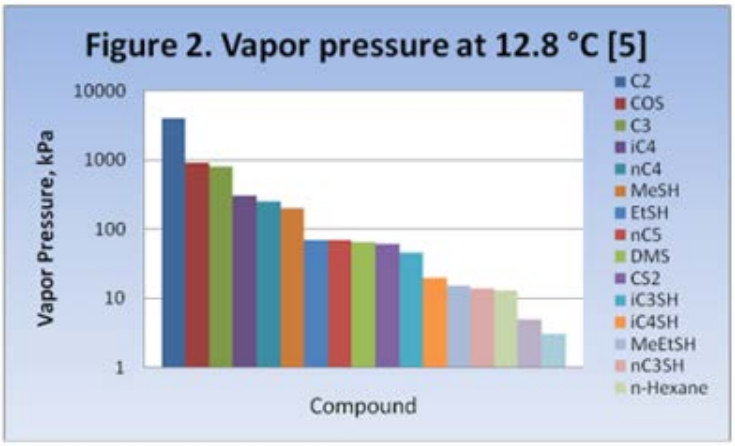

Results of Computer Simulation:

The NF plant described in the previous section was simulated using HYSYS [7] based on the Peng-Robinson equation of state (EOS) [8]. In this study, the HYSYS built-in binary interaction parameters were used even though we recommend insertion of VLE data regression into the EOS interaction parameters. This regression is required to adequately model the systems dealing with mercaptans. Table 3 presents the mole percent recovery of each component in the product and gas streams predicted by HYSYS. The mole percent recovery is defined as the number of moles of a component in the product stream divided by the moles of the same component in the feed stream (Stream 5). Table 3 also presents the vapor fraction, temperature, pressure, and flow rate of each stream. The focus of this study is on the distribution (% recovery) and concentration (PPM) of the sulfur-containing compounds in the product streams. Table 4 presents the PPM concentration of sulfur-containing compounds in the product streams.

Table 3. Mole % recovery of each component in the gas and product streams

Component	Flash Vapor 9 Gas	deC2 Top 13 Gas	deC1 Top 16 Gas	deC1 Bot 17 C2	deC2 Bot 15 C3	deC4 Top 20 C4	deC5 Top 23 C5	deC5 Bot 24 C_6+
H_2S	11.98	12.12	8.62	67.15	0.13	0.00	0.00	0.00
CO_2	22.49	20.38	28.68	28.45	0.00	0.00	0.00	0.00
Methane	35.06	29.08	35.85	0.00	0.00	0.00	0.00	0.00
Ethane	11.86	11.31	7.57	69.11	0.15	0.00	0.00	0.00
Propane	4.58	0.01	0.00	0.25	95.12	0.03	0.00	0.00
i-Butane	0.07	0.00	0.00	0.00	3.23	96.67	0.02	0.00
n-Butane	0.00	0.00	0.00	0.00	0.09	97.78	2.12	0.00
i-Pentane	0.00	0.00	0.00	0.00	0.00	9.90	89.97	0.13
n-Pentane	0.00	0.00	0.00	0.00	0.00	0.62	98.11	1.27
n-Hexane	0.00	0.00	0.00	0.00	0.00	0.00	0.00	100.00
n-Heptane	0.00	0.00	0.00	0.00	0.00	0.00	0.00	100.00
n-Octane	0.00	0.00	0.00	0.00	0.00	0.00	0.00	100.00
n-Nonane	0.00	0.00	0.00	0.00	0.00	0.00	0.00	100.00
n-Decane	0.00	0.00	0.00	0.00	0.00	0.00	0.00	100.00
COS	5.39	0.31	0.09	5.25	88.96	0.00	0.00	0.00
MeSH	2.65	0.00	0.00	0.00	84.31	13.04	0.00	0.00
EtSH	0.00	0.00	0.00	0.00	0.01	77.04	22.95	0.00
CS_2	0.00	0.00	0.00	0.00	0.00	58.91	41.09	0.00
iC_3SH	0.00	0.00	0.00	0.00	0.00	0.01	67.00	32.99
iC_4SH	0.00	0.00	0.00	0.00	0.00	0.00	0.00	100.00
Properties:								
Vapor Fraction	1.00	1.00	1.00	0.00	0.00	0.00	0.00	0.00
Temperature, °C	17.6	-18.2	-20.2	-1.6	60.9	25.0	71.2	132.8
Pressure, kPa	2190.5	1991.0	2304.6	2317.3	2160.0	758.6	343.2	362.8
Molar Flow, kmole/h	248.8	164.8	131.5	787.5	1473.1	1027.2	400.2	255.6

Table 4. Concentration (PPM, mole) of sulfur containing compounds in the gas and product streams

Component	Feed 5	Flash Vapor 9 Gas	deC2 Top 13 Gas	deC1 Top 16 Gas	deC1 Bot 17 C2	deC2 Bot 15 C3	deC4 Top 20 C4	deC5 Top 23 C5	deC5 Bot 24 C_6+
H_2S	32.3	69.8	106.6	95.0	123.6	0.1	0.0	0.0	0.0
COS	3.6	3.5	0.3	0.1	1.1	9.7	0.0	0.0	0.0
MeSH	124.7	59.5	0.0	0.0	0.0	320.4	71.1	0.0	0.0
EtSH	95.8	0.0	0.0	0.0	0.0	0.0	322.4	246.5	0.0
CS_2	12.5	0.0	0.0	0.0	0.0	0.0	32.1	57.5	0.0
iC_3SH	17.8	0.0	0.0	0.0	0.0	0.0	0.0	133.9	103.2
iC_4SH	13.4	0.0	0.0	0.0	0.0	0.0	0.0	0.0	234.7

Figures 3 through 9 present bar-graphs of the recovery of each sulfur-containing compound in the product streams.

H_2S: Figure 3 shows the distribution and recovery of H_2S in the gas, C_2 and C_3 streams. As expected, the majority of the H_2S distributes in the gas and the C_2 streams.

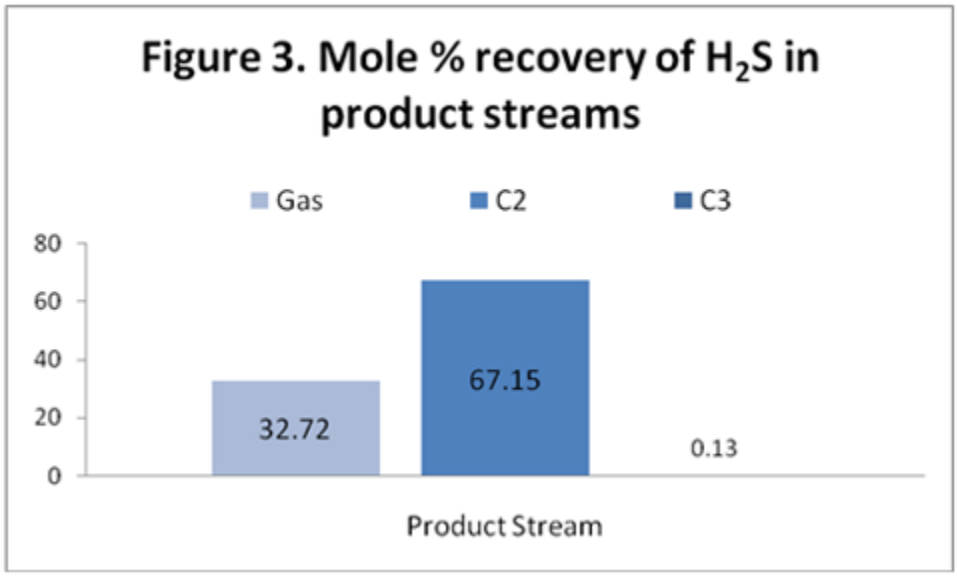

COS: Figure 4 shows the distribution and recovery of COS in the gas, C_2, and C_3. As expected, the majority of the COS ends up in the C_3 stream.

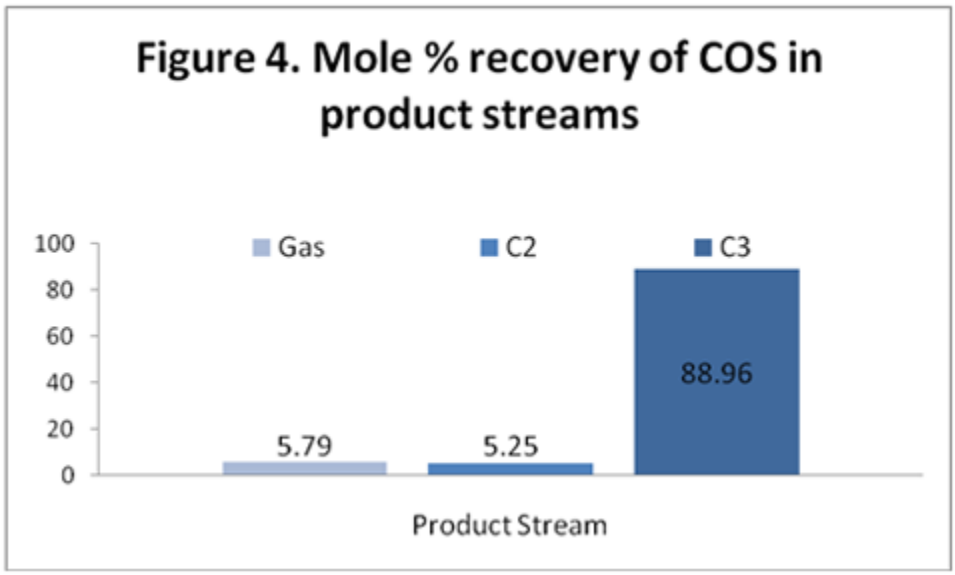

MeSH: Figure 5 shows the distribution and recovery of MeSH in the gas, C_3, and C_4 streams. Contrary to the data presented in Figure 2, the majority of the MeSH distributes to the C_3 stream rather than to the C_4 stream.

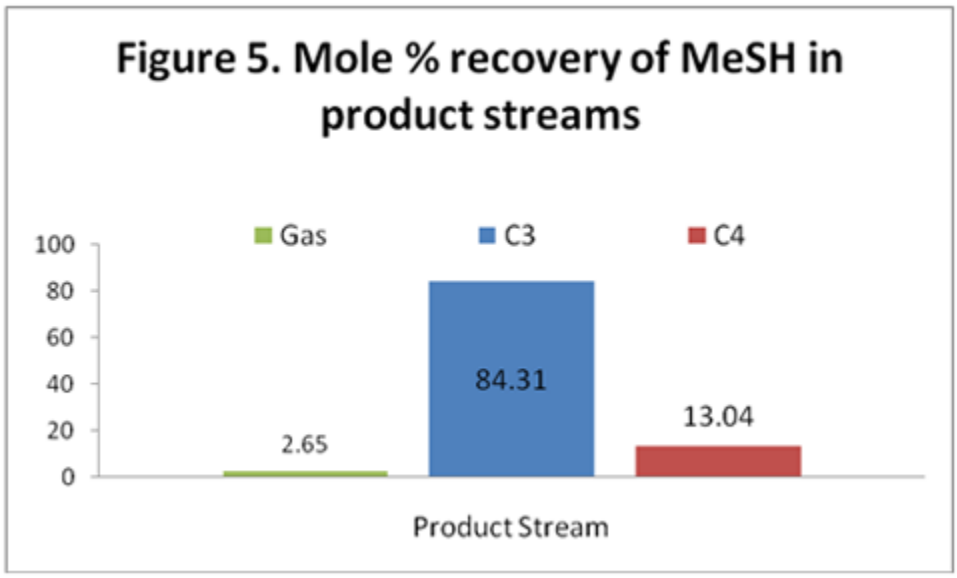

EtSH: Figure 6 shows the distribution and recovery of EtSH in the C_3, C_4, and C_5 streams. Unexpectedly, the majority of the EtSH ends up in the C_4 stream rather than C_5 as would be expected in Figure 2.

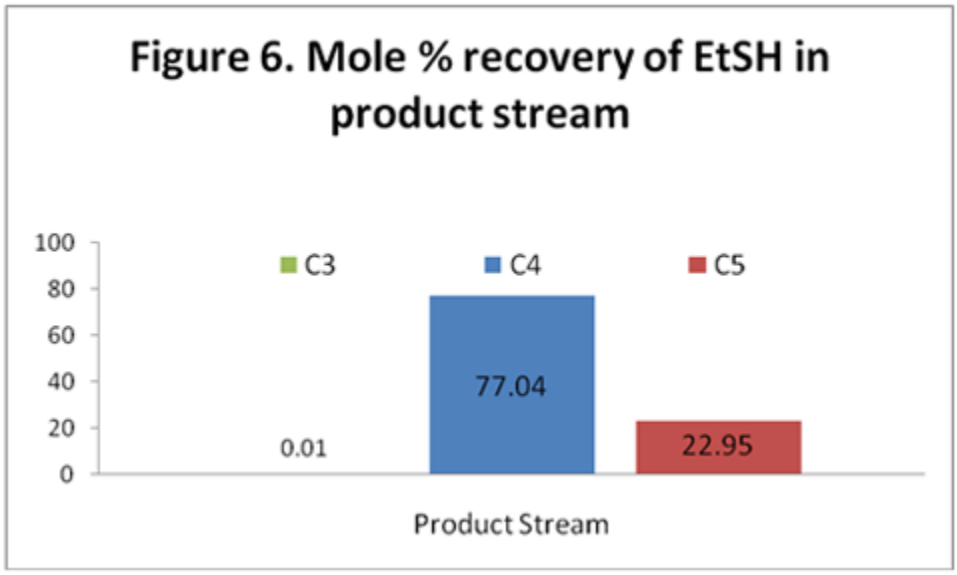

CS_2: Figure 7 shows the distribution and recovery of CS_2 in the C_4, and C_5 streams. Contrary to the pure CS_2 behavior (Figure 2), the majority of the CS_2 ends up in C_4 stream.

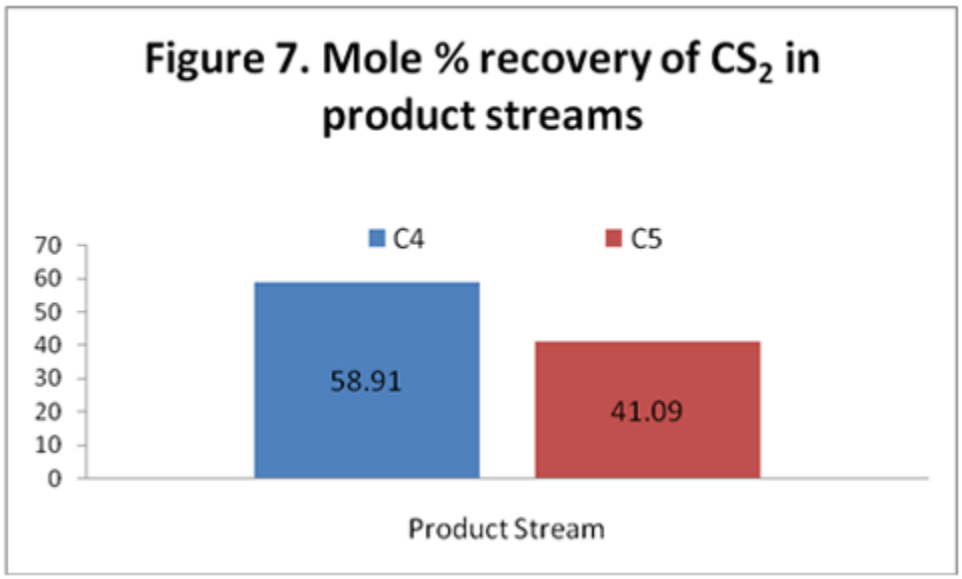

iC_3SH: Figure 8 shows the distribution and recovery of iC_3SH in the C_4, C_5 and C6+. As expected, iC_3SH ends up in C_5 and C6+ streams.

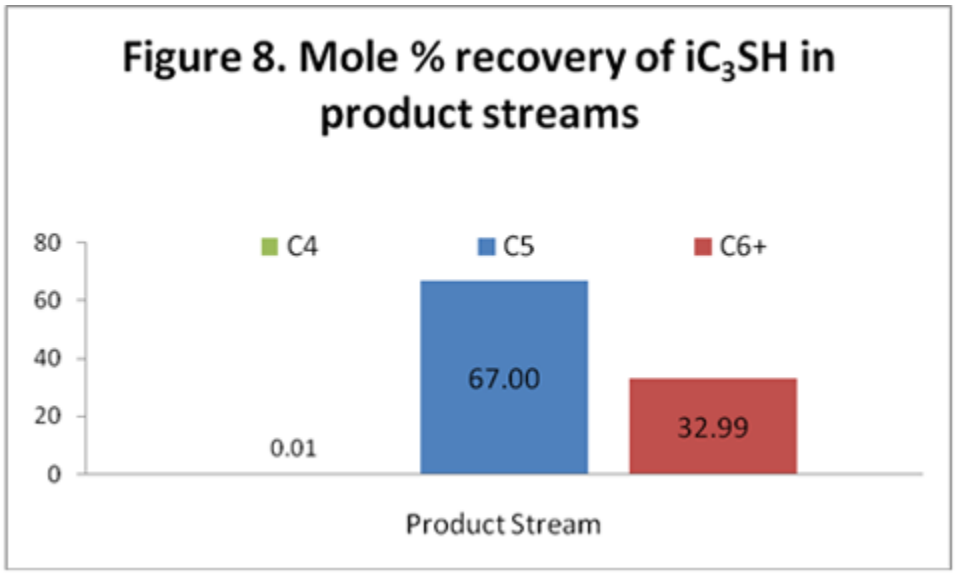

iC_4SH: Figure 9 shows recovery of iC_4SH in the C6+ stream. As expected, all of the iC_4SH ends up in the C6+ stream.

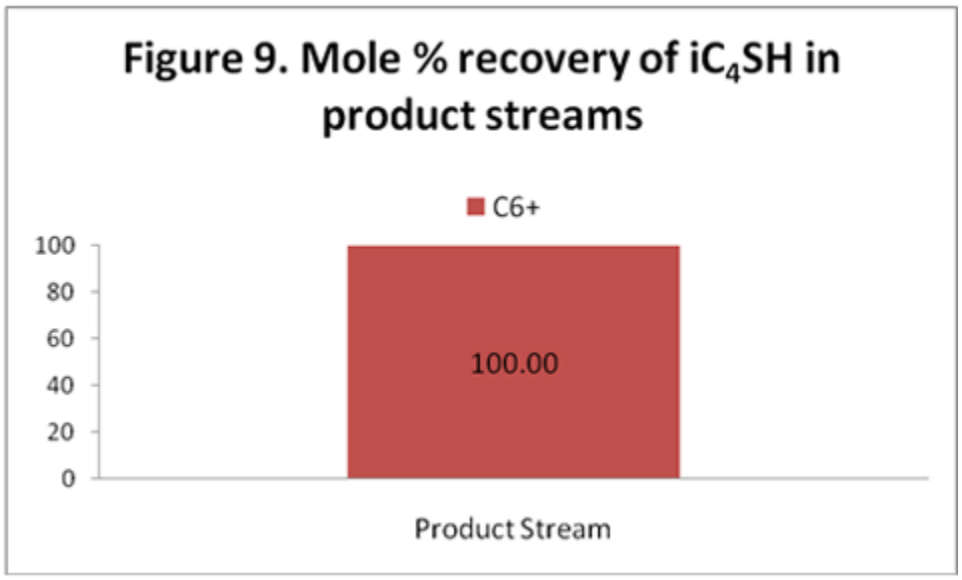

Conclusions:

The calculation results presented and discussed here are specific to the liquid fractionation plant studied here, but there are some general conclusions that can be drawn from this study.

The results indicate that the highest concentration of ethyl mercaptan (EtSH) and carbon disulfide (CS_2) are present in the C_4 product (stream 20) and C_5 Product (stream 23), respectively. The highest concentration of methyl mercaptan (MeSH) is present in the C_3 product (stream 15).

The binary interaction parameters used in the EOS play an important role in the VLE behavior of the system under study, and affect the distribution of the sulfur-containing compounds present in the feed. Use of improper or incorrect binary interaction parameters may generate erroneous results. Care must be taken to use correct values of binary interaction parameters. In this study, the HYSYS library values of the binary interaction parameters were used.

Some of the sulfur-containing compounds (i.e. MeSH, EtSH, and CS_2) were not distributed among the hydrocarbon products in the same the way one would expect from their volatilities and concentrations. This may be explained by the conclusion reported by Harryman and Smith who wrote “iC3SH is formed during fractionation within the depropanizer and the deethanizer”.

This should be a good reason to perform laboratory tests and detailed thermodynamic tray calculations to determine process flow rates and composition. Detailed process analysis should always be made to justify and prove correct decisions as to selection of process flow schemes.

REFERENCES

1. Maddox, R. N. and L. Lilly, “Gas Conditioning and Processing, Computer Applications for Production/Processing Facilities,” John M. Campbell and Company, Norman, Oklahoma, 1995.
2. Maddox, R. N. and D. J. Morgan, “Gas Conditioning and Processing, Gas Treating and Sulfur Recovery Vol. 4," John M. Campbell and Company, Norman, Oklahoma, 2006.
3. Harryman, J.M. and B. Smith, “Sulfur Compounds Distribution in NGL’s; Plant Test Data – GPA Section A Committee, Plant design,“ Proceedings 73rd GPA Annual Convention, New Orleans, Louisiana, March, 1994.
4. Harryman, J.M. and B. Smith, “Update on Sulfur Compounds Distribution in NGL’s; Plant Test Data – GPA Section A Committee, Plant design,“ Proceedings 75th GPA Annual Convention, Denver, Colorado, March, 1996.
5. Likins, W. and M. Hix, “Sulfur Distribution Prediction with Commercial Simulators,” the 46th Annual Laurance Reid Gas Conditioning Conference Norman, OK 3 - 6 March, 1996.
6. Al-Sayegh, A.R., Moshfeghian, M. Abbszadeh, M.R., Johannes, A. H. and R. N.
7. Maddox, “Computer simulation accurately determines volatile sulfur compounds,” Oil and Gas J., Oct 21, 2002.
8. ASPENone, Engineering Suite, HYSYS Version 7.0, Aspen Technology, Inc., Cambridge, Massachusetts U.S.A., 2009.
9. Peng, D.,Y. and D. B. Robinson, Ind. Eng. Chem. Fundam. 15, 59-64, 1976.

Pressure Relief System Design Pit-falls

by Kindra Snow-McGregor

In this tip of the month, we will discuss how miscalculations and incorrect analysis of potential process upsets can affect process safety. There are many aspects in facility design engineering and process safety engineering that should be considered when designing a new facility or debottlenecking an existing one. During these times of compressed schedules and budgets, it can become difficult to ensure all project deliverables receive the proper amount of checking and documentation. Mistakes in engineering design and operations of the following systems can result in serious safety incidents which must be avoided. Quality control, technical training, calculation checking and method verifications can aid in minimizing safety risks in these systems. This months' tip will focus on Pressure Relief Systems.

Pressure Relief Systems:

A primary process system in oil and gas facilities requiring careful attention is the Pressure Relief System. The most common components in upstream pressure relief systems are:

- Protected Equipment
- Emergency Shut Down Valves
- Depressurization Valves
- Pressure Safety Valves (PSV)
- Pressure Safety Valves Inlet and Discharge Piping
- Flare Header
- Flare Knock Out Drum
- Flare Stack / Tip

The primary purpose of the pressure relief system is to ensure that the operation's personnel and equipment are protected from overpressure conditions that happen during process upsets, power failures, and from external fires. In some locations and facilities, it is accepted practice to vent the pressure safety valves directly to atmosphere provided the process fluid is discharged at sufficient velocity to ensure good dispersion and that the fluids molecular weight is lighter than air. In this TOTM we will be discussing components in the pressure relief system in which detailed engineering calculations must be completed to select and install properly.

Pressure Safety Valves:

The purpose of a pressure safety valve is to protect equipment and / or piping from any possible overpressure scenario. There are multiple industry recommended practices and standards that govern the sizing, selection and installation of pressure safety valves. Many of these are referenced in this TOTM. A study that was conducted by Berwanger, et al. [1] determined that only 65% of upstream processing facility pressure safety valves meet the existing standards. Accurate pressure safety valve relieving requirements, scenario analysis and installation design is critical to ensure safety of the equipment and the operations staff during an upset condition. The American Institute of Chemical Engineering found that roughly 30% of process industry losses have been found to be partially attributed to deficient pressure relief systems [2]. If an upset process condition occurs with a system that has a pressure safety valve that is missing, undersized, or not properly installed, there is a potential that the equipment will not be protected and will mechanically fail. This could result in a significant loss of fluid containment and potential fatalities depending upon the fluids contained within the process.

On March 4, 1998, there was a major vessel failure at a Sonat Exploration facility in Pitkin Louisiana. The vessel failure and subsequent fire resulted in four deaths. A cause of the incident was failure of a low pressure vessel open to a high pressure gas source that was not provided with any pressure relief devices [3].

In determining the relevant relieving scenarios for a pressure relief valve, it is essential that the engineer doing the evaluation has a solid understanding of the process and the process control design within the facility. If the lead engineer is conducting an existing plant review or working on the design of a new facility, it is critical that they evaluate all potential relieving scenarios that may be required. If a scenario is missed, then there is a possibility that the system will not be protected if that missed scenario was the limiting case. ANSI / API Standard 521 ISO 23251, 5th Edition [5] specifies requirements and provides guidelines for examining the principal causes of overpressure; determining individual relieving rates; and selecting and designing disposal systems, including the details on specific components of the disposal system. Only with experience and training do engineers develop the competency level to complete these evaluations effectively. Participation in Process Safety Hazards Reviews and Analyses promote the development of an engineer's skills in identifying and resolving potential process hazards, and can help develop a junior engineer's skills and understanding of the evaluation of these systems.

API Recommended Practice 520, 7th Edition, Part 1 [4], and the International Organization for Standardization (ISO) Standards in the 4126 series (will not all be referenced here, and it should be noted that these only apply to systems designed and installed in the European Union Member States), addresses the methods to determine the pressure safety valve sizing requirements for the different relieving scenarios and provides guidance on how to select the proper relief valve type.

Both over-sizing and under-sizing a relief valve can result in mechanical failures, thus it is critical that the valve sizing and selection are correct.

If a facility is being debottlenecked and modified all pressure safety valves that will be affected by the modification must be checked for adequate capacity. Many facilities are not applicable to the U.S. Occupational Safety and Health Administration (OSHA) Process Safety Management (PSM) Standard 29 CFR 1910.119 [6].It is strongly recommended that a Management of Change (MOC) procedure be used to ensure that no facility modification will pose a safety risk or undermine the existing safety equipment provided within the facility. Pressure safety valves for all modified systems must be verified to safely handle the new required rates and compositions that result from debottlenecking the facility.

In addition, it is essential that operation's personnel are trained in the proper handling and testing of relief valves. There have been cases when operations and maintenance personnel have increased the set pressure on a pressure relief valve that was frequently relieving. The increase in set pressure results in the vessel operating above the stamped maximum allowable working pressure and may result in mechanical failure. Trained staff will understand that the solution to the problem is to correct the process condition that is resulting in the high pressure, not increase the set point on the pressure safety valve.

PSV Inlet and Discharge Piping

Another area that requires close attention is the proper design of the inlet and discharge piping of the pressure safety valves. API Recommended Practice 520, 5th Edition, Part 2 [7], and ANSI / API Standard 521 [5] provide guidance on the installation and design of the inlet and discharge piping for pressure safety valves.

For inlet piping to pressure safety valves, the recommended practice is to maintain the inlet hydraulic losses at no more than 3% of the set pressure of the pressure safety valve. This is because the relief valve is designed to normally close at 97% of the set pressure. A PSV with no inlet flow will sense the same pressure as exists in the protected equipment. Once open however, the pressure at the inlet to the relief will be the pressure at the protected equipment minus the friction loss in the inlet line. If this friction loss exceeds 3%, the valve will close and then reopen once the flow stops. This chattering can destroy the valve. Over sizing of a pressure safety valve can also result in "chatter" from essentially the same phenomenon. There is a potential for pressure relief valve or piping failure from prolonged "chattering" due to mechanical fatigue and potentially thermal fatigue.

If the inlet piping design cannot be configured to meet this requirement, then the use of a remote sensing pilot pressure safety valve can be used. This is not preferred due to the potential for the sensing line to plug or freeze.

Typically, relief valves are mounted almost directly on the equipment they protect. You will often find, however, that in existing plants this is not always the case. Some pressure safety valves may be located remotely with long inlet lines and the 3% criteria must be carefully checked. Even

with new plant designs, there are times when the piping designer must locate the pressure safety valve remotely. It is important to always check the inlet line losses by utilizing the piping isometric drawings.

A study conducted by Berwanger, et al [1], found that 16% of all pressure safety valve installations reviewed were out of compliance with accepted engineering practices and standards as a result of improper installations. 35.5 % of these valves were out of compliance due to excessive inlet pressure drop. Experience indicates that in many older plants, the pressure safety valve inlet and discharge piping is set at the inlet size and outlet size of the pressure safety valve and the pressure drop calculations were not performed – or were performed on incorrect assumptions for inlet pipe routing. A crude oil fire occurred in a Shell facility as a result of improper inlet piping design. This caused severe vibration and caused a 6" flange to fail, losing containment of the process stream [8].

For systems with 600# ratings and above, the valve manufacturer may supply a relief valve with an inlet flange rating of 600# and an outlet flange rating of 300#. Be aware that a "typical" 150# flange rating on the PSV discharge piping is not always acceptable for the higher pressure systems. The velocity at the outlet of the pressure safety valve can not exceed sonic. Thus, for high pressure systems the flow through the relief valve may require a pressure greater than the max pressure rating of a 150# system to maintain sonic flow. It is important to check the pressure required to maintain sonic based on the size of the pressure safety valve outlet. If a 300# flange is required then a 300# pipe fitting is installed to expand the pipe to a diameter where the pressure corresponding to a 150# system is not exceeded. For large systems, it is recommended to use a flare network software program to predict the backpressure at the outlet of each pressure safety valve for various relief scenarios. During a fire, several reliefs may open simultaneously and the backpressure must be known at the outlet of each relieving pressure safety valve under these circumstances.

The piping design for the inlet and discharge of pressure safety valves should be reviewed to determine that the piping can meet the mechanical and thermal stresses that will develop when the pressure safety valves relieve. Threaded connections for high set pressure safety valves or on pressure safety valves that are installed near vibrating equipment are not recommended. The threaded connections have a tendency to fail or become "unscrewed" from the vibrations, and / or forces during relieving.

Proper valve and discharge piping support design is essential. Piping and valve support becomes more critical on larger pressure safety valves and pressure safety valves that have high set pressures discharging to atmosphere. The reaction forces that can develop from the valves relieving to atmosphere can be significant. Even though the outlet piping may not be excessively long, the internal thrust created at the 90 degree elbow as the discharge piping turns up can be excessive. The flow will most likely be sonic velocity at the elbow and the discharge vent must be adequately supported to prevent failure. One incident occurred when the inlet piping on a 4X6 pressure safety valve set at 1350 psig failed. The valve became a projectile as a result. Fortunately, no one was hurt by flying debris and the gas line was isolated before the vapor cloud was ignited. This "near miss" was likely

the direct result of poor welding and poor support on the valve installation.

The reaction forces in closed systems tend to be less, but in some cases the reaction forces in a closed system can become significant if there are sudden large pipe expansions or during unsteady flow conditions within the piping. Inadequate design and supports for pressure safety valves and the associated piping can result in mechanical failure during a relieving event.

Flare Header Design

If the pressure safety valve discharges into a flare header the superimposed and built up back pressure is critical and can impact the valves relieving capacity if the actual back pressure is higher than the originally calculated or assumed back pressure. The maximum allowable back pressure at which a pressure safety valve can function properly depends upon the type of the pressure safety valve. A study conducted by Berwanger, et al [1], found that almost 24% of all PSV installations reviewed were out of compliance with accepted engineering practices and standards because of improper installations. 12 % of these valves were out of compliance due to the outlet pressure drop being too high. If the built up back pressure is greater than the maximum value the valve can function with, then the upstream pressure of the valve will increase above the set pressure of the valve as a result. This condition increases the likelihood of a failure.

A flare network software program should be used to calculate backpressure in large relief systems. For most pressure safety valves the maximum flow that can pass through the orifice size is larger than the required relieving flow. The maximum flow must be used to calculate the inlet line loss and the resulting backpressure. Modulating pilot valves can be used, if required, to control the maximum flow that is required to be relieved. In the design of the flare system, several types of valves are available, as explained in API 520 Part 1 [4]. Conventional, bellows, and pilot valves are typically used. The valve manufacturer must be consulted to define the maximum flow and backpressure requirements for each type of valve. The final flare design can not be completed until the actual pressure safety valves have been selected.

Depending upon the fluids which are being relieved and the pressures involved, it is possible to have relieving events that require stainless steel discharge piping, Flare Header, Flare KO Drum and Flare Stack because of cryogenic relieving temperatures from the Joule-Thompson Effect through the pressure safety valve. There have been multiple cases where carbon steel flare headers have failed due to the cryogenic relieving temperatures that developed during relieving events. The failure of a flare header completely undermines the purpose of the Pressure Relief System, and can result in a catastrophic event.

In today’s’ market, the recovery of NGL’s from natural gas is quite common. Particular attention is required in designing the relief systems for the cryogenic vessels. The pressure safety valves most likely will be relieving cold (at -20 F or below) two phase fluids. The pressure safety valve downstream piping will be exposed to very cold temperatures when the valves relieve. The recommended method for sizing two phase flow valves is by utilizing the DIERS equations. API 520

Part 1, Appendix D [4] summarizes these equations and provides an example calculation. The calculation procedure is long and tedious but it is recommended to perform a hand calculation before utilizing in house spreadsheets. The couple of hours spent performing the calculation will provide valuable insight to the key parameters used in the equations and will serve as a verification check of a spreadsheet.

There should be no dead legs in any piping from the discharge of the relief valve to the Flare KO Drum. Any pockets or dead legs can fill with liquids which may result in excess back pressure during relieving events There may also be large reaction forces in the flare header as a result of the slug of liquids forced down the header. In 1999, the flare header of a Tosco refinery in California was overpressured due liquid accumulation at a low point in the flare header. This resulted in a facility shutdown. There were no injuries reported [9].

Flare KO Drum and Flare Stack / Tip

Flare KO Drum and Flare Stack sizing is also critical to the safety of the plant. Oil and Gas Industry Flares are designed to destroy vapor streams only and require an adequately sized Flare KO Drum to prevent flammable liquids from raining out of the flare tip. In determining the sizing, it is important that a Flare Study be conducted to determine the worst case scenario for Flare KO Drum and Stack capacity and to select the proper droplet size separation criteria that the selected flare tip can adequately destroy. ANSI / API Standard 521[5] provides guidance on sizing, design and selection of this equipment.

A good example of the consequences of liquids flowing out of a Vent Stack was the Texas City Refinery explosion of 2005. This catastrophic incident resulted in a process upset where the amount of liquids that flowed to the KO Drum overwhelmed the drum size, and flowed up the vent stack and to the surrounding atmosphere which resulted in the tragic explosion [10]. If a Flare would have been installed in the Texas City Refinery rather than a Vent Stack, the consequences of the event would have been reduced. The vapor phase hydrocarbons that were originally flowing to the vent stack would have been destroyed in the Flare Tip, and the vapor cloud that exploded would have been prevented. Flowing liquid hydrocarbons to a Flare Tip is still a dangerous situation. If a Flare KO Drum were overwhelmed with hydrocarbon liquids the Flare Stack would likely be raining fire, and not liquid hydrocarbons.

Based on the stack sizing, ANSI / API Standard 521 [5] outlines procedures to estimate the radiation effect from the flare. With today's' specialized design of flare stacks, consultation with the flare manufacturer is recommended for the radiation confirmation.

Depressurization Valves

In the gas processing industry, it has become a standard practice to block in the treating facility with Emergency Shut Down (ESD) Valves rather than depressure the entire facility to the

flare. One primary reason for this philosophy is that natural gas fires are not equivalent to liquid hydrocarbon pool fires. Natural gas fire protection and mitigation requires different protection methods than for those used for fighting liquid hydrocarbon pool fires, which can be extinguished using a fire water system or a foam system. . It is standard natural gas industry practice to isolate the hydrocarbon gas sources to the facility and evacuate all personnel from the facility. Once the source of the gas is isolated, the feed to the fire is terminated and the fire is quickly extinguished from lack of fuel.

In the case where a facility must be depressurized in an upset condition, careful attention must be given to the design of the depressurization valves, their timing and flare capacity. There exists the potential to overwhelm the Flare Tip if the Tip was not designed for the high depressurization rates. In addition, consideration for required depressurization time, resulting Flare Header temperatures, and depressurization control schemes must be given close attention. These systems can be highly complex due to the transient nature of the process and require careful design procedures to ensure a safe Depressurization System.

.

REFERENCES

1. Non-Conformance of Existing Pressure Relief Systems with Recommended Practices, A Statistical Analysis, Patrick C. Berwanger, PE, Robert A Kreder, and Wai-Shan Lee. Berwanger, Inc., 2002.
2. AIChE. Emergency Relief System (ERS) Design Using DIERS Technology. American Institute of Chemical Engineers, New York, NY, 1995.
3. U.S. Chemical Safety and Hazard Investigation Board, Investigation Report, Catastrophic Vessel Overpressurization, Report No. 1998-002-I-LA.
4. Sizing, Selection, and Installation of Pressure-Relief Devices in Refineries, Part 1 – Sizing and Selection, API Recommended Practice 520, 7th Edition, January 2000.
5. ANSI / API Standard 521, / ISO 23251, Pressure Relieving and Depressuring Systems, 5th Edition, January 2007.
6. Occupational Safety and Health Standards, Process Safety Management of Highly Hazardous Chemicals, 29-CFR-OSHA-1910.119, 57 FR 23060, June 1, 1992; 61 FR 9227, March 7, 1996.
7. Sizing, Selection, and Installation of Pressure-Relief Devices in Refineries, Part 2 – Installation, API Recommended Practice 520, 5th Edition, August 2003.
8. Poor Relief Valve Piping Design Results in Crude Unit Fire, Politz, FC., API Mid-year Refining Meeting, 14 May 1985, Vol / Issue 64.
9. Contra Costa County, California, USA Contra Costa Health Services, Major Accidents at Chemical / Refinery Plants, Copyright © 2000–2009.
10. U.S. Chemical Safety and Hazard Investigation Board, Investigation Report, Refinery Explosion and Fire, REPORT NO. 2005-04-I-TX, March 2007.

Variation of Properties in the Dense Phase Region; Part 2 – Natural Gas

By Dr. Mahmood Moshfeghian

In the last tip of the month (TOTM) we described the dense phase of a pure compound and how it impacted processes. We illustrated how thermophysical properties change in the dense phase as well as in the neighboring phases. The application of dense phase in the oil and gas industry was discussed briefly. In this TOTM, we will discuss the dense phase behavior of multi-component systems, like natural gases.

When a natural gas, is compressed above the *cricondenbar* in the region between *critical temperature* and *cricondentherm*, it becomes a dense, highly compressible fluid that demonstrates properties of both liquid and gas. Figure 1 presents different regions of the phase envelope for a typical natural gas mixture with the composition shown in Table 1.

Table 1. Composition of the natural gas used in this study

Component	Mole %
Methane	80.00
Ethane	8.00
Propane	4.00
i-Butane	3.00
n-Butane	2.00
i-Pentane	1.00
n-Pentane	0.50
n-Hexane	0.50
n-Heptane	0.25
n-Octane	0.25
n-Nonane	0.25
n-Decane	0.25

For simplicity and convenience, we define the dense phase to be within *critical temperature* and *cricondentherm* if the pressure is above the *cricondenbar*. In practice, there is no clear line (i.e. *critical temperature*) dividing dense phase from liquid phase or other single line (i.e. *cricondentherm*) dividing the dense phase from the gas phase.

Both the left bound (*critical temperature*) and the right bound (*cricondentherm*) should be replaced by a transition region. There is a gradual transition from the gas phase to the dense phase and another gradual transition from the dense phase to the liquid phase. The dense phase is often referred to as a "dense fluid" to distinguish it from normal gas and liquid (see Figure 1). Dense phase is a fourth (Solid, Liquid, Gas, *Dense*) phase that cannot be described by the senses.

The word "fluid" refers to anything that will flow and applies equally well to gas and liquid. *The dense phase has a viscosity similar to that of a gas, but a density closer to that of a liquid*. Because of it's unique properties, dense phase has become attractive for transportation of natural gas.

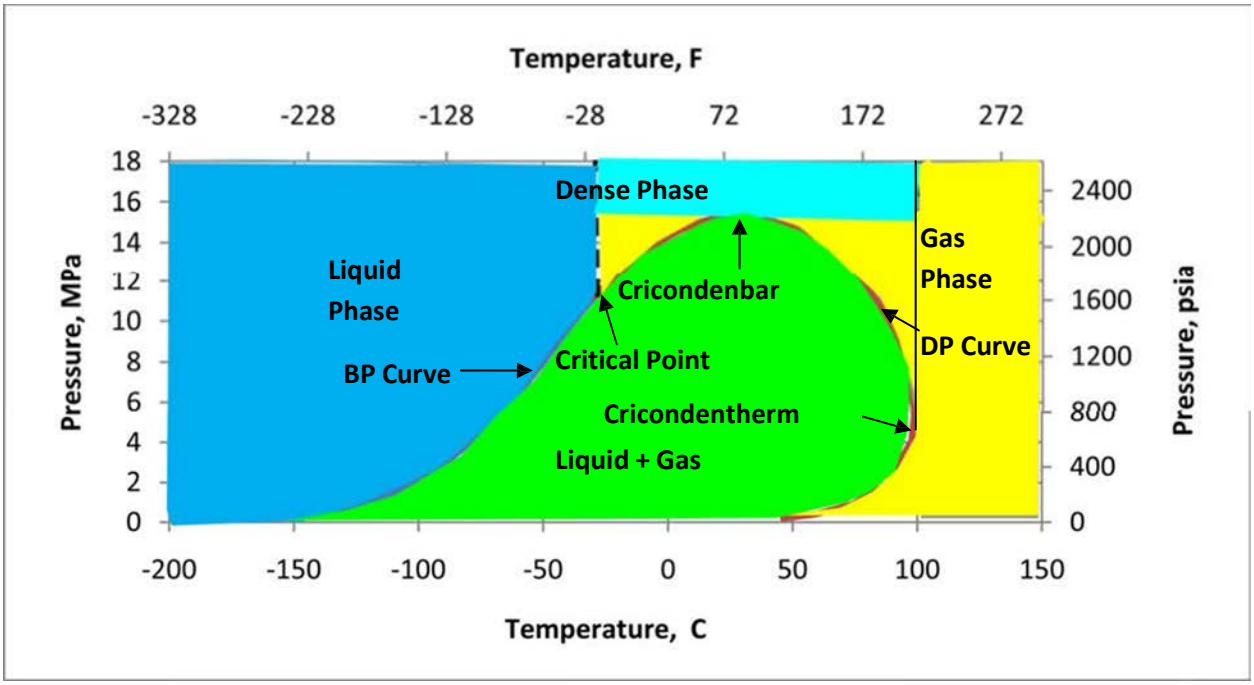

Figure 1. Identifying different phases for a typical natural gas

Pipelines have been built to transport natural gas in the dense phase region due to its higher density. This also provides an added benefit of no liquids formation in the pipeline, reducing pigging and pressure drop which results in lower OPEX. The higher density at higher pressure in the dense phase allows transporting more mass per unit volume, resulting in higher CAPEX. However, the OPEX reduction usually offsets the CAPEX increment. As shown in the following sections, the value of the dense phase viscosity is very similar to gas phase viscosity. The dense phase density is closer to the liquid phase density.

In the next section we will illustrate the variation of thermophysical properties in the dense phase and its neighboring phases. Natural gas properties have been calculated with HYSYS software for a series of temperatures and pressures. Table 2 presents, the pressures and temperatures and their paths used in this study.

The calculated thermophysical properties are plotted as a function of pressure and temperature in Figures 2 to 9. The thermophysical property is shown on the left- hand side y-axis, temperature on the x-axis and pressure on the right-hand side y-axis.

Table 2. Pressure-Temperature combination and the paths chosen for natural gas

Point	Location	Temperature		Pressure		Path
		°C	°F	MPa	Psia	
1	A (BP)	-50.2	-58.4	8.0	1160	A to B: Bubble point liquid to subcooled liquid
2	B	-100.0	-148	8.0	1160	B to C: Isothermal, subcooled liquid to compressed liquid
3		-100.0	-148	11.0	1595	
4		-100.0	-148	14.0	2030	
5		-100.0	-148	17.0	2466	
6	C	-50.0	-58	17.0	2466	C to D: Isobaric, compressed liquid to dense phase (Dense Fluid)
7		0.0	31	17.0	2466	
8		50.0	122	17.0	2466	
9		100	212	17.0	2466	
10		125	257	17.0	2466	
11		125	257	14.0	2030	
12	D	125	257	11.0	1595	D to E: Isothermal, dense phase (Dense fluid) to gas
13		125	257	8.0	1160	
14	E	100	212	8.0	1160	E to F: Isobaric, gas to dewpoint, two phase and bubble point liquid
15	(DP)	95.2	203.4	8.0	1160	
16		50	122	8.0	1160	
17		0.0	32	8.0	1160	
18	F	-50.0	-58	8.0	1160	

Critical Temperature = -29.45 °C = -21.0 °F and Critical Pressure = 11.23 MPa = 1628 Psia

Cricondentherm = 98.86 °C = 210 °F and cricondenbar = 15.35 MPa = 2225 Psia

Density:

Figure 2 presents the variation of density in different phases as a function of pressure and temperature. In the isobaric subcooling path of AB, liquid density increases sharply. However, in the isothermal compression of BC path, a small increase of density is observed. In the isobaric CD path, compressed liquid density decreases gradually as temperature is increased well into the dense phase region. However, as the temperature increases further in the dense phase, density reduction is accelerated. Reduction of density is further accelerated during isothermal expansion of DE. Isobaric cooling of gas along EF path corresponds with a sharp increase in density. It can be noted the values of dense phase density are close to the liquid phase density in some areas of the dense phase region, and is overall significantly higher than the gas phase densities.

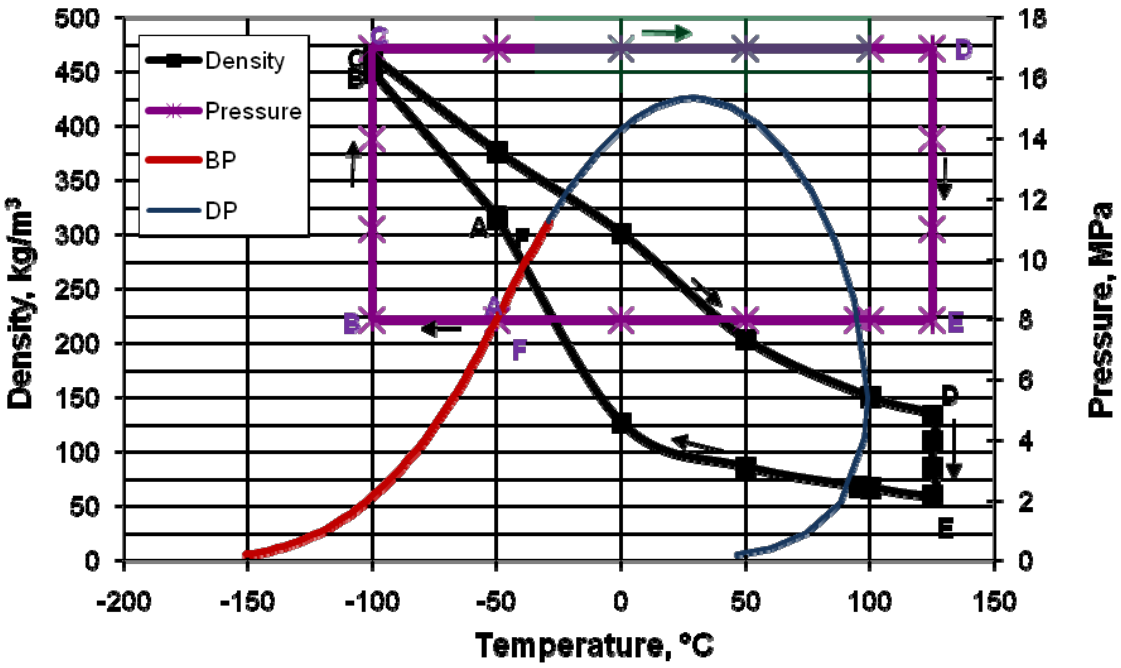

Figure 2. Density as a function of pressure and temperature

Viscosity:

Figure 3 presents the variation of viscosity in different phases as a function of pressure and temperature. In the isobaric subcooling path of AB, liquid viscosity increases sharply. However, in the isothermal compression of BC path, a very small change of viscosity is observed. In the isobaric CD path, compressed liquid viscosity decreases linearly and sharply as temperature is increased well into the dense phase region. As the temperature increases further in the dense phase, viscosity reduction becomes gradual and approaches the gas phase values. Reduction of viscosity is quite small during isothermal expansion of DE. Isobaric cooling of gas along EF path up to the dew point temperature corresponds with no appreciable change in viscosity but increases noticeably in the two phase region. For the sake of completing the graph, the two phase viscosity was estimated by: $\mu = \mu_{Saturated\ Vapor}(V/F) + \mu_{Saturated\ Liquid}(L/F)$ where (V/F) and (L/F) are vapor and liquid mole fractions, respectively.

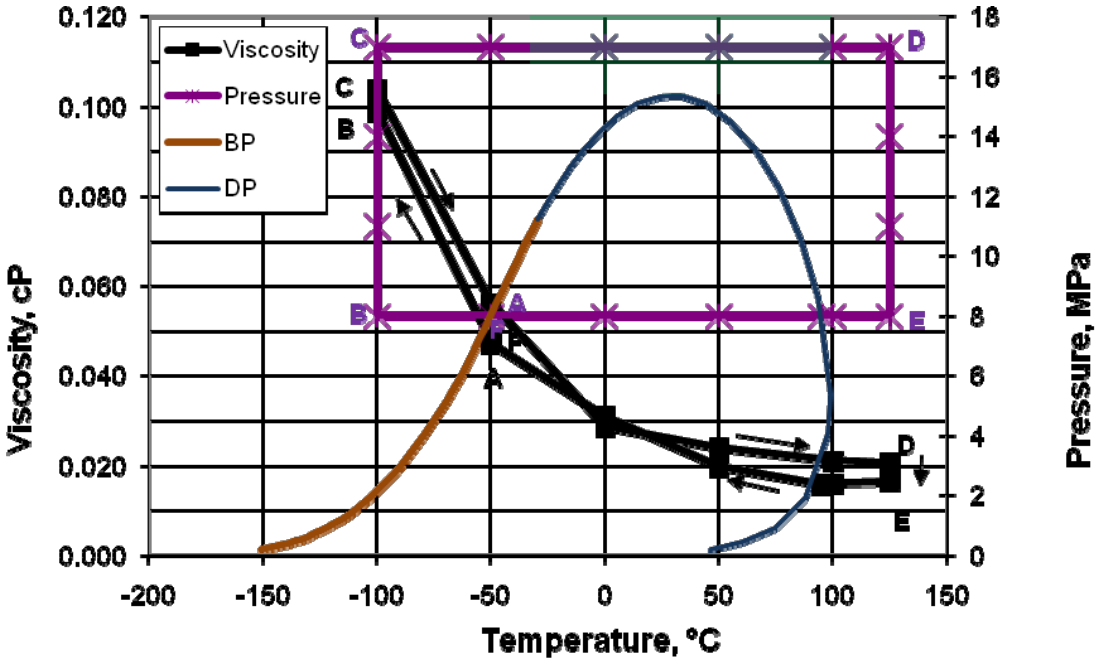

Figure 3. Viscosity as a function of presure and temperature

Compressibility Factor:

In general, the compressibility factor, Z, calculated by an equation of state is not accurate for the liquid phase. Therefore, Figure 4 which presents compressibility factor as a function of pressure and temperature should be considered for qualitative study only. In the isobaric subcooling path of AB, Z decreases. However, in the isothermal compression of BC path, Z increases drastically. In the isobaric CD path, Z remains almost constant in the compressed liquid region but increases gradually as temperature is increased well into the dense phase region. As the temperature increases further in the dense phase, the increase in Z is accelerated. The increase in Z is further accelerated during isothermal expansion of DE. Isobaric cooling of gas along EF path corresponds with a gradual decrease in Z. In the two-phase region, Z is not applicable and its value is not plotted.

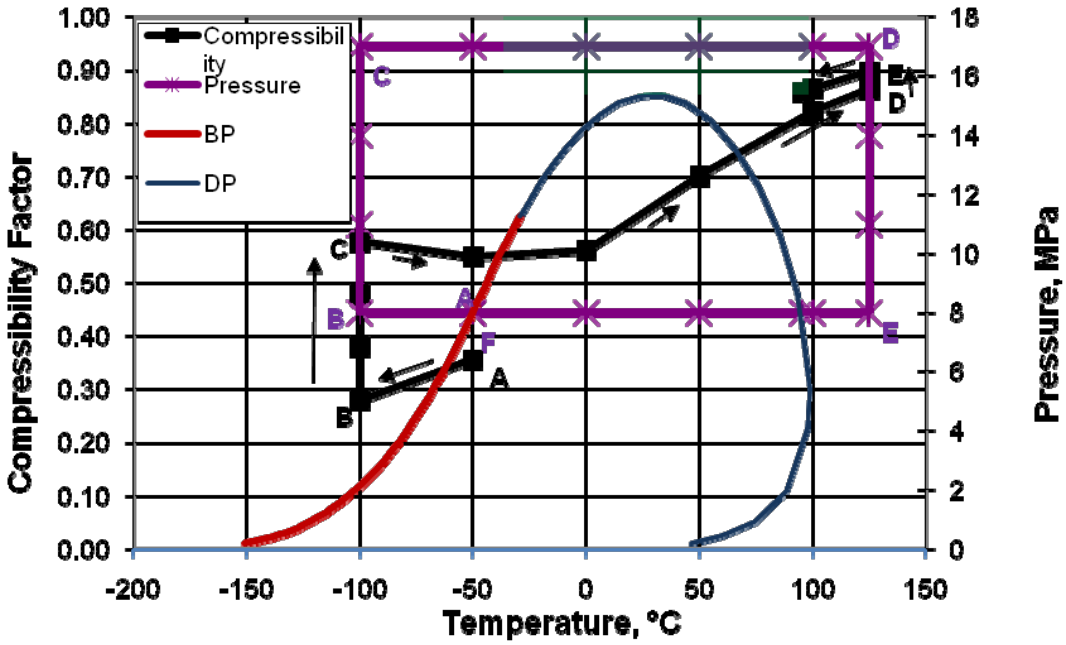

Figure 4. Compressibility factor as a function of pressure and temperature

Surface Tension:

Figure 5 shows that in the liquid phase, surface tension is a strong function of temperature but independent of pressure. In the gas phase, surface tension is not applicable and its value is zero. In the two-phase region, it reached a maximum value.

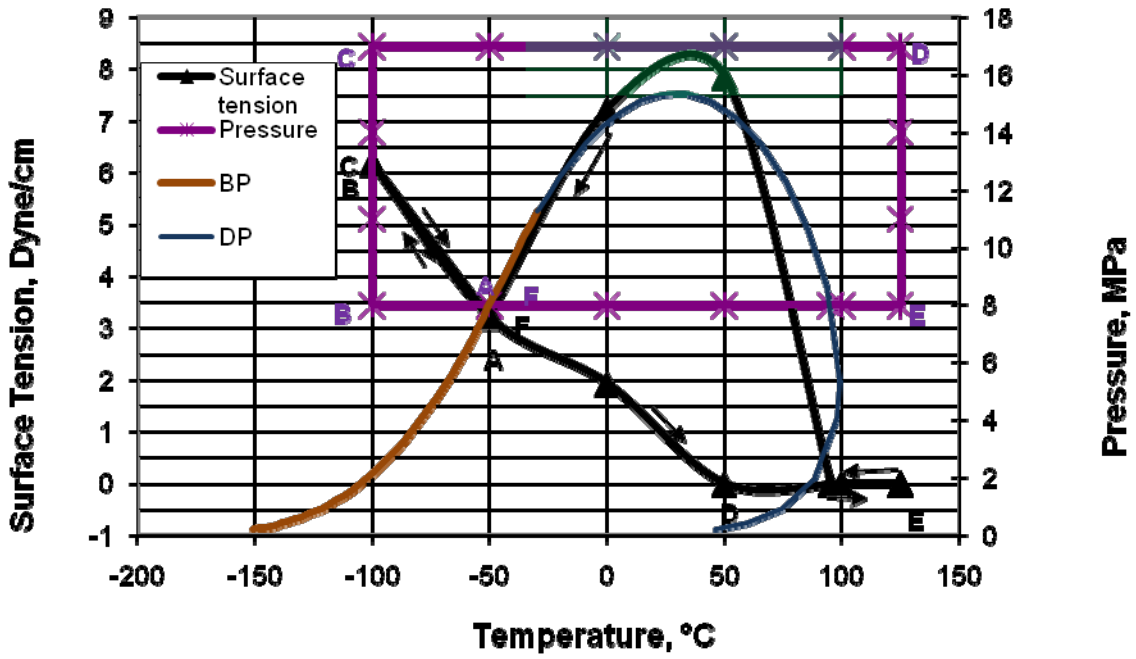

Figure 5. Surface tension as a function of pressure and temperature

Heat Capacity:

Generally, heat capacity is applicable in a single phase region and should not be used when there is a phase change. Figure 6 presents the variation of heat capacity in different phases as a function of pressure and temperature. In the isobaric subcooling path of AB, liquid heat capacity decreases. In the isothermal compression of BC path, a small increase of heat capacity is observed. In the isobaric CD path, compressed liquid heat capacity increases sharply as temperature is increased but starts to decrease in the dense phase region. As the temperature increases further in the dense phase, heat capacity decreases. This is strange behavior and surprisingly high values are

calculated. Similar results were obtained for pure methane in the previous TOTM. Increase of heat capacity is further noticed during isothermal expansion of DE. Isobaric cooling of gas along EF path corresponds with a gradual increase in heat capacity up to a maximum point and then starts to decrease in the two phase region.

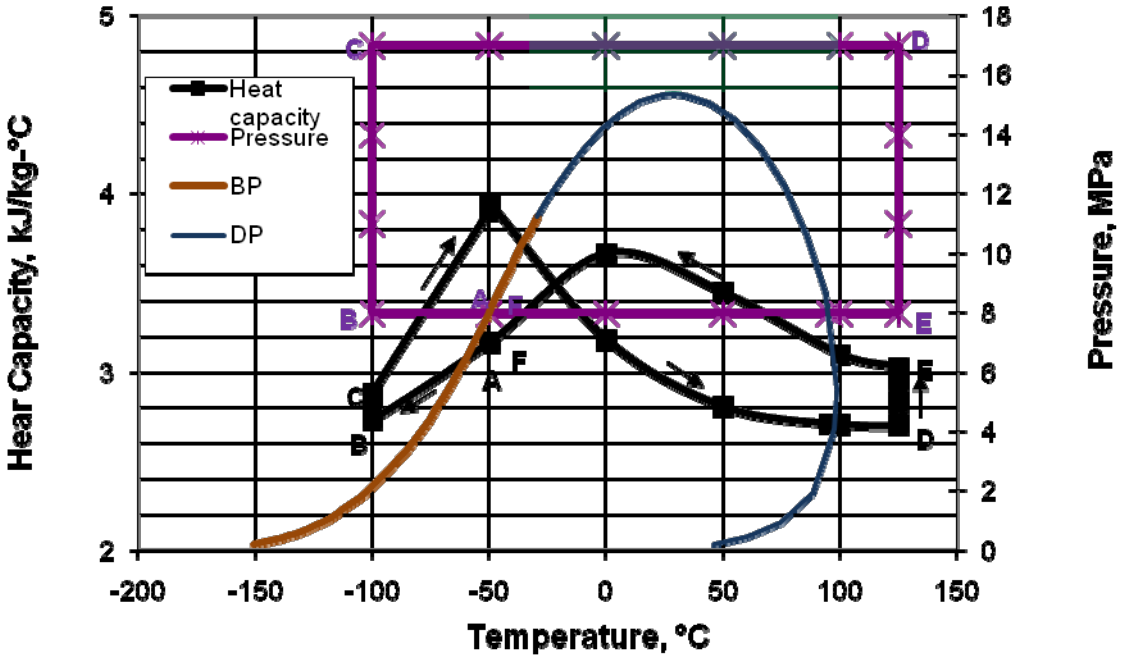

Figure 6. Heat capacity as a function of pressure and temperature

Thermal Conductivity:

Figure 7 presents the variation of thermal conductivity in different phases as a function of pressure and temperature. In the isobaric subcooling path of AB, liquid thermal conductivity increases sharply. In the isothermal compression of BC path, no change is observed. In the isobaric CD path, compressed liquid thermal conductivity decreases sharply as temperature is increased well into the dense phase region. However, as the temperature increases further in the dense phase, thermal conductivity reduction is gradual. Reduction of thermal conductivity is further noticed during isothermal expansion of DE. Isobaric cooling of gas along EF path corresponds with a small decrease in thermal conductivity and goes up in the two-phase region. The two phase thermal conductivity was calculated in the same manner as described in the viscosity section.

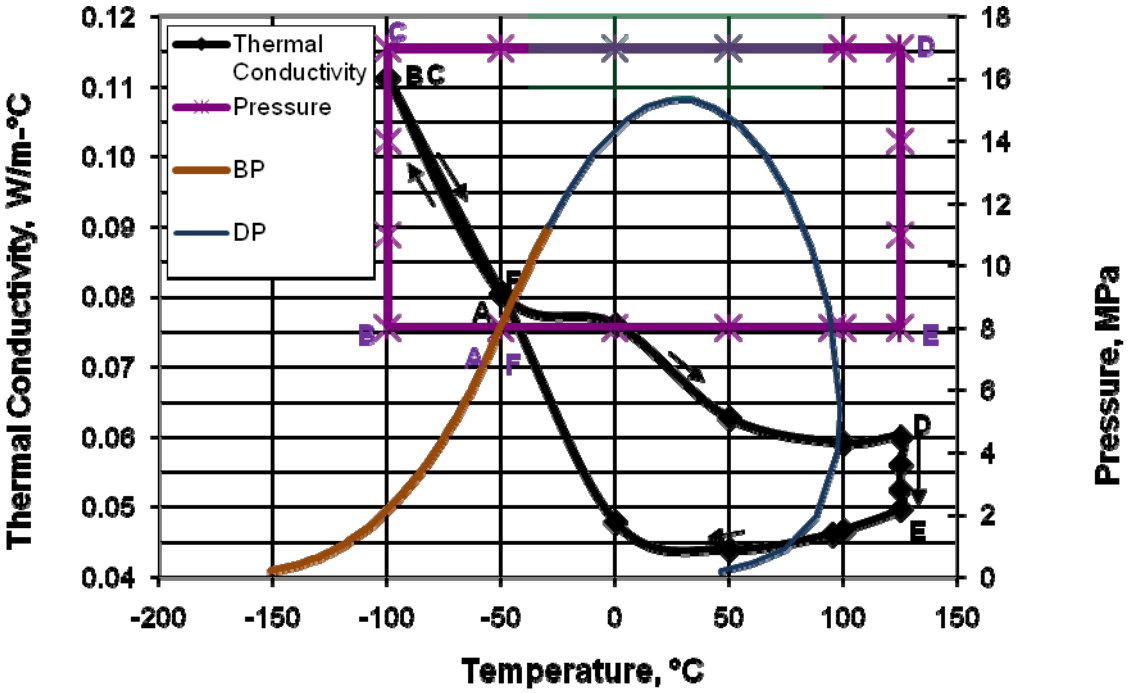

Figure 7. Thermal conductivity as a function of pressure and temperature

Enthalpy and Entropy:

Figures 8 and 9 present the variation of enthalpy and entropy in different phases as a function of pressure and temperature. As shown in these figures, their qualitative variations are similar. In the isobaric subcooling path of AB, liquid enthalpy and entropy decrease. In the isothermal compression of BC path, no change is observed. During the isobaric CD path, compressed liquid enthalpy and entropy values increase gradually as temperature is increased well into the dense phase region. The increase in enthalpy and entropy is further noticed during isothermal expansion of DE. Isobaric cooling of vapor along EF path corresponds with a decrease in enthalpy and entropy.

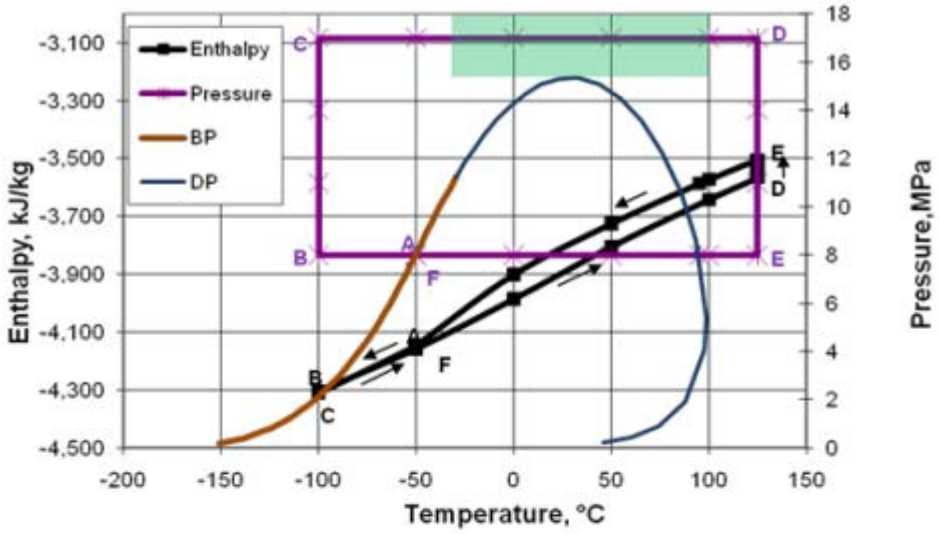

Figure 8. Enthalpy as a function of pressure and temperature

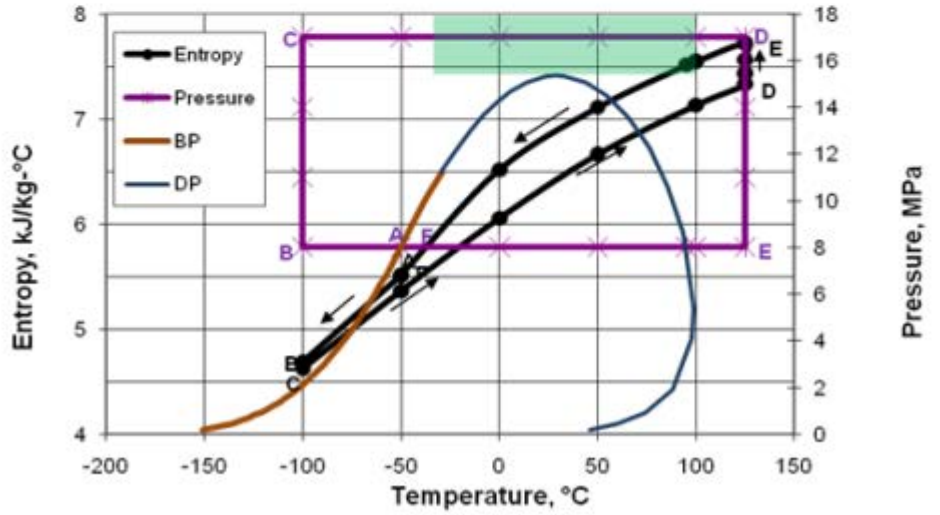

Figure 9. Entropy as a function of pressure and temperature

Conclusions:

Dense phase behavior is unique and has special features. The thermophysical properties in this phase may vary abnormally. Care should be taken when equations of state are used to predict thermophysical properties in dense phase. Evaluation of equations of state should be performed in advance to assure their accuracy in this region. Many simulators offer the option to use liquid-based algorithms (e.g. COSTALD) for this region. It is also recommended not to use heat capacity in the two-phase (gas- liquid) and in the dense phase. In these regions, enthalpy should be used for heat duty and energy balance calculations.

There is a gradual change of phase transition from gas-to-dense and dense-to- liquid phases or vice versa. Dense phase is a highly compressible fluid that demonstrates properties of both liquid and gas. The dense phase has a viscosity similar to that of a gas, but a density closer to that of a liquid. This is a favorable condition for transporting natural gas in dense phase.

REFERENCE

1. ASPENone, Engineering Suite, HYSYS Version 2006, Aspen Technology, Inc., Cambridge, Massachusetts U.S.A., 2006.

The Hybrid Hydrate Inhibition

By: Dr. Mahmood Moshfeghian

The best way to prevent hydrate formation (and corrosion) is to keep the pipelines, tubing and equipment **dry** of liquid water. There are occasions, right or wrong, when the decision is made to operate a line or process containing liquid water. If this decision is made, and the process temperature is below the hydrate point, inhibition of this water is necessary.

Many materials may be added to water to depress both the hydrate and freezing temperatures. For many practical reasons, a thermodynamic hydrate inhibitor (THI) such as an alcohol or one of the glycols is injected, usually methanol, diethylene glycol (DEG) or monoethylene glycol (MEG). All may be recovered and recirculated, but the economics of methanol recovery may not be favorable in many cases. Hydrate prevention with methanol and or glycols can be quite expensive because of the high effective dosage required (10% to 60% of the water phase). Large concentrations of solvents aggravate potential scale problems by lowering the solubility of scaling salts in water and precipitating most known scale inhibitors. The total injection rate of inhibitor required is the amount/concentration of inhibitor in the liquid water phase for the desired hydrate temperature suppression, plus the amount of inhibitor that will distribute in the vapor and liquid hydrocarbon phases. Any inhibitor in the vapor phase or liquid hydrocarbon
phase has little effect on hydrate formation conditions. Due to the accuracy limitations of the hydrate depression calculations and flow distribution in the process, it is recommended that the hydrate formation temperature with inhibition be chosen with a design factor below the coldest expected operating temperature of the system to ensure adequate inhibitor injection rates.

Determination of the amount and concentration of inhibitors and their distribution in different phases are very important for practical purposes and industrial applications. Therefore, to determine the required amount and concentration of these inhibitors, several thermodynamic models for hand and rigorous calculations have been developed and incorporated into computer software.

Low dosage inhibitors are relatively new and only recently reaching the “proven technology” stage in oil and gas processing. Although these systems move the hydrate formation line to the left, it is only temporary. In typical systems they will “delay” the formation of hydrates for about 12 hours.

Low Dosage Hydrate Inhibitors (LDHIs) are two class of chemicals: Kinetic inhibitors (KHIs) and Anti-Agglomerants (AAs). A KHI can prevent hydrate formation but cannot dissolve an already formed hydrate. Current KHIs have a difficult time overcoming a subcooling temperature (ΔT) threshold of 15 °C (27 °F). AAs allow hydrates to form and maintain a stable dispersion of hydrate crystals in the hydrocarbon liquid. AAs form stable water in oil micro-emulsion. AAs adsorb onto the hydrate crystal lattice and disrupt further crystal growth but must have a liquid hydrocarbon phase and the maximum water oil ratio is about 40-50%.

Laboratory studies and field experiences indicate hydrate-inhibition synergy is gained through the combination of two or more THIs [1] or THI and LDHI [2]. This is termed a hybrid hydrate inhibition (HHI).

In this TOTM we will demonstrate the synergy effect of mixed THIs like NaCl and MEG solution. In the next TOTM, we will discuss the results of a successful application of combined methanol and a KHI solution for a well producing natural gas, condensate and water in the Gulf of Mexico (GOM).

Combined THIs (MEG + NaCl or MEG + KCl)

The produced water from natural gas reservoirs contains an electrolyte solution such as NaCl, KCl, and $CaCl_2$. In order to estimate the hydrate formation temperature in the presence of mixed thermodynamic inhibitors, we propose to add up the depression temperature due to each individual inhibitor. The steps are summarized below:

1. Using a conventional method described in reference [3], estimate the hydrate formation temperature in the presence of pure water, T_o.
2. Using a method similar to Javanmardi *et al.* [1], estimate the hydrate depression temperature due to the presence of salt solution, salt ΔT.
3. Using a method similar to Hammerschmidt [4], estimate the hydrate depression temperature due to the presence of MEG solution, MEG ΔT.
4. Add up Salt ΔT and MEG ΔT, Total ΔT.
5. The hydrate formation temperature is calculated by subtracting total ΔT from T_o.

As an example, Table 1 presents the detail of calculation and the contribution of each inhibitor to the hydrate formation temperature for methane gas at different pressures and mixed inhibitor concentration. Comparison of the estimated hydrate formation temperature (last column of Table 1) with the experimental data (the fifth column) measured by Masoudi *et al.* [5] indicates a relatively good agreement. Figures 1 and 2 also present the contribution of each inhibitor to the hydrate formation temperature as described above for mixed solution of NaCl + MEG and KC l+ MEG, respectively.

Table 1. Contribution of different inhibitor to methane hydrate depression temperature

Salt	Salt Conc (Wt%)	MEG Conc (Wt%)	Exp P (kPa)	Exp T (°C)	Pure water T_o, °C	Salt HFT, °C	MEG HFT, °C	Salt ΔT, °C	MEG ΔT, °C	Total ΔT, °C	HFT, °C
NaCl	15.0	21.3	5068	-10.9	7.3	0.8	1.3	6.5	5.98	12.48	-5.2
NaCl	15.0	21.3	11431	-4.8	14.7	6.7	8.6	8	6.02	14.02	0.6
NaCl	15.0	21.3	27758	1.2	21.5	8.7	15.3	12.75	6.21	18.96	2.5
NaCl	15.0	21.3	46698	4.8	25.4	6.8	18.9	18.64	6.48	25.12	0.3
NaCl	12.0	30.8	6957	-10.8	10.31	5.01	2.02	5.3	8.29	13.59	-3.3
NaCl	12.0	30.8	13610	-5.8	16.06	9.45	7.8	6.61	8.26	14.87	1.2
NaCl	12.0	30.8	22946	-2.8	20.05	11.33	11.71	8.72	8.34	17.06	3.0
NaCl	12.0	30.8	46691	2.1	25.41	10.94	16.71	14.47	8.7	23.17	2.2
KCl	10.0	23.0	4164	-7.6	2.62	-0.26	-3.75	2.88	6.37	9.25	-6.6
KCl	10.0	23.0	10356	0.3	13.83	10.22	7.43	3.61	6.4	10.01	3.8
KCl	10.0	23.0	22760	6.0	19.99	14.71	13.47	5.28	6.52	11.8	8.2
KCl	10.0	23.0	44513	10.8	25.03	16.49	18.19	8.54	6.84	15.38	9.7
KCl	8.0	35.0	3930	-13.9	4.81	2.53	-4.89	2.28	9.7	11.98	-7.2
KCl	8.0	35.0	9935	-6.1	13.48	10.71	3.95	2.77	9.53	12.3	1.2
KCl	8.0	35.0	23442	-0.1	20.21	16.02	10.65	4.19	9.56	13.75	6.5
KCl	8.0	35.0	45050	4.5	25.13	18.4	15.24	6.73	9.89	16.62	8.5

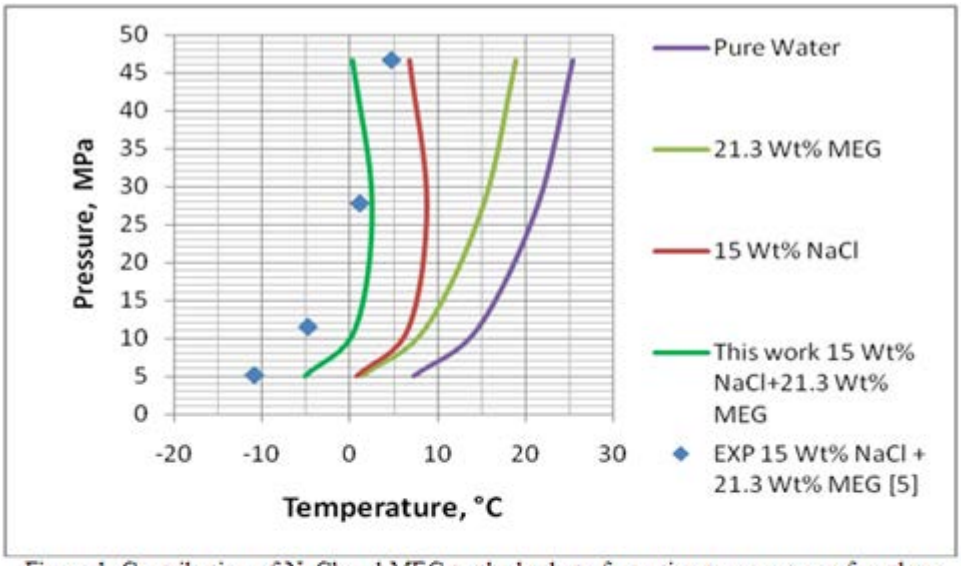

Figure 1. Contribution of NaCl and MEG to the hydrate formation temperature of methane

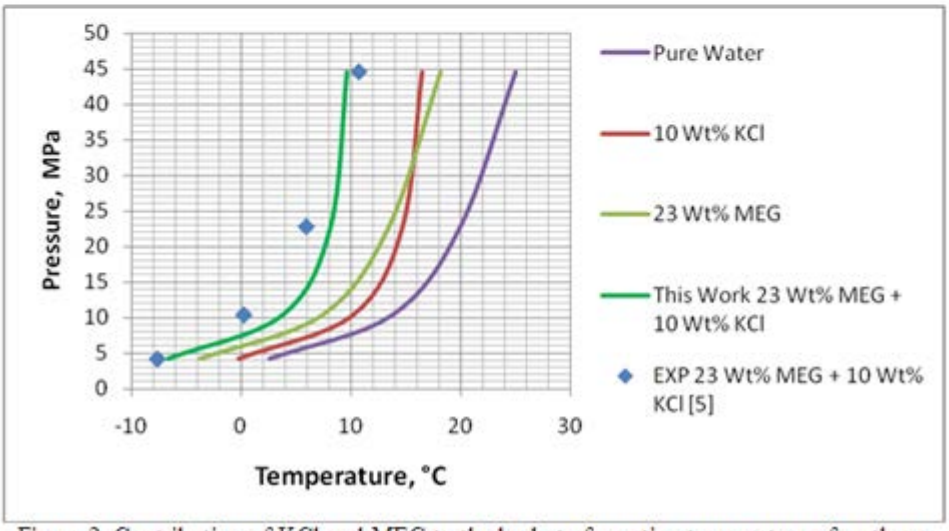

Figure 2. Contribution of KCl and MEG to the hydrate formation temperature of methane

Table 2 presents a comparison between the accuracy of the proposed method with Javanmardi *et al.* method against the experimental data for methane gas in the presence of mixed inhibitors. Table 2 also indicates an average absolute temperature difference of 4.7 and 3.5 °C for the proposed method and Javanmardi *et al.* method, respectively.

Table 2. Comparison between the accuracy of the proposed method with Javanmardi *et al.* method against the experimental data [5] for methane gas in the presence of mixed inhibitors

Salt	Salt Conc (Wt %)	MEG Conc (Wt%)	Exp P (kPa) Ref [5]	Exp T (°C) Ref [5]	This work T (°C)	This work ΔT (°C)	Javanmardi *et al.*, T (°C)	Javanmardi *et al.*, ΔT (°C)
NaCl	15	21.3	5068	-10.85	-5.2	5.65	-7.11	3.74
NaCl	15	21.3	11431	-4.75	0.6	5.35	-0.58	4.17
NaCl	15	21.3	27758	1.15	2.5	1.35	5.21	4.06
NaCl	15	21.3	46698	4.75	0.25	4.5	8.57	3.82
NaCl	12	30.8	6957	-10.75	-3.28	7.47	-5.96	4.79
NaCl	12	30.8	13610	-5.85	1.18	7.03	-1.12	4.73
NaCl	12	30.8	22946	-2.85	3	5.85	2.11	4.96
NaCl	12	30.8	46691	2.05	2.24	0.19	6.47	4.42
KCl	10	23	4164	-7.65	-6.63	1.02	-5.94	1.71
KCl	10	23	10356	0.25	3.82	3.57	1.73	1.48
KCl	10	23	22760	5.95	8.15	2.2	8.19	1.18
KCl	10	23	44513	10.75	9.65	1.1	11.5	0.75
KCl	8	35	3930	-13.85	-7.17	6.68	-9.07	4.78
KCl	8	35	9935	-6.15	1.18	7.33	-1.63	4.52
KCl	8	35	23442	-0.15	6.46	6.61	3.85	4
KCl	8	35	45050	4.45	8.51	4.06	7.81	3.36
Average Absolute Difference						4.7		3.5

In summary, a simple procedure is proposed for estimation of the hydrate formation temperature in the presence of mixed THIs such as MEG plus a salt solution. This procedure can be used for a mixture of glycol and electrolyte solutions. The procedure is relatively simple and its accuracy is good enough for facility calculations. For more accurate prediction of hydrate formation temperature in the presence of electrolytes, the readers should refer to the papers presented by Javanmardi *et al.* [1] and Masoudi *et al.* [5].

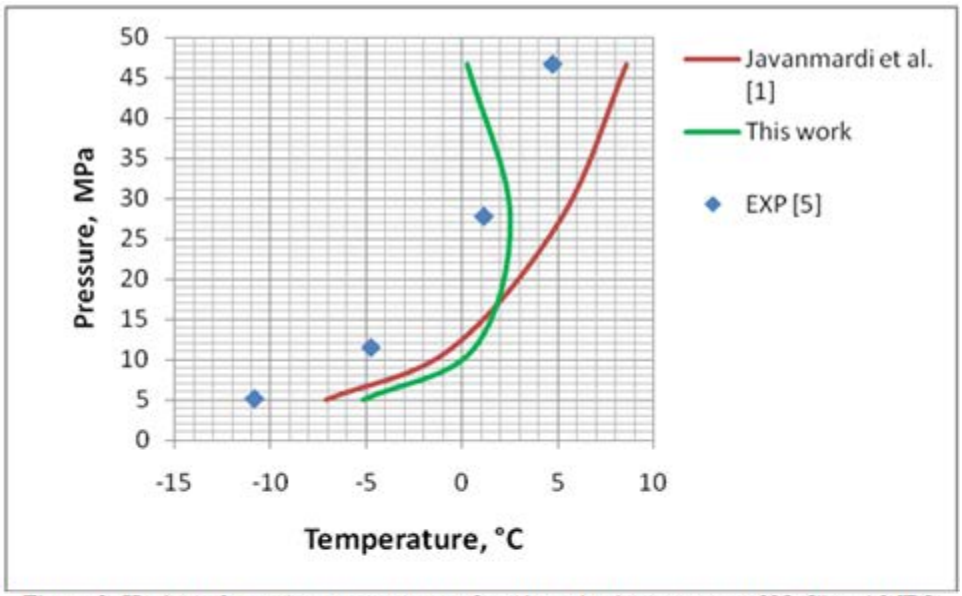

Figure 3. Hydrate formation temperature of methane in the presence of NaCl and MEG

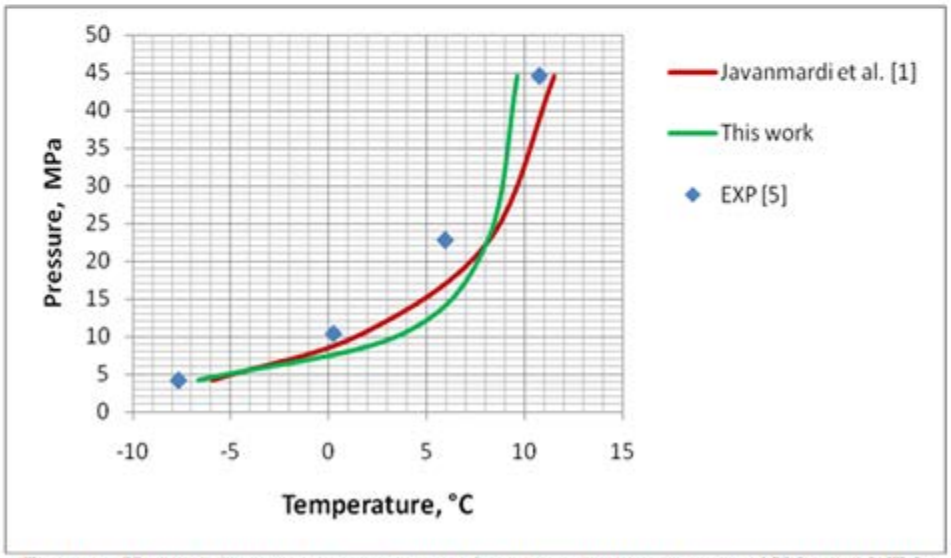

Figure 4. Hydrate formation temperature of methane in the presence of KCl and MEG

REFERENCES

1. Javanmardi, J., Moshfeghian, M. and R. N. Maddox, "An Accurate Model for Prediction of Gas Hydrate Formation Conditions in Mixture of Aqueous Electrolyte Solutions and Alcohol,"Canadian J. of Chemical Engineering, 79, 367-373, (2001).

2. Szymczak, S., Sanders, K., Pakulski, M., Higgins, T.; “Chemical Compromise: A Thermodynamic and Low-Dose Hydrate-Inhibitor Solution for Hydrate Control in the Gulf of Mexico,” SPE Projects, Facilities & Construction, (Dec 2006).
3. Campbell, J. M., "Gas Conditioning and Processing", Vol. 1, The Basic Principles, 8th Ed., Second Printing, J. M. Campbell and Company, Norman, Oklahoma, (2002).
4. Hammerschmidt, E. G. "Formation of Gas Hydrate in Natural Gas Transmission Lines", Ind. Eng. Chem., 26, 851-855, (1934).
6. Masoudi, R., Tohidi, B., Anderson, R., Burgass, R., and Yang, J. “Experimental Measurement and Thermodynamic Modelling of Clathrate Hydrate Equilibria and Salt Solubility in Aqueous Ethylene Glycol and Electrolyte Solutions,” Fluid Phase Equilibria, 219, 157-163 (2004).

The Hybrid Hydrate Inhibition-Part 2: Synergy Effect of Methanol and KHI

By: Dr. Mahmood Moshfeghian

Many materials may be added to water to depress the hydrate temperature. For many practical reasons, a thermodynamic hydrate inhibitor (THI) such as an alcohol or one of the glycols is injected, usually methanol, diethylene glycol (DEG) or monoethylene glycol (MEG). All may be recovered and recirculated, but the economics of methanol recovery may not be favorable in many cases. Hydrate prevention with methanol and or glycols can be quite expensive because of the high effective dosage required (10 to 60% of the water phase). Large concentrations of solvents can aggravate potential scale problems by lowering the solubility of scaling salts in water and precipitating most known scale inhibitors. The high rates of methanol create a logistical problem as well as a health, safety, and environmental (HS&E) concern because of the handling issues associated with methanol. The total injection rate of inhibitor required is the amount/concentration of inhibitor in the liquid water phase for the desired hydrate temperature suppression, plus the amount of inhibitor that will distribute in the vapor and liquid hydrocarbon phases. Any inhibitor in the vapor phase or liquid hydrocarbon phase has little effect on hydrate formation conditions. Due to the accuracy limitations of the hydrate depression calculations and flow distribution in the process, it is recommended that the hydrate formation temperature with inhibition be chosen with a design factor below the coldest expected operating temperature of the system to ensure adequate inhibitor injection rates.

Low dosage hydrate inhibitors (LDHIs) are relatively new and only recently reaching the "proven technology" stage in oil and gas processing. Although LDHIs move the hydrate formation line to the left, it is only temporary. In typical systems they will "delay" the formation of hydrates for about 12 hours. The LDHIs are two classes of chemicals: Kinetic inhibitors (KHIs) and Anti-Agglomerants (AAs). A KHI can prevent hydrate formation but contrary to methanol cannot dissolve an already formed hydrate. Current KHIs have a difficult time overcoming a subcooling temperature (ΔT) threshold of about 15 °C (27 °F). AAs allow hydrates to form and maintain a stable dispersion of hydrate crystals in the hydrocarbon liquid. AAs form stable water in oil micro-emulsion. AAs adsorb onto the hydrate crystal lattice and disrupt further crystal growth but must have a liquid hydrocarbon phase present and the maximum water to oil ratio is about 40-50%.

Laboratory studies and field experiences indicate hydrate-inhibition synergy is gained through the combination of a THI and LDHI [1]. This is termed a hybrid hydrate inhibition (HHI). In the June 2010 tip of the month (TOTM) we demonstrated the synergy effect of mixed THIs like NaCl and MEG solution and presented a shortcut method to estimate the synergy effect of brine and MEG solution. In this TOTM, we will discuss the results of a successful application of combined methanol and a KHI solution for a well producing natural gas, condensate and water in the Gulf of Mexico (GOM). The following sections are based on the paper presented by Szymczak *et al.* [1].

As mentioned earlier, THIs are used in concentration ranging from 10 to 60 weight percent in water and LDHIs are used in concentration normally less than 5 weight percent. Proper combination of THI and LDHI will result in lower injection rates of the combined inhibitor mixture while controlling hydrate formation. In addition, the combined inhibitor mixture provides the ability to dissociate any hydrates that may form. Table 2 extracted from reference [1] presents the cost comparison between LDHI and methanol for various related activities. As can be seen in this table the cost of HHI for most activities is low and medium for unit cost and volume usage.

Table 1- Cost comparison of LDHI, Methanol and HHI for an offshore application [1]

Cost Factor	LDHI	Methanol	HHI
Unit Cost	Very High	Low	Medium
Transportation	Low	High	Low
Pump	High	High	Low
Storage	Low	High	Low
Crane Lifts	Low	High	Low
Corrosion	Low	High	Low
Volume	Low	High	Medium

Field Study:

To demonstrate the synergy effect of THI plus LDHI (HHI) and to illustrate the advantage of using HHI, we will discuss the results of a field study in the GOM reported by Szymczak *et al.* [1]. The well production flows 5.6 km (3½ miles) through 114 mm (4½-in) flowline to a production platform where natural gas, condensate and water are separated. There was a seven- line umbilical bundle that included a 9.5 mm (3/8-in) outside diameter line for methanol and/or LDHI injection. The hydrate-inhibitor injection point was at the tree. The recent gas composition is presented in Table 2 while detailed system information is shown in Table 3.

Table 2- Field Gas Composition [1]

Component	Mole %
Nitrogen	0.2045
Carbon Dioxide	0.5893
Methane	95.7432
Ethane	0.4462
Propane	0.3431
i-Butane	0.1508
n-Butane	0.1823
i-Pentane	0.1262
n-Pentane	0.1088
Hexane	0.1663
C_{7+}	1.9392

To inhibit hydrate formation, a sufficient rate of methanol was injected to assure hydrate-free operation. Knowing the rate of water production, methanol was injected at approximately 0.019 m^3/h (5 gal/hr). The injection rates were monitored and adjusted by comparing the chemical feed-line pressure at the wellhead and the flowline pressure measured at the platform.

Monitoring pressure drop between the inlet and outlet of pipelines is an industry-wide standard method of flow assessment. Fluctuating pressure drop values provide the operator with instant information concerning flow irregularities or obstructions. Only formed and dislodged hydrates manifest as rapid pressure fluctuations, whereas flow regime change or wax and scale build up result in gradual pressure changes. The GOM facilities operating experience showed that with only

methanol in the system, the pressure difference between the wellhead and the flowline at the platform changed rapidly. The differential pressure changed as much as 345 kPa (50 psi) daily and was always between 1034 and 1724 kPa (150 and 250 psi) [1].

Table 3- Flowline Data [1]

Terrain	Flat
Gas Flow Rate	0.5663 x10^6 std m^3/d (20 MMSCF/D)
Line Length	5.6 km (3.5 miles)
Line Diameter	114 mm (4.5 in)
Water Flow Rate	0.023 m^3/d (6 gal/day)
Condensate	Traces
High Pressure	35, 853 kPa (5,200 psi)
Low Pressure	7,584 kPa (1,100 psi)
Average Pressure	27,579 kPa (4,000 psi)
Flow Speed	3.66 to 6.096 m/s (12 to 20 ft/sec)
Practical Methanol Rate	0.019 m^3/h (5 gal/hr)
Sea Temperature	5 °C (41 °F)
Outlet Temperature	12.8 °C (55 °F)

Table 4 presents a summary of Szymczak *et al.* [1] calculation results for the worst case-scenario methanol injection rate. The relatively large dosage of methanol required was the result of a combination of temperature and gas volume conditions in the pipeline resulting in most of the injected methanol going into the vapor phase of the system at equilibrium conditions. For the detail of calculations, refer to Chapter 6, Volume 1, Gas Conditioning and Processing [2]. For methanol concentration below 25 weight percent, the Hammerschmidt [3] equation may be used. The practical 0.019 m^3/h (5 gal/hr) rate of methanol applied resulted in borderline operating conditions between obstructed flow and line plugging. Szymczak *et al.* stated that the short fluid residence time in the flowline prevented the formation of a complete hydrate plug. Note that the high values of subcooling temperature eliminated KHI as the sole hydrate-prevention method. Known KHIs become ineffective inhibitors at approximately $\Delta T>15$ °C ($\Delta T>27$ °F) [1].

HHI Results

Szymczak *et al.* [1] reported that the inhibitor usage was reduced dramatically from 0.019 m^3/h (5 gal/hr) of methanol to 0.0028 m^3/h (0.75 gal/hr) of HHI and the pressure drop showed a lowering trend. They optimized the HHI dosage at approximately 0.0025 m^3/h (0.67 gal/hr), a HHI rate sufficient to protect the flowline from producing hydrates in any case of rate or pressure/temperature fluctuation. This HHI rate represented an 80% reduction compared to the methanol injection rate. As a result of the injection rate reduction, the costs of transportation, pump maintenance, storage on the platform, corrosion inhibition of the flowline, labor and safety costs related to crane lifts, and pressure drop were reduced. For further detail on this field study, refer to Szymczak *et al.* paper [1].

Table 4- The worst case-scenario theoretical methanol injection rate requirement

Flowline Pressure Option	**35, 853 kPa (5,200 psi)**	**27,579 kPa (4000 psi)**
Hydrate depression (Subcooling)	23 °C (41.4 °F)	20 °C (36 °F)
Weight % methanol in water phase	23	20
Injection rate	0.045 m^3/h (12 gal/hr)	0.035 m^3/h (9.2 gal/hr)

In summary, HHI provides both thermodynamic and LDHI inhibition. From a cost standpoint, the HHI is cost-efficient compared to THIs. Additionally, the HHI can reduce corrosion and may eliminate the need for corrosion inhibitor. From an offshore operational standpoint, the HHI significantly reduces logistical costs related to shipping, storage, handling, and chemical pumping. In addition to cost reduction, the problems related to health, safety, and environment (HS&E) would reduce too.

REFERENCE

1. Szymczak, S., Sanders, K., Pakulski, M., Higgins, T.; "Chemical Compromise: A Thermodynamic and Low-Dose Hydrate-Inhibitor Solution for Hydrate Control in the Gulf of Mexico," SPE Projects, Facilities & Construction, (Dec 2006).
2. Campbell, J. M., "Gas Conditioning and Processing", Vol. 1, The Basic Principles, 8th Ed., Second Printing, J. M. Campbell and Company, Norman, Oklahoma, (2002).
3. Hammerschmidt, E. G. "Formation of Gas Hydrate in Natural Gas Transmission Lines", Ind. Eng. Chem., 26, 851-855, (1934).

Variation of Natural Gas Heat Capacity with Temperature, Pressure, and Relative Density

By: Dr. Mahmood Moshfeghian

The change in enthalpy for a fluid where no phase change occurs between Points (1) and (2) can be expressed as:

$$\Delta h = \int_{T_1}^{T_2} C_P dT + \int_{P_1}^{P_2} \left[V - T\left(\frac{\partial V}{\partial T}\right)_P \right] dP \qquad (1)$$

The second term on the right hand side of this equation is generally not convenient to solve manually. However, it is trivial or zero for the following cases: (1) ideal gases, (2) constant pressure, $dP = 0$, and (3) for a liquid considered incompressible. For all three cases enthalpy is a mathematical function only of temperature. *Cp* is commonly expressed by equations of the form:

$$C_P = A + BT + CT^2 \qquad (2)$$

Where A, B, and C are constants that depend on system composition and T is the absolute temperature. In most instances it is sufficiently accurate to find a *Cp* at the average temperature T_{Avg}, where:

$$T_{Avg} = (T_1 + T_2)/2 \qquad (3)$$

C_{PAvg} is then found at this average temperature and

$$\Delta h = \int_{T_1}^{T_2} C_P dT = C_{PAvg}(T_2 - T_1) \qquad (4)$$

This approximate solution to the first integral, although not exact, is satisfactory for most applications. Heat capacity values for pure substances are readily available from many handbooks and similar reference material. As noted in Chapter 7 of Volume 1, Gas Conditioning and Processing [1], values of heat capacity can be found from the slope of h vs. T plots at a given pressure. The C_P for hydrocarbon liquid mixtures may be estimated from the equations presented in Volume 1 [1].

For a non-ideal, compressible fluid like natural gas, the second term on the right hand side of Eq.(1) can't be ignored. Therefore, in process simulation software, an equation of state like Soave-Redlich-Kwong (SRK) [2] or Peng-Robinson (PR) [3] is used to calculate Δh. For many calculations involving the heat capacity of natural gas, Figure 8.3 in Volume 1 is appropriate. Heat capacity at system pressure and average temperature is read off the graph and multiplied by gas mass flow rate and ΔT to obtain the heat load Q.

$$Q = (m)(C_{PAvg})(T_2 - T_1) \qquad (5)$$

In this Tip of The Month (TOTM), the variation of heat capacity of natural gases with temperature, pressure, and relative density (composition) will be demonstrated. Then an empirical correlation will be presented to account for these variations. This correlation will be used to estimate natural gas heat capacity for wide ranges of pressure, temperature, and relative density. Finally, the accuracy of the proposed correlation will be discussed.

Development of a Generalized C_P Correlation:

As mentioned earlier, C_P can be defined from the slope of h vs. T plots at constant pressure. Mathematically, this is expressed by:

$$C_P = \left(\frac{\partial h}{\partial T}\right)_P \qquad (6)$$

The derivative on the right hand side of Eq (6) may be obtained from an equation of state (EOS) but it is too tedious for hand calculations. Therefore, the PR EOS option in ProMax [4] was used to generate C_P values for various values of pressure, temperature, and relative density. The total number of C_P values calculated was 715. Table 1 presents the composition of five different natural gas mixtures used in this study.

Table 1. Gas compositions used for generating C_P values

Component	Natural Gas Mixtures, (Mole %)				
	A	B	C	D	E
CH_4	94.4	88.9	83.2	78.0	74.9
C_2H_6	2.6	5.2	8.8	10.5	10.1
C_3H_8	2.0	3.7	4.2	6.5	7.2
iC_4H_{10}	0.5	0.7	1.1	1.5	2.4
nC_4H_{10}	0.5	0.7	1.1	1.5	2.4
iC_5H_{12}	0.0	0.4	0.8	1.0	1.5
nC_5H_{12}	0.0	0.4	0.8	1.0	1.5
MW	17.389	18.827	20.279	21.724	23.183
SG	0.60	0.65	0.70	0.75	0.80

Figures 1 through 5 present variations of C_P with pressure, temperature and gas relative density. The red highlighted regions in Figures 3, 4, and 5 identify the two phase region of gas and liquid where the C_P concept is not valid. It should be noted that the isobar of 20 MPa represents a single phase even at low temperatures. However, at low temperature, the fluid is dense phase.

In order to correlate all the curves shown in Figures 1-5 by a single equation, the following expression is proposed.

$$C_p = \left[ab^T T^c + de^P P^f \right] \left(\frac{SG}{0.60} \right)^{0.025} \qquad (7)$$

Where T is temperature, P is pressure and C_P is heat capacity. A non-linear regression algorithm was used to determine the optimum values of parameters "a" through "f". First, C_P values of each gas in Table 1 were used to determine "a" through "f". Then all of the generated C_P values were used to determine a set of generalized parameters. These parameters were tuned and rounded to best represent all five gases covering a wide range of relative density from 0.60 to 0.80. For each case, the parameters and the summary of statistical error analysis are presented in Table 2. Note that the C_P values of the two phase region were not used for the regression process. The general range of this correlation is from 20 to 200 °C (68 to 392 °F) and from 0.10 to 20 MPa (14.5 to 2900 Psia).

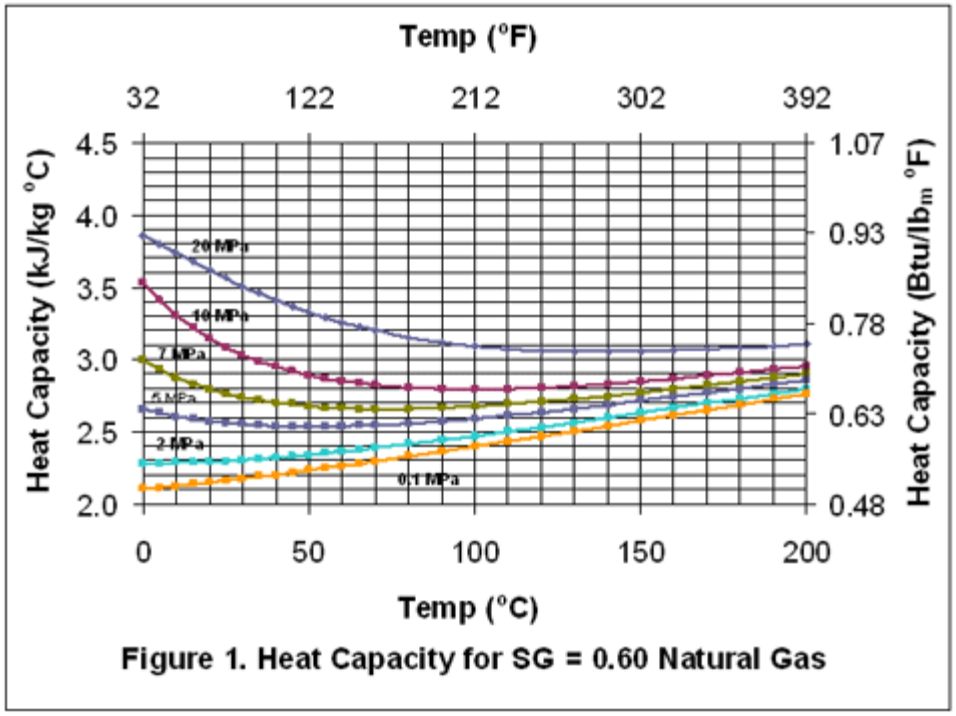

Figure 1. Heat Capacity for SG = 0.60 Natural Gas

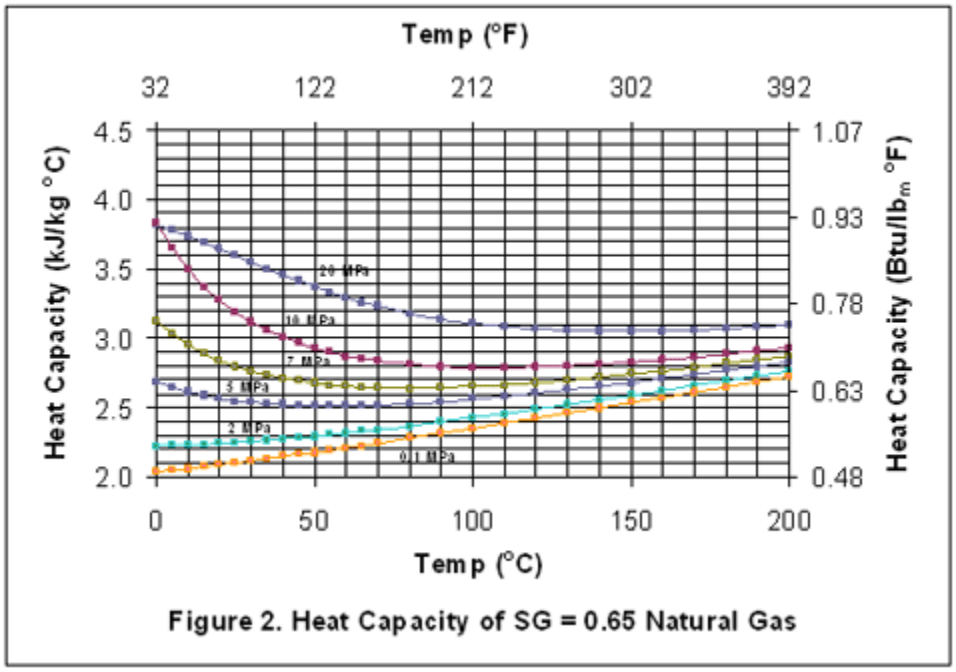

Figure 2. Heat Capacity of SG = 0.65 Natural Gas

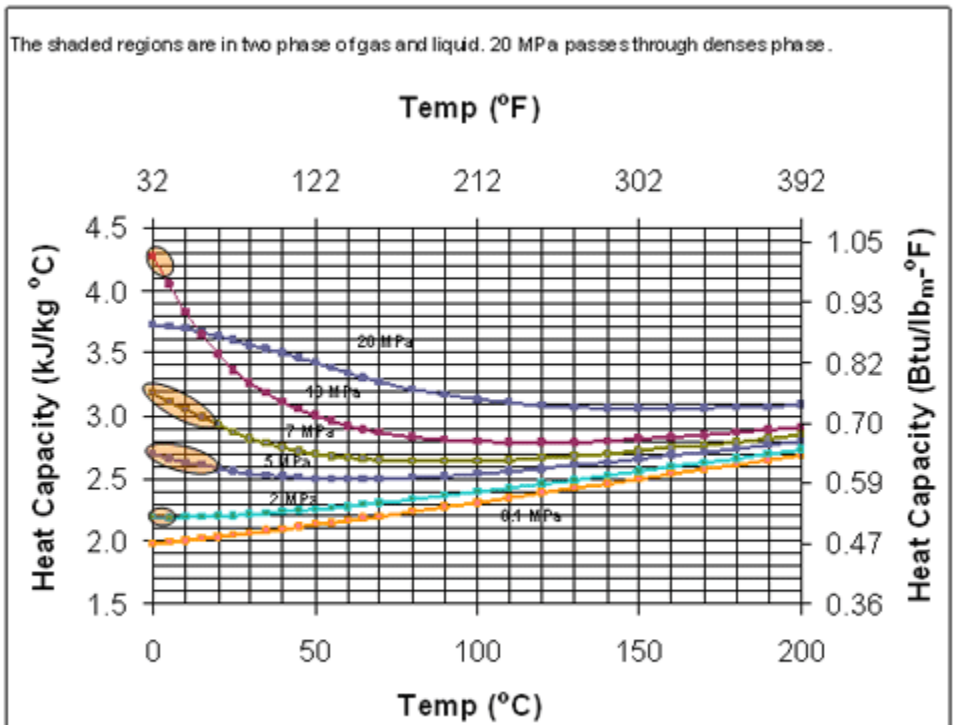

Figure 3. Heat Capacity of SG =0.70 Natural Gas

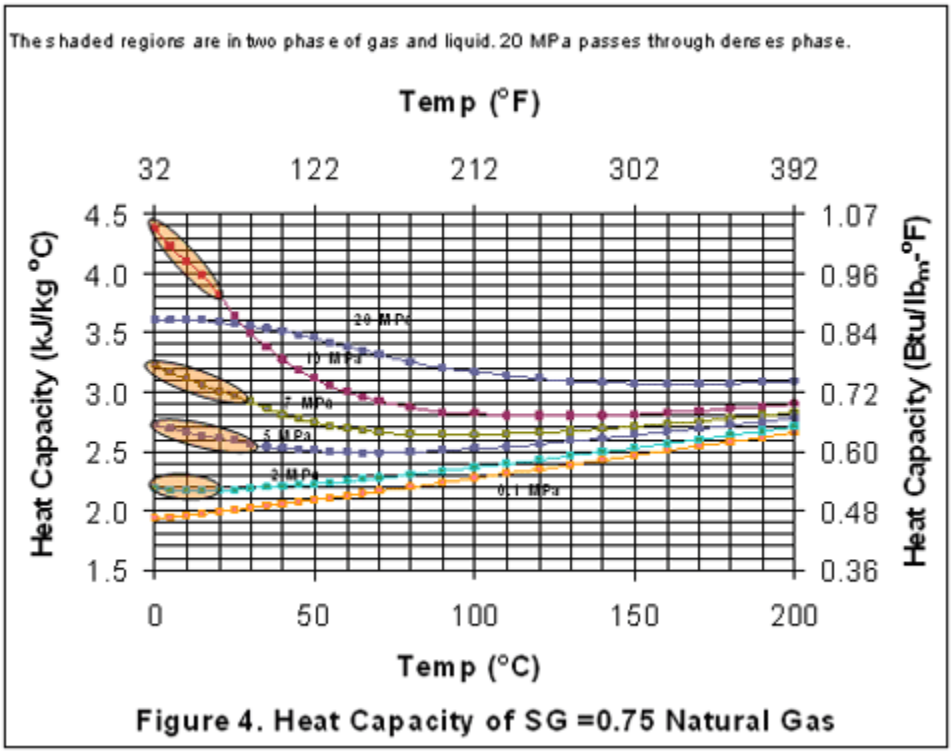

Figure 4. Heat Capacity of SG =0.75 Natural Gas

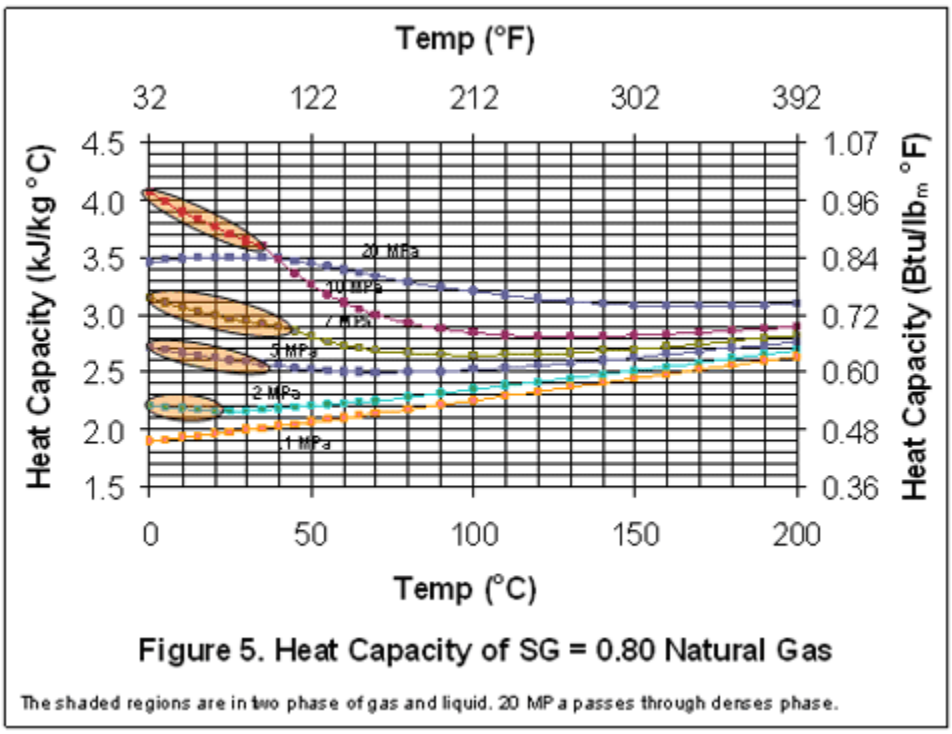

Figure 5. Heat Capacity of SG = 0.80 Natural Gas

The shaded regions are in two phase of gas and liquid. 20 MPa passes through denses phase.

Discussion and Conclusions

A single and relatively simple correlation has been developed to estimate heat capacity of natural gases as a function of pressure, temperature, and relative density (composition). This correlation covers wide ranges of pressure (0.10 to 20 MPa, 14.5 to 2900 Psia), temperature (20 to 200 °C, 68 to 392 °F), and relative density (0.60 to 0.80). A generalized set of parameters in addition to an individual set of parameters have been determined and reported in Table 2. The error analysis reported in Table 2 indicates that the accuracy of this equation is quite good and can be used for natural gas heat duty calculations. For the generalized set of parameters, the average absolute percentage error (AAPD) and the maximum absolute percent deviations (MAPD) for the total of 715 points are 4.34 and 23.61, respectively. The applicable ranges of the proposed correlation are shown in Table 2.

Table 2. Parameters for the proposed correlation; Eq. (7) in SI and FPS system

T in °C, P in MPa, and Cp in kJ/kg-°C (0.10 to 20 MPa)										
Gas SG	a	b	c	d	E	f	AAPD	MAPD	T range, °C	NPT
0.60	0.9426	1.0106	-0.5260	2.1512	1.0140	0.0155	3.43	12.10	15 to 200	150
0.65	1.1684	1.0123	-0.6476	2.1436	1.0146	0.0188	3.94	16.05	15 to 200	150
0.70	0.2633	1.0200	-0.7330	2.2486	1.0146	0.0204	4.39	20.44	20 to 200	147
0.75	1.8455	1.0194	-1.0665	2.1972	1.0148	0.0246	4.83	22.88	30 to 200	139
0.80	0.0133	1.0053	0.3912	2.1488	1.0155	0.0234	4.45	21.34	40 to 200	129
Overall							4.21	22.88		715
Gas SG	a	b	c	d	E	f	AAPD	MAPD	T range, °C	NPT
0.60-0.8	0.90	1.014	-0.700	2.170	1.015	0.0214	4.34	23.19	See above	715
T in °F, P in Psia/1000, and Cp in Btu/lbm-°F (14.5 to 2900 Psia)										
Gas SG	a	b	c	d	E	f	AAPD	MAPD	T range, °F	NPT
0.60	1.1231	1.0057	-0.7351	0.5126	1.1032	0.0161	3.43	12.35	59 to 392	150
0.65	1.9309	1.0068	-0.9104	0.5170	1.1075	0.0195	3.94	16.31	59 to 392	150
0.70	1.6987	1.0108	-1.2230	0.5506	1.1062	0.0209	4.39	20.27	68 to 392	147
0.75	8.7046	1.0108	-1.4945	0.5437	1.1079	0.0250	4.83	22.83	86 to 392	139
0.80	0.0014	1.0030	0.4652	0.5372	1.1118	0.0235	4.45	21.30	104 to 392	129
Overall							4.21	22.83		715
Gas SG	a	b	c	d	E	f	AAPD	MAPD	T range, °F	NPT
0.60-0.8	1.15	1.008	-0.944	0.533	1.110	0.0216	4.34	23.61	See above	715

AAPD= Average Absolute Percent Deviation and
MAPD= Maximum Absolute Percent Deviation
NPT= Number of Points and
SG = Relative Density (Specific Gravity)
Note: Below the above the temperature ranges for pressures 2, 5, 7, and 10 MPa (14.5 to 1450 Psia), the gas mixture may be in two phase (gas and liquid) region.

It should be noted that the concept of heat capacity is valid only for the single phase region. Figures 3 through 5 indicate that for low temperatures, liquid forms and irregular behavior of C_P is observed.

REFERENCE

1. Campbell, J. M., "Gas Conditioning and Processing, Vol. 1, the Basic Principals, 8th Ed., Campbell Petroleum Series, Norman, Oklahoma, 2001
2. G. Soave, Chem. Eng. Sci. 27 (1972) 1197-1203.
3. D.-Y. Peng, D.B. Robinson, Ind. Eng. Chem. Fundam. 15 (1976) 59-64.
4. **ProMax®**, Bryan Research & Engineering Inc, Version 2.0, Bryan, Texas, 2007

Corrosion Monitoring and Inspection – Is There a Difference?

By Alan Foster

Introduction

To many people involved in the Oil and Gas production and refining industry, the terms monitoring and inspection are used interchangeably when referring to corrosion issues. However, this lack of differentiation can lead to misunderstandings and errors. It is our contention that a clear differentiation is needed and that engineers should strive to use the correct terminology. In order to achieve that differentiation it is necessary to first define these terms 'corrosion monitoring' and 'inspection'. A review of some of the named techniques and methods used in these areas will help to consolidate an understanding of which terms fall into the inspection bracket and which are viewed as corrosion monitoring devices.

Definitions

The following definitions may not be exactly scientific in nature, but they do help to show two major differences between the two sets of valuable corrosion management tools.

'Corrosion monitoring' – is a way of determining how corrosive the fluids are within a specific environment. The various techniques available are typically used to give frequent, short time interval measurements, thereby allowing the day-to- day control of corrosion mitigation / prevention approaches such as corrosion inhibition. (The one exception to the 'short time interval' description is the weight-loss coupon).

'Inspection' – is the means by which corrosion (and other) damage may be located in a structure, as well as gaining insight to the amount and severity of that damage. Usually inspection tools are used less frequently than corrosion monitoring devices, often on an annual or even longer basis. However, the frequency of measurement should be determined via a process of risk based analysis to give a programme of 'risk based inspection' (RBI).

The Methods and Techniques

It is important to point out at the outset that the use of any corrosion monitoring device or inspection tool should be within the bounds of prudent process safety engineering. In the first place only trained personnel should be allowed to operate and maintain the various pieces of equipment. Secondly, they should learn about the system to be monitored / inspected, so that they clearly understand what risks are involved with respect to carrying out their monitoring/inspection activities.

Corrosion Monitoring Techniques

The most commonly used corrosion monitoring devices are included in the following list of equipment:

- Weight-loss coupons
- Spool pieces
- Electrical resistance probes
- Linear polarisation probes
- Galvanic probes
- Hydrogen pressure probes
- Hydrogen electrochemical patch probes
- Electrochemical noise probes
- Field Signature Method™
- Bioprobes

The majority of these techniques are classed as 'intrusive', in that for internal measurement there must be an access fitting to allow the measuring probe to be inserted into the process fluids. The exceptions on this list are the hydrogen electrochemical patch probes and the Field Signature Method™, which are attached to the outside surface of vessels and pipes.

Weight loss coupons, spool pieces and bioprobes, give one-off readings. In order to determine the result, each of these items must be withdrawn from the system and carefully examined and tested. The other devices can be left in place for some time, measurements being obtained either manually or automatically collected via hard wire connections or radio transmission devices.

Inspection Tools

The inspection tools are either arranged on the external surfaces of structures, or inserted into tubing via wireline and into pipelines installed in 'intelligent pigs'. The following list of these methods is not exclusive:

- Visual inspection
- Eye and magnifying glass
- Boroscopes
- Fiberscopes
- Robotic crawlers
- Cameras
- Calliper tools (on wireline or in intelligent pigs)
- Ultrasonic thickness (UT) measurements
- 'Spot' UT (compression mode) / straight beam (UTL)
- Pulse-echo contact method
- Shearwave mode (UTS)
- Phased array
- Automated UT (both in compression and shear modes)

- Long range UT (LRUT, or guided wave inspection - GWI)
- Radiography (RT)
- Dye penetrant (PT)
- Magnetic flux leakage (for example in intelligent pigs)

These first six methods are the most commonly used. Others include the following:

- Dry magnetic particle
- Wet magnetic particle
- Wet fluorescent magnetic particle testing (WFMP or WFMT)
- Magnetostrictive guided wave testing (MGWT)
- Eddy current
- Pulsed eddy current (PEC)
- Neutron backscatter (for CUI – corrosion under insulation)
- Tangential radioscopy
- Magnetic flux exclusion
- Acoustic emission (AE)
- Acousto ultrasonics

Specialist application of some of these inspection tools allows the detection of cracking damage, including sub-surface cracks. Early detection of the latter can obviously prevent subsequent catastrophic failures.

Finally

This ‘Tip of the Month’ has concentrated on the need to differentiate between corrosion monitoring and inspection, to show that each play a part in the overall corrosion management of an oil and gas production / processing system.

How Sensitive is Pressure Drop Due to Friction with Roughness Factor?

By Dr. Mahmood Moshfeghian

In the February 2007 tip of the month (TOTM), Joe Honeywell [1] presented a procedure for calculating fluid pressure drop for liquid in a **piping** system due to friction. Continuing Honeywell's TOTM, we will outline procedures for calculation of friction losses in oil and gas **pipelines**. From an engineer's point of view the question may arise "how sensitive is friction pressure drop with the wall roughness factor?" Of course the answer is "it depends". To explain this answer quantitatively and qualitatively, we will study the effect of wall roughness factor for two case studies in this month's TOTM. In the first case study, an oil pipeline with a flow rate of 0.313 m^3/s (170,000 bbl/day) and in the second case, a natural gas pipeline with a flow rate of 22.913 Sm^3/s (70 MMSCFD) will be studied and calculation results will be presented in tabular and graphical format.

Friction Factor

The Moody diagram in Figure 1 is a classical representation of the fluid behavior of Newtonian fluids and is used throughout industry to predict fluid flow losses. It graphically represents the various factors used to determine the friction factor. For example, for fluids with a Reynolds number of 2000 and less, the flow behavior is considered a stable laminar fluid and the friction factor is only dependent on the Reynolds number [2]. The friction factor, *f*, for the Laminar zone is represented by:

$$f = \frac{64}{\mathrm{Re}} \tag{1}$$

Where *Re* is the Reynolds number and is expressed as the ratio of inertia force to viscous force and mathematically presented as.

$$\mathrm{Re} = \frac{(V)(D)(\rho)}{\mu} \tag{2}$$

Fluids with a Reynolds number between 2000 and 4000 are considered unstable and can exhibit either laminar or turbulent behavior. This region is commonly referred to as the critical zone and the friction factor can be difficult to accurately predict. Judgment should be used if accurate predictions of fluid loss are required in this region. Either Equation 1 or 3 are commonly used in the critical zone. If the Reynolds number is beyond 4000, the fluid is considered turbulent and the friction factor is dependent on the Reynolds number and relative roughness. For Reynolds numbers beyond 4000, the Moody diagram identifies two regions, transition zone and completely turbulent zone. The friction factor represented in these regions is given by the Colebrook formula which is used throughout industry and accurately represents the transition and turbulent flow regions of the Moody diagram.

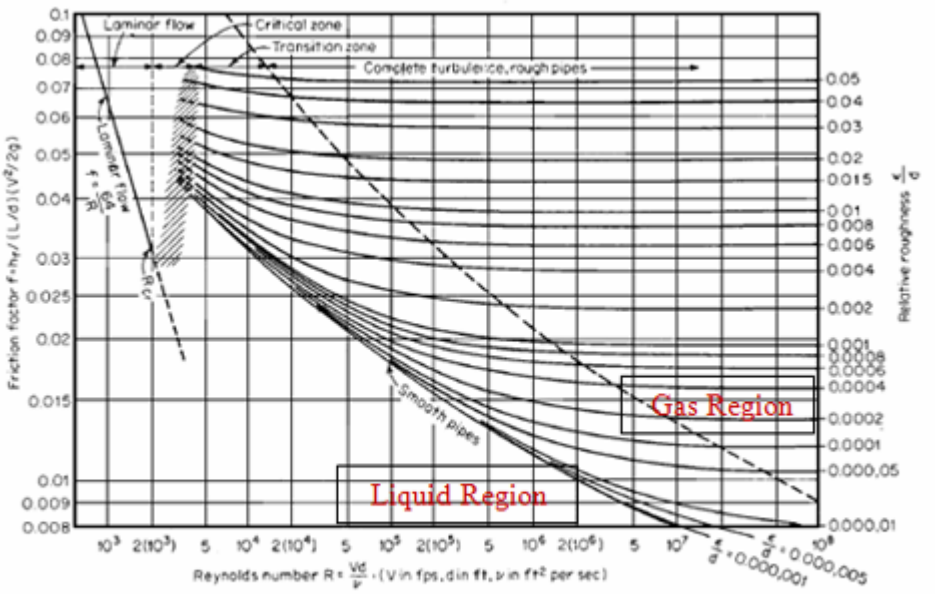

Figure 1. Moody Friction Factor Diagram [1]

The Colebrook formula for Reynolds number over 4000 is given in equation 3.

$$\frac{1}{\sqrt{f}} = -2\log_{10}\left(\frac{\varepsilon/D}{3.7} + \frac{2.51}{\mathrm{Re}\sqrt{f}}\right) \tag{3}$$

(3)

Where:

f = Moody friction factor, dimensionless

Re = Reynolds Number

V = Fluid average velocity, m/s (ft/sec)

D = Inside diameter, m (ft)

ε = Absolute wall roughness, m (ft)

ρ = Fluid density, kg/m^3 (lb$_m$/ft^3)

μ = Fluid viscosity, kg/(m-s) or lb$_m$/(ft-sec)

The roughness factor is defined as the absolute roughness divided by the pipe diameter or ε/D. Typical values of absolute roughness are $5.9x10^{-4}$ in (0.0015 mm) for PVC, drawn tubing, glass and 0.0018 in (0.045 mm) for commercial steel/welded steel and wrought iron [3].
The Colebrook equation has two terms. The first term, $(\varepsilon/D)/3.7$, is dominate for gas flow where the Re is high. The second term, $\frac{2.51}{\mathrm{Re}\sqrt{f}}$, lines converge (smooth pipes). In the "Complete Turbulence" region, the lines are "flat", meaning that they are independent of the Reynolds Number. In the "transition Zone", the lines are dependent on Re and ε/D. When the lines converge in the "smooth zone" the fluid is independent of relative roughness.

Liquid (Incompressible) Flow

For liquid flow, equation 4 has been used by engineers for over 100 years to calculate the pressure drop in pipe due to friction. This equation relates the various parameters that contribute to the friction loss. This equation is the modified form of the Darcy-Weisbach formula which was derived by dimensional analysis.

$$\Delta P_{Friction} = f \frac{L}{D} \frac{V^2}{2g_c} (\gamma)(\rho_{water}) \qquad (4)$$

(4)

Where:

$\Delta P_{Friction}$	= Pressure loss due to friction, MPa or psi
f	= Moody friction factor, calculated by Equation 3, dimensionless
L	= Pipe length, km or mile
D	= Inside diameter, mm or inch
V	= Average fluid velocity, m/s or ft/sec
γ	= Relative density (specific gravity), dimensionless
ρ_{water}	= Density of water, kg/m^3 or lb$_m$/ft^3

The friction factor in this equation is calculated by equation 3 for a specified Reynolds number and roughness factor using an iterative method or a trial and error procedure.

Gas (Compressible) Flow

For gas flow, density is a strong function of pressure and temperature, and the gas density may vary considerably along the pipeline. Due to the variation of density, equation 5 should be used for calculation of friction pressure drop.

$$\Delta P_{Friction} = P_{in} - \sqrt{P_{in}^2 - 5.7 \times 10^{-4} f L Z_{avg} T_{avg} \rho_{std} \frac{Q_{std}^5}{D^5}}$$

Where:

$\Delta P_{Friction}$	= Pressure loss due to friction, MPa or psi	(5)
Pin	= Inlet pressure, MPa or psia	
f	= Moody friction factor, calculated by Equation 3, dimensionless	
L	= Pipe length, km or mile	
D	= Inside diameter, mm or inch	
Z_{avg}	= Average compressibility factor	
ρ_{std}	= Gas density at standard condition	
Q_{std}	= Gas volume flow rate at standard condition	
T_{avg}	= Average pipeline temperature, K or °R	

Again, the friction factor in this equation is calculated by equation 3 for a specified Reynolds number and roughness factor using a trial and error procedure. Actual volume flow rate is needed to calculate the velocity of gas in the line from which the Reynolds number is calculated. Equation 6 may be used to convert the volume flow rate at standard condition to the actual volume flow rate.

$$Q_{act} = Z_{avg} \left(\frac{T_{avg}}{T_{std}} \right) \left(\frac{P_{std}}{P_{avg}} \right) Q_{std} \qquad (6)$$

Where:

Q_{std}	= Gas volume flow rate at standard condition
Q_{act}	= Actual gas volume flow rate
T_{std}	= Standard condition temperature, K or °R
P_{std}	= Standard condition pressure, MPa or psia
T_{avg}	= Average pipeline temperature, K or °R
P_{avg}	= Average pipeline pressure, MPa or psia
Z_{avg}	= Average compressibility factor

Case Study 1: Oil Pipeline

Consider a 16-inch (inside diameter of 395 mm) oil export line for transportation of 170,000 bbl/day (0.313 m^3/s) of a 43 API crude oil (relative density of 0.81) from an offshore platform to the shore oil terminal. The total length of pipe is 55 km. The ambient temperature is 5 °C and the crude oil viscosity at the average pipe temperature is 0.001 cP. The pipe line inlet pressure is 14.9 MPa (absolute). Since the objective is to study the effect of roughness factor on friction pressure drop, we will ignore elevation change.

To study the effect of roughness factor on friction pressure drop, ε/D was varied from $1x10^{-6}$ to $1x10^{-3}$. The roughness factor of $\varepsilon/D = 1x10^{-6}$ represents a very smooth pipe. The calculated friction pressure drop as a function of the roughness factor is plotted in Figure 2. For each value of roughness factor, the percent change in frictional pressure drop was calculated in comparison to a very smooth pipe ($\varepsilon/D = 1x10^{-6}$) and the results are presented in Figure 3. The calculated results are also presented in Table 1.

Case Study 2: Gas Pipeline

Let's consider an 8-inch (inside diameter of 190 mm) gas export line for transportation of 70 MMSCFD ($22.913x10^6$ Sm^3/d) of natural gas with a molecular weight of 19.3 (relative density of 0.67) from an offshore platform to the shore. The total length of pipe is 43 km. The ambient temperature is 5°C and the gas viscosity at the average pipeline temperature is $1.1x10^{-6}$ cP. The gas inlet temperature is 35°C and pressure is 13.0 MPa (absolute). Since the objective is to study the effect of roughness factor on friction pressure drop, we will again ignore elevation change.

Similar to the oil pipeline, the roughness factor, ε/D was varied from $1x10^{-6}$ to 0.006. Note, for a roughness factor greater than 0.006, a higher inlet pressure, a larger diameter or lower flow rate was needed. The calculated friction pressure drop as a function of roughness factor is presented in Figure 2. For each value of roughness factor, the percent change in frictional pressure drop in comparison to a very smooth pipe ($\varepsilon/D = 1x10^{-6}$) was calculated and the results are presented in Figure 3.

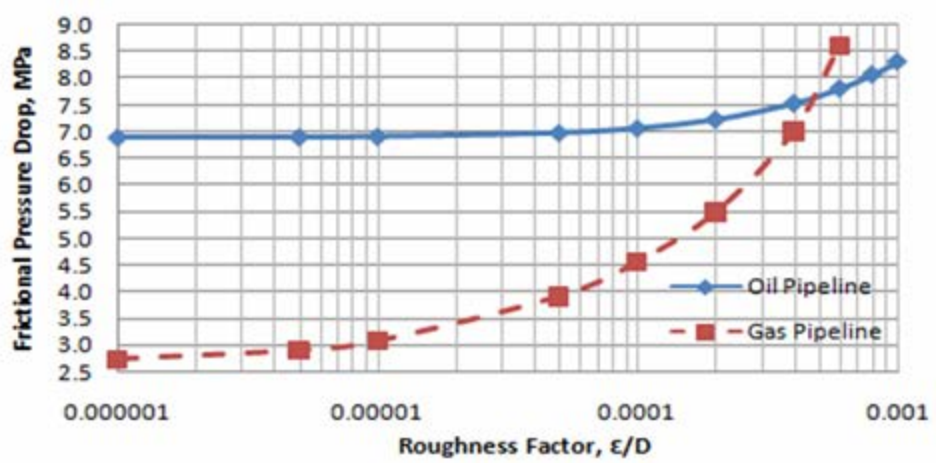

Figure 2. The sensivity of frictional pressure drop with roughness factor in oil and gas pipelines

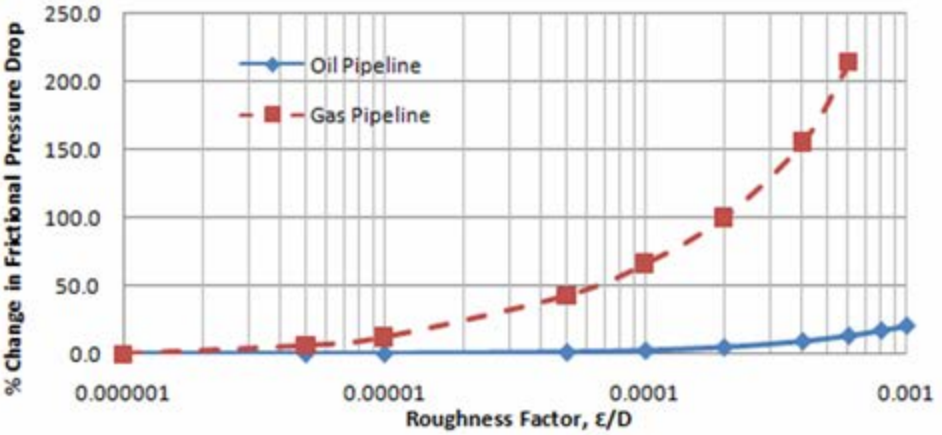

Figure 3. Impact of roughness factor on % change of frictional pressure drop relative to a smooth pipeline in oil and gas transmission lines

Table 1. Calculated friction factor and pressure drop for a range of roughness factor

	Oil Pipeline				Gas Pipeline			
ε/D	Re	f	$\Delta P_{Friction}$ MPa	$\Delta P_{Friction}$ Psi	Re	f	$\Delta P_{Friction}$ MPa	$\Delta P_{Friction}$ Psi
0.000001	81,680	0.0188	6.901	1001.0	$1.152x10^7$	0.0081	2.731	396.1
0.000005	81,680	0.0188	6.908	1002.0	$1.152x10^7$	0.0085	2.898	420.3
0.00001	81,680	0.0188	6.917	1003.3	$1.152x10^7$	0.0089	3.069	445.1
0.00005	81,680	0.0190	6.986	1013.3	$1.152x10^7$	0.0108	3.906	566.5
0.0001	81,680	0.0192	7.071	1025.6	$1.152x10^7$	0.0121	4.548	659.7
0.0002	81,680	0.0197	7.234	1049.3	$1.152x10^7$	0.0138	5.477	794.4
0.0004	81,680	0.0205	7.538	1093.3	$1.152x10^7$	0.0159	6.989	1013.7
0.0006	81,680	0.0213	7.816	1133.7	$1.152x10^7$	0.0174	8.583	1244.9
0.0008	81,680	0.0220	8.075	1171.2	N/A	N/A	N/A	N/A
0.001	81,680	0.0226	8.316	1206.2	N/A	N/A	N/A	N/A

.

Discussion and Conclusions

The analysis of Figure 2 indicates that for the oil pipeline, the friction pressure drop is almost independent of the roughness factor in the range of $1x10^{-6} < \varepsilon/D < 1x10^{-4}$; however, for $\varepsilon/D > 1x10^{-4}$, it will increase with ε/D. For liquid lines, the Reynolds number is normally in the range of $5x10^4$ to $1x10^6$. For this range, the friction factor curves in Figure 1 approach close to each other so the values of friction factors become close to each other.

Contrary to the oil pipeline, the friction pressure drop for the gas pipeline is a strong function of ε/D. As can be seen in Figure 2, friction pressure drop increases very rapidly with the roughness factor. Figure 3 shows the comparison of percent change of friction pressure drop between oil and gas pipelines as a function of roughness factor. For the liquid pipeline, the maximum change is 20 % but for the gas pipeline the maximum change is more than 200 %. Again this can be explained by referring to Figure 1. For gas pipelines, the Reynolds number is higher than in the liquid line and the range is normally $5x10^6 < Re < 1x10^8$. For this range, the friction factor curves in Figure 1 are apart from each other, so the friction factors are not close.

In summary, contrary to liquid pipelines the gas pipelines are very sensitive to wall roughness and using smooth pipe can reduce friction pressure drop considerably. This in turn lowers the OPEX. Therefore, regular pigging to clean the pipe surface is done to lower the roughness factor. The modern gas transmission companies will add a Fusion Bounded Epoxy (FBE) liner to gas pipelines because the pipe is sensitive to roughness. This lowers OPEX for the long term. It should be noted that the smoother the pipe, the higher the CAPEX, so as always, detailed total cost analysis should be performed for engineering applications. Due to the sensitivity of gas pipelines to roughness factor and other operation parameters, there are numerous gas flow equations (e.g. Weymouth, Panhandle A and B, AGA) to best fit certain design conditions [1].

REFERENCES

1. Honeywell, Joe, "Friction Pressure Drop Calculation," Campbell Tip of the Month, Feb 2007
2. Campbell, J. M., "Gas Conditioning and Processing, Vol. 1, the Basic Principals, 8th Ed., Campbell Petroleum Series, Norman, Oklahoma, 2001
3. Menon, E.S, Piping Calculations Manual, McGraw-Hill, New York, 2005

The Parameters Affecting a Phase Envelope in the Dense Phase Region

By Dr. Mahmood Moshfeghian

Because phase envelope generation and its impact on design and performance of gas processing plants is so important it has been the topic of several Tips Of The Month (TOTM). As emphasized by Rusten *et al.* [1], there are several challenges that have to be addressed in order to succeed with the phase envelope modeling of real natural gases. The most important are:

1. Sampling procedures
2. Sample preparations
3. Chromatographic gas analysis. A detailed composition is required for satisfactory input to thermodynamic models
4. Thermodynamic models that correctly predict the phase envelope

In this TOTM we will demonstrate the impact of thermodynamic modeling for rich gases in the dense phase region. For a discussion on the dense phase, please see the January 2010 TOTM. The value of the dense phase viscosity is very similar to gas phase viscosity. The dense phase density is closer to the liquid phase density. Therefore, it has become attractive to transport rich natural gas in the dense phase region. In October 2005 we discussed several methods of C7+ (heavy ends) characterization and checked the accuracy of several methods and presented tips to improve the accuracy of each method. These methods are presented briefly below. For more detail, please refer to Gas Conditioning and Processing, Volume 3, Advanced Techniques and Applications [2].

Method A: The C7+ is treated as a single hypothetical component based on its molecular weight (MW) and specific gravity (SG). The normal boiling point is predicted; the critical temperature, critical pressure, and acentric factor are also predicted using correlations similar to the ones by Riazi and Duabert [3].

Adjusting MW (or Tc) in Method A: By adjusting the molecular weight of the C7+ fraction we can closely match the measured dew point. The critical temperature (Tc) can also be adjusted to make the phase envelope curve pass through the measured dew point. The Tc adjustment is preferred because less work is involved to match the calculated and experimental values.

Method B: The C7+ is broken into Single Carbon Numbers (SCN) ranging from SCN 7 to SCN 17+ using the exponential decay procedure presented by Katz [4] and applied by others [5-7].

Method C: The large number of SCN components of **Method B** may be lumped into 4 cuts. The properties of the lumped cuts are estimated from the individual SCN components.

Method D: This method is similar to **Method B** except that 12 normal parafins (alkanes) are used to represent the C7+ instead of SCN components. The advantage of this method is that n-alkane

components are readily available in many commercial software packages but the SCNs may not be.

Tuning MW in Method D: The distribution (i.e. mole %) of the alkane part of the C_{7+} depends on the assumed value of the C_{7+} MW.

Tuning the binary interaction parameters, k_{ij}, in Methods B and C: A common correlation to estimate the binary interaction parameter is:

$$k_{ij} = 1 - \left[\frac{2\sqrt{v_{c_i}^{1/3} \; v_{c_j}^{1/3}}}{v_{c_i}^{1/3} + v_{c_j}^{1/3}} \right]^{n}$$

In the above equation, v_{ci} and v_{cj} represent the critical volumes of components i and j, respectively. The default value of exponent n is normally set to 1.2 but it can be used as a tuning parameter to match the experimentally measured dew point.

In this TOTM we will generate the dew point curve for the rich gas shown in Table 1 using the C_{7+} characterization methods described above. The dew point curve portion of the phase envelope for this gas was generated using both HYSYS [8] and ProMax [9] simulation software by the Soave-Redlich-Kwong (SRK) [10] (Figure 1) and Peng-Robinson (PR) [11] (Figure 2). The experimentally measured dew point pressure [12] is also show in these two figures as a red triangle.

Table 1. Feed composition and condition [12]

Component	Mole Fraction
C1	0.8238
C2	0.0428
C3	0.0351
IC4	0.0161
nC4	0.0303
IC5	0.0060
nC5	0.0068
C6	0.0099
C7+	0.0292
MW C7+	125
SG C7+	0.74
T, °C	4.44
Experimental Dew Point, kPa	21340

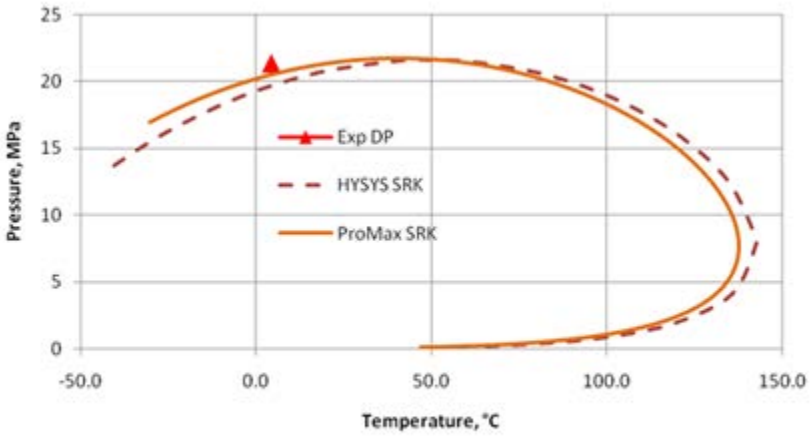

Figure 1. Dew point curve by SRK EOS of HYSYS and ProMax

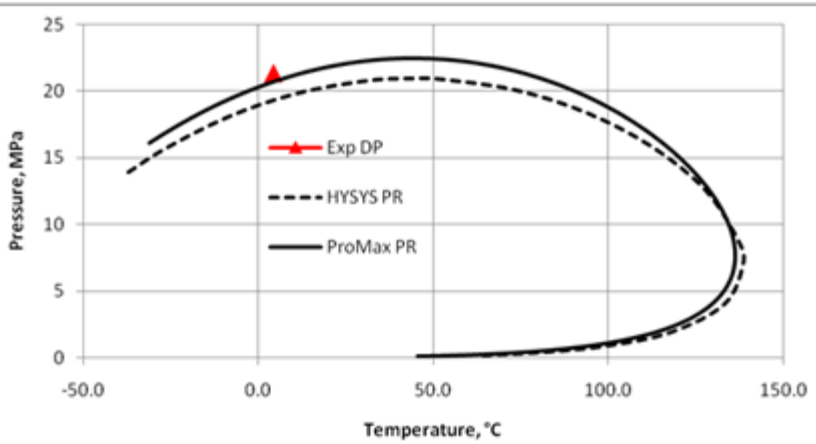

Figure 2. Dew point curve by PR EOS of HYSYS and ProMax

Figures 1 and 2 were generated using a single C_{7+} cut with the relative density and molecular weight shown in Table 1. Other required properties were estimated using the default options of the simulation software. As can be seen in these figures using the PR Equation of State with ProMax gives the closest prediction of the experimentally measured dew point. As described above the MW can be adjusted to match experimental and calculated data.

The single carbon number (SCN) analysis as described in Method B above was used for further tuning of the thermodynamic model, The predicted dew point pressures for the different cases studied here are shown in Table 2. Figure 3 demonstrates the same information graphically.

Table 2. Predicted dew point pressure in kPa at 4.44 °C by ProMax using the PR EOS

No of Cuts	SCN	Molecular weight of C_{7+}			
		125	120	118.2	115
3	C7-C9	NA	21408	21091	20553
4	C7-C10	22642	21698	21360	20746
5	C7-C11	22897	21905	21532	20891
6	C7-C12	23139	22091	21698	21015
7	C7-C13	23373	22249	21843	21125
8	C7-C14	23580	22387	21960	21201

Using Method B, the experimental dew point is most closely represented using four SCNs with a combined molecular weight of 118.2. The properties and mole percent distribution of these four SCN components for the optimum case are given in Table 3.

Table 3. The properties and mole % distribution of SCN for the optimum case (MW=118.2)

SCN	Average Boiling Point, °C	Relative Density	MW	Mole% in Feed
7	91.9	0.722	96	0.5047
8	116.7	0.745	107	0.6161
9	142.2	0.764	121	0.7941
10	165.8	0.778	134	1.0051
Total			118.2	2.9200

Table 4 shows the improvement made in the dew point prediction by using four SCNs with a modified molecular weight of 118.2 instead of a single C_{7+} cut. The ProMax PR EOS is used for both cases. The predicted dew point curves for these two cases can be seen in Figure 4.

Table 4. The dew point prediction improvement by using four SCNs

Dew point Pressure, kPa			Error %	
Experimental	C7+	4 SCN	C7+	4 SCN
21340	20741	21360	2.8	-0.1

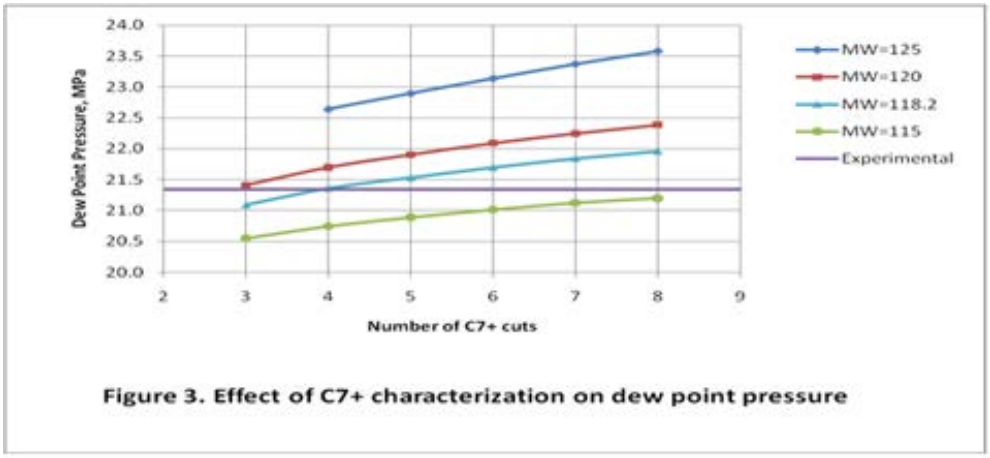

Figure 3. Effect of C7+ characterization on dew point pressure

As can be seen in Figure 4, proper characterization of the heavy components (see Tables 3 and 4) can improve the quality of the phase envelope and match the experimentally measured dew point in the dense phase region. For a detailed discussion of this topic, the readers may refer to the Rusten *et al.* paper [1].

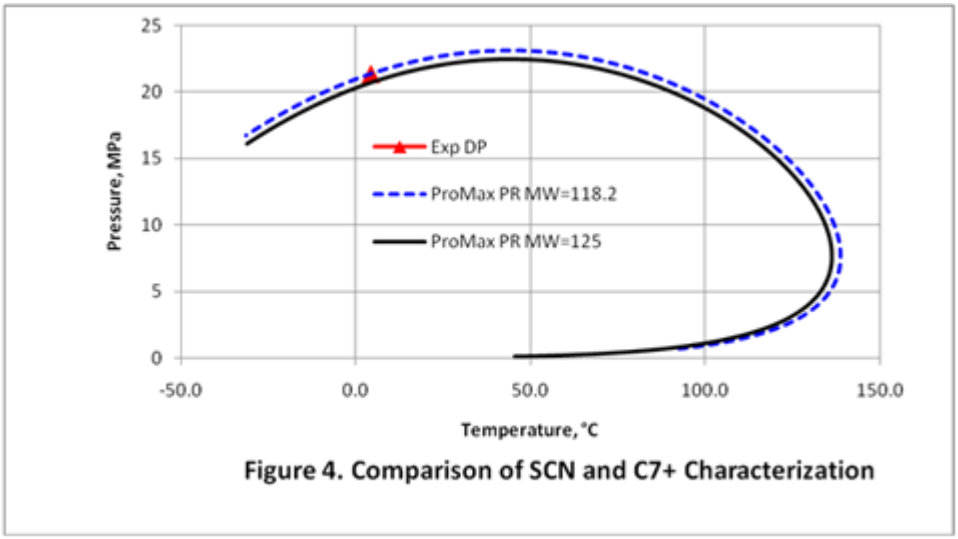

Figure 4. Comparison of SCN and C7+ Characterization

REFERENCES

1. Rusten, B.H., Gjertsen, L.H., Solbraa, E., Kirkerød, T., Haugum, T. and Puntervold, s., "Determination of the phase envelope – crucial for process design and problem solving," presented at the 87th GPA National Convention, Grapevine, 2008
2. Maddox, R. N. and L. Lilly, "Gas Conditioning and Processing, Computer Applications for Production/Processing Facilities," John M. Campbell and Company, Norman, Oklahoma, 1995.
3. Riazi, M.R. and T.E. Daubert, Hydr. Proc. P. 115, (March) 1980
4. Katz, D. *J. Petrol. Technol.*, 1205-1214, (June) 1983.
5. Whitson, C. H. *SPE J.*, 683-694, (August) 1983
6. Starling, K. E. Presented at the American Gas Association Operations Conference, Orlando, FL, April 27-30, 2003
7. Moshfeghian, M., Maddox, R.N., and A.H. Johannes, "Application of Exponential Decay Distribution of C_{6+} Cut for Lean Natural Gas Phase Envelope," J. of Chem. Engr. Japan, Vol 39, No 4, pp.375-382, 2006
8. ASPENone, Engineering Suite, **HYSYS** Version 7.0, Aspen Technology, Inc., Cambridge, Massachusetts U.S.A., 2009.
9. **ProMax®**, Bryan Research & Engineering Inc, Version 3.2, Bryan, Texas, 2009
10. Soave, G., Chem. Eng. Sci. 27, 1197-1203, 1972.
11. Peng, D.,Y. and D. B. Robinson, Ind. Eng. Chem. Fundam. 15, 59-64, 1976.
12. Sage, B.H, and R.H. Olds, AIME 170, 156–173, 1947.

The Sensitivity of k-Values on Compressor Performance

By: Joe Honeywell

One of the most important physical properties of a gas is the ratio of specific heats. It is used in the design and evaluation of many processes. For compressors, it is used in the design of components and determination of the overall performance of the machine. Engineers are frequently asked to evaluate a compressor performance utilizing traditional equations of head, power and discharge temperature. While these simplified equations may not give exact results, they give useful information needed to troubleshoot a machine, predict operating conditions, or a long-term trend analysis. The accuracy of the performance information will depend on the proper selection of the ratio of specific heats. This Tip of the Month (TOTM) will investigate the application of the ratio of specific heats to compressors, its sensitivity to the determination of machine performance and give recommendations for improved accuracy.

Background of k-value

The ratio of specific heats is a physical property of pure gases and gas mixtures and is known by many other names including: adiabatic exponent, isentropic exponent, and k-value. It is used to define basic gas processes including adiabatic and polytropic compression. It also appears in many of the traditional equations commonly used to determine a compressor head, gas discharge temperature, gas power, and polytropic exponent. The k-value also influences the operating speed of a compressor, but we will simplify the present analysis by deleting speed from our evaluation. The following commonly used compressor performance equations show how the k-value is utilized in the design and evaluation of compressors.

Ideal adiabatic (also call isentropic) gas compression process [1]:

$$P_S \upsilon_S^k = P_D \upsilon_D^k = \text{constant} \qquad (1)$$

Ideal adiabatic head [5] (see Note):

$$H_{AD} = \frac{Z_S}{A}\frac{R}{MW} T_S \frac{k}{k-1}\left[R_P^{\frac{k-1}{k}} - 1\right] \qquad (2)$$

Gas discharge temperature [5]:

$$T_D = T_S \frac{R_P^{\frac{k-1}{k}} - 1}{\eta_{AD}} + T_S \qquad (3)$$

Gas power [5]:

$$PWR_{GAS} = \frac{mH_{AD}}{B\eta_{AD}} \qquad (4)$$

Polytropic exponent [5, 7]:

$$\frac{n}{n-1} = \frac{k}{k-1}\eta_P \qquad (5)$$

Note: The actual Z-value will vary from the suction to discharge conditions. ZS is sometimes replaced with ZAVE to approximate the variations in compressibility value [1, 5]. See the nomenclature at the end of this TOTM.

The above equations are written in terms of the adiabatic process with the exception of Equation 5, which refers to the polytropic process. Both compression processes are similar and will give the same actual results. The adiabatic and polytropic methods are extensively used by manufacturers to design compressors, and make use of k-values to calculate their performance. However, as will be seen, the effect of the k-value and the calculated results will influence both compression processes alike. For simplicity, this Tip of the Month will use the adiabatic process.

It can be seen from Equations 1-5 that the k-value has an effect on a compressor head, temperature, power, and polytropic exponent. In order to determine how small changes in the k- value can influence a compressor performance, let us first define the k-value of a pure gas. The thermodynamic definition of a gas k-value is given by Equation 6. It shows the relationship to the specific heat at constant volume, C_V and specific heat at constant pressure, C_p. Both values vary with temperature and pressure.

$$k = \frac{C_P}{C_V} \qquad (6)$$

For a pure gas there are many references that give C*p* and C_V values at various conditions. One useful source is National Institute of Standards and Technology. Their website is http://webbook.nist.gov/chemistry/fluid/

The method of determining the k-value for gas mixtures is more complex. The major difference is that a gas mixture does not behave as any one of its components but as an "equivalent" gas. Therefore, to determine the k-value of the mixture, we must know the mole fraction of each component, y_i and the molar specific heat at constant pressure for each component, MC_{Pi}. Equation 7 can be used to determine the k-value of an ideal gas mixture [1, 5]. Real gases may deviate from the calculated value.

$$k = \frac{\sum_i y_i MC_{Pi}}{\sum_i y_i MC_{Pi} - D} \qquad (7)$$

While Equations 1-7 are applicable for manual calculations methods, it is important to note that process simulation packages determine the compressor head and discharge temperature utilizing equations of state. The results are the same but the methods are very different.

K-value Sensitivity Analysis

In the compression process the temperature and pressure of the process gas both increase. Not knowing what k-value to select for evaluating the compression process can lead to errors. For example, a typical propane compressor may have a k-value at suction conditions of 1.195. At the compressor

discharge conditions the k-value is 1.254. The difference in the two values varies by 4.94 percent and can have a significant influence in the performance evaluation. The following example illustrates how minor changes in the k-value can influence the calculated compressor head, temperature, power and the polytropic coefficient.

Example 1: A natural gas compressor is operating at the conditions given below. Only the k-value is varied from 1.20 to 1.28, all other given parameters remain constant. Figure 1 illustrates how the "apparent" performance of a compressor can change by varying the k-value.

Given: MW=18.0 Z_S=0.95 Z_S=0.93
η_{AD}=0.75 η_P=0.77 R_P=2.5
Mass flow=1000 lbm/min (453.6 kg/min) T_S=100 °F (37.7 °C)

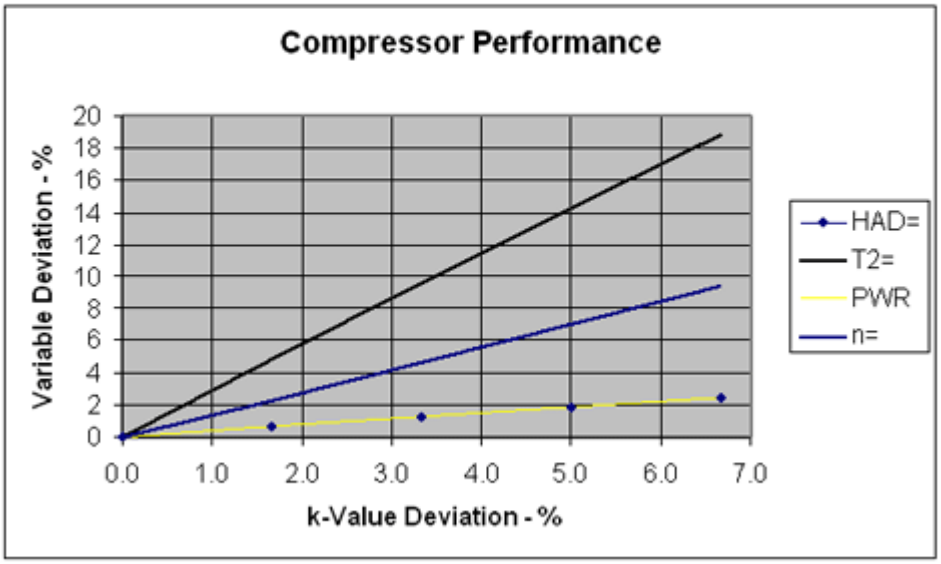

Figure 1 – Compressor Performance Deviations with k-Value Changes

It can be seen from Figure 1 that the discharge temperature deviated over 18.8 percent by only changing the k-value by 6.7 percent. In this case the k-value varied from a value of 1.20 to 1.28; which is the typical range for natural gas. Similarly, the power changed by 2.5 percent, polytropic exponent by 9.5 percent, and adiabatic head by 2.5 percent for the same variation of the k-value. The changes in compressor performance described in Figure 1 can be much larger depending on the gas composition and the operating temperature and pressure.

Corrected k-Value Recommendations

The k-value sensitivity for a single-stage machine is not nearly the problem as a multi-stage compressor. For a single-stage machine, the pressure ratio is typically lower and the temperature and pressure changes are less. As a result the changes in k-value are not as great and accurate results can be obtained by approximating the k-value at the suction conditions. However, for multi-stage machines, where the pressure and temperature ratios are higher, the k-value sensitivity is more of a factor in evaluating compressor performance. Most compressor manufacturers calculate the k-value for each stage of compression and avoid errors introduced by utilizing an overall k-value. Without their software,

we are left with a corrected k-value by empirical methods.

There are many useful approximations that will correct for changes in the k-value as the process gas passes through the compressor. Normally the k-value will decrease during compression but not always. Utilizing the suction conditions to estimate the k-value will generally give higher values of temperature, heat, and power. The polytropic exponent generally decreases as the adiabatic exponent decreases. To avoid potential discrepancies, a k-value correct may be warranted. The following are six methods of determining the corrected k-value commonly used in industry.

1) At T_S and P_S: This method determines the k-value at suction conditions and is useful for single stage compressors or applications where there is little change in the k-value. The k-value is easy to determine and tends to overestimate results, especially if the temperature and pressure do not change significantly. For greater values of R_P the results may become so conservative they become useless.

$k = k_S$ at suction conditions

2) At T_D and P_D: This method determines the k-value at discharge conditions. The k-value is less conservative and tends to underestimate results. The k-value may be difficult to determine, especially if the discharge temperature is unknown. For gases with highly variable k-values, an iterative solution may be required to estimate the discharge temperature and corrected k-value.

$k = k_D$ at discharge conditions

3) At T_{AVE} and P_{STD} [5]: This method utilizes the average operating temperature at standard pressure and determines the k-value. Numerous reference books propose this method. Errors are introduced because the k-value at standard pressure may not accurately represent values at the operating pressure.

k = at average operating temperature and standard pressure

4) At T_{AVE} and P_{AVE}: This method utilizes the k-value at the average operating temperature and pressure.

k = at average operating temperature and pressure

5) Average value [1, 3]: This empirical method takes the average k-value at compressor inlet conditions and outlet conditions. Utilizing the average k-value will result in performance values that are closer to the actual performance of the compressor.

$$k = \frac{k_S + k_D}{2}$$

6) Weighted average value [4]: This empirical method takes the weighted average of the suction, mid-point and discharge conditions. Note that the mid-pressure is determined by equivalent pressure ratios, $P_{MD} = \sqrt{P_D / P_S}$. The mid-temperature is estimated from the mid-pressure. This method considers the staged k-value to change with diverging isentropic and pressure lines on Mollier chart.

$$k = \frac{k_S + 2k_{MD} + k_D}{4}$$

Example 2 illustrates the various methods used to determine corrected k-values given above. It also compares the range of the resulting values.

Example 2: A propane compressor is operating at the given conditions shown below. Table 1 lists the k-values attributed to various operating and reference conditions [6].

Given: T_S=0 °F (-18 °C), T_{AVE}=85 °F (29 °C), T_{MID}=100 °F (41 °C), T_D=171 °F (77 °C)

P_S = 38 psia (262 kPa), P_{AVE} = 144 psia (262 kPa), P_{MID} = 98 psia (672 kPa), P_D = 250 psia (1723 kPa), P_{STD} = 14.696 psia (101.3 kPa)

Table 1
Comparison of k-values at Various Conditions

Method	Temperature		Pressure		Corrected	Deviation
	°F	°C	psia	kPa	k-Value	%
1	0	-18	38	262	1.195	0
2	171	77	250	1723	1.254	4.94
3	85	29	14.696	101.3	1.134	-5.11
4	85	29	144	992.3	1.271	6.36
5	0/171	-18/77	38/250	262/1723	1.225	2.51
6	0/100/171	-18/38/77	38/98/250	262/672/1723	1.206	0.92

Summary

This Tip of the Month has defined the physical property of process gases called the k-value or ratio of specific heats. It has shown that small changes in the k-value can have a significant effect on the calculated values of head, power, gas discharge temperature, and polytropic exponent. Recommendations were also given to improve the accuracy by utilizing different k-value methods.

Nomenclature

A	=	conversion constant	1,000	1
B	=	conversion constant	3,600	33,000
C_P	=	specific heat at constant pressure	Cal/C-kg	Btu/^{0}F-lbm
C_V	=	specific heat at constant volume	Cal/C-kg	Btu/^{0}F-lbm
D	=	conversion constant	8.314	1.986
H_{AD}	=	adiabatic head	kN-m/kg	ft-lbf/lbm
k	=	adiabatic exponent	-	-
m	=	mass flow rate	kg/min	lbm/min
MC_P	=	molar specific heat at constant pressure	Cal/kg-mol-C	Btu/lb-mol-^{0}F
MW	=	molecular weight	kg/kg-mol	lbm/lbm-mol
n	=	polytropic exponent	-	-
P	=	pressure	kPa	psia
PWR_{GAS}	=	gas power	kW	hp
R	=	universal gas constant	8,314	1,545
R_P	=	pressure ratio (P_D/P_S)	-	-
T	=	temperature	K	^{0}R
y	=	mole fraction of each component in the mixture	decimal	decimal
Z_{AVE}	=	average compressibility factor	-	-
υ	=	specific volume	kg/m^3	lbm/ft^3
η_{AD}	=	adiabatic efficiency	decimal	decimal
η_P	=	polytropic efficiency	decimal	decimal
AVE	=	subscript at average conditions	-	-
D	=	subscript at outlet or discharge conditions	-	-
MID	=	subscript at middle conditions	-	-
S	=	subscript at inlet or suction conditions	-	-
i	=	component i of gas mixture	-	-

REFERENCES

1. Ronald P Lapina, *Estimating Centrifugal Compressor Performance*, Vol. 1, Gulf Publishing, 1982.
2. John M. Campbell, *Gas Conditioning and Processing*, Vol. 2, John M. Campbell & Co., 8th Edition.
3. Elliott Compressor Refresher Course,
4. John M. Schultz, "The Polytropic Analysis of Centrifugal Compressors", Journal of Engineering for Power, January 1962.
5. Gas Processor Suppliers Association, *Engineering Data Book*, Section 13, 2004 National Institute of Standards and Technology, Web Site for Properties of Propane, Fluid Data.
6. ASME PTC10-1997, Performance Test Codes, "Compressors and Exhausters", R2003

Distribution of Sulfur-Containing Compounds in NGL Products by Three Simulators

By Dr. Mahmood Moshfeghian

In the February 2010 tip of the month (TOTM) we presented the distribution and concentration of sulfur-containing compounds in an NGL Fractionation (NF) plant using HYSYS [1] with the Peng-Robinson equation of state (PR EOS) [2]. In this TOTM we will present the distribution and concentration of the sulfur-containing compounds in the same NF plant using ProMax [3] and VMGSim [4] both using the PR EoS. These two simulation results will be compared with the HYSYS [1] results. The software's built-in binary interaction parameters were used in this study. The NF plant is the same as the one described by Alsayegh *et al.* [5]. The feed composition, rate, condition, and product specifications are shown in Tables 1 and 2 and the plant process flow diagram is shown in Figure 1 of the February 2010 TOTM. An overall tray efficiency of 90 percent was used for all columns.

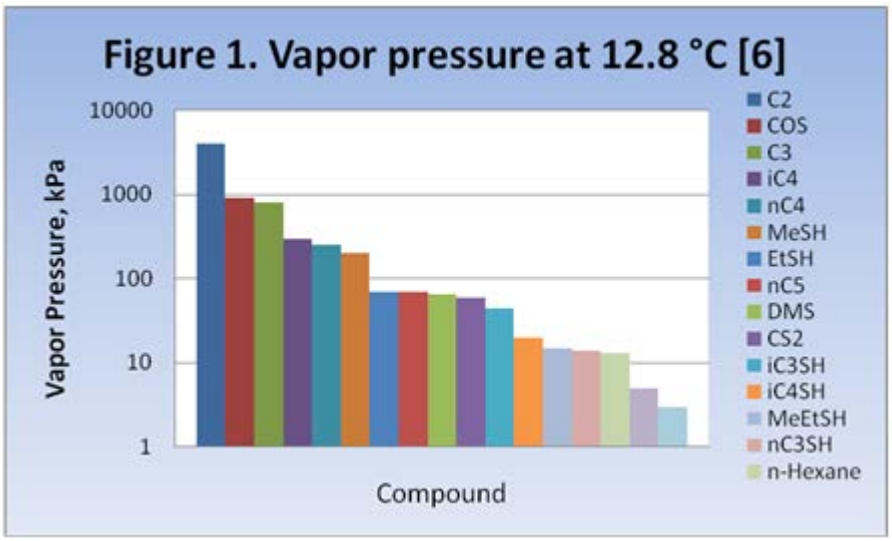

Expected Product Distribution:

Figure 1, reproduced from Figure 9 of a paper published by Likins and Hix [6], shows a descending order log scale bar-graph of the pure compounds vapor pressure for the components of interest to this study. This figure shows that COS should distribute to both the ethane and the propane streams. MeSH, with a vapor pressure close to n- butane should distribute primarily with the butanes with a small amount distributing to the pentane stream. EtSH, having a vapor pressure between butane and pentane, should distribute primarily with butane and pentane. CS2 should distribute primarily to the pentane and the C_6^+ streams with only minor distribution to the butane stream. The heavier sulfur compounds should end up almost entirely in the C_6 stream.

Results of Computer Simulation:

The NF plant described in the previous section was simulated using HYSYS [1], ProMax and VMGSim based on the PR EOS [2]. In this study, the respective software built-in (library) binary interaction parameters were used even though we recommend evaluating the accuracy of VLE results against experimental data and if necessary the insertion of VLE data regression into the EOS interaction parameters. This regression may be required to adequately model the systems dealing with mercaptans.

Component	5 Feed	9 Gas	13 Gas	16 Gas	17 C2	15 C3	20 C4	23 C5	24 C6+
HYSYS Results									
H2S	32.3	69.8	106.6	95.0	123.6	0.1	0.0	0.0	0.0
COS	3.6	3.5	0.3	0.1	1.1	9.7	0.0	0.0	0.0
MeSH	124.7	59.5	0.0	0.0	0.0	320.4	71.1	0.0	0.0
EtSH	95.8	0.0	0.0	0.0	0.0	0.0	322.4	246.5	0.0
CS2	12.5	0.0	0.0	0.0	0.0	0.0	32.1	57.5	0.0
iC3SH	17.8	0.0	0.0	0.0	0.0	0.0	0.0	133.9	103.2
iC4SH	13.4	0.0	0.0	0.0	0.0	0.0	0.0	0.0	234.7
ProMax Results									
H2S	32.3	69.3	103.7	94.1	119.9	0.0	0.0	0.0	0.0
COS	3.6	4.2	1.1	0.5	3.6	9.5	0.0	0.0	0.0
MeSH	124.7	9.2	0.0	0.0	0.0	58.0	461.9	1.6	0.0
EtSH	95.8	0.0	0.0	0.0	0.0	0.0	221.1	509.1	0.1
CS2	12.5	0.0	0.0	0.0	0.0	0.0	9.6	109.9	0.2
iC3SH	17.8	0.0	0.0	0.0	0.0	0.0	0.0	182.4	30.3
iC4SH	13.4	0.0	0.0	0.0	0.0	0.0	0.0	0.0	228.3
VMGSim Results									
H2S	32.3	71.9	105.7	93.0	123.6	0.1	0.0	0.0	0.0
COS	3.6	3.6	0.5	0.2	1.6	9.3	0.0	0.0	0.0
MeSH	124.7	63.6	0.0	0.0	0.0	332.4	53.9	0.0	0.0
EtSH	95.8	0.0	0.0	0.0	0.0	0.0	230.4	482.9	0.0
CS2	12.5	0.0	0.0	0.0	0.0	0.0	35.3	49.7	0.0
iC3SH	17.8	0.0	0.0	0.0	0.0	0.0	0.0	132.7	104.9
iC4SH	13.4	0.0	0.0	0.0	0.0	0.0	0.0	0.0	235.5

The focus of this study is on the distribution (% recovery) and concentration (PPM) of the sulfur-containing compounds in the product streams. Table 1 presents the PPM concentration of sulfur-containing compounds in the feed and product streams. Figures 2 through 8 present bar-graphs of the recovery of each sulfur-containing compound in the gas and product streams. The mole percent recovery is defined as the number of moles of a component in the product stream divided by the moles of the same component in the feed stream (Stream 5). In these figures, the gas and product streams are followed by letters H, P, and V representing HYSYS, ProMax, and VMGSim results, respectively.

H_2S: Figure 2 shows the distribution and recovery of H_2S in the gas, C_2 and C_3 product streams. As expected, the majority of the H_2S distributes in the gas and the C_2 product streams. As can be seen in this figure, the results of the simulators are the same.

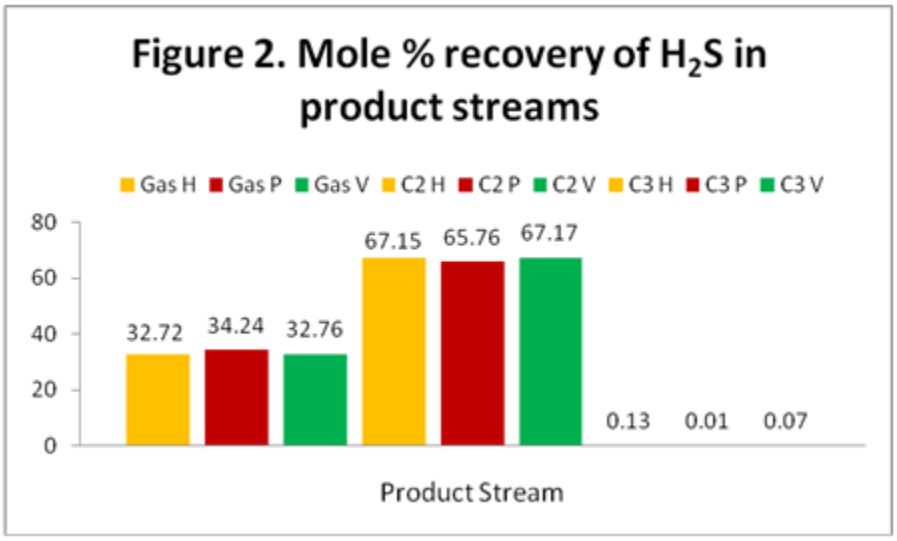

COS: Figure 3 shows the distribution and recovery of COS in the gas, C_2, and C_3. As expected, the majority of the COS ends up in the C_3 product stream. As can be seen in this figure, the results of the three simulators are almost the same.

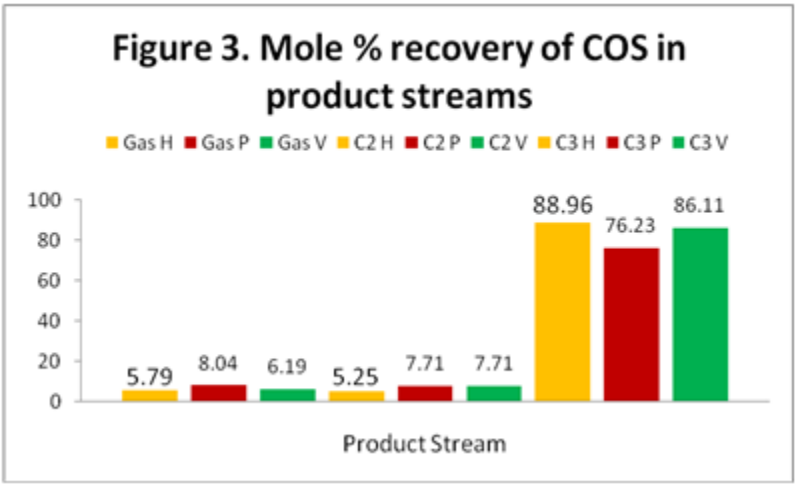

MeSH: Figure 4 shows the distribution and recovery of MeSH in the gas, C_3, and C_4 product streams. For HYSYS and VMGSim, contrary to the data presented in Figure 1, the majority of the MeSH distributes to the C_3 stream rather than to the C_4 stream. However, the ProMax result follows the same trend as in Figure 1 and the majority of MeSH distributes to the C_4 stream.

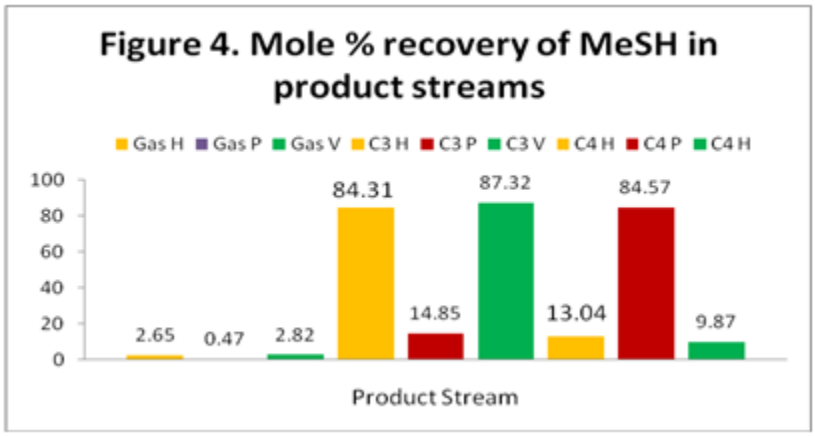

EtSH: Figure 5 shows the distribution and recovery of EtSH in the C_3, C_4, and C_5 streams. Unexpectedly, HYSYS predicts that the majority of the EtSH ends up in the C_4 stream rather than the C5 product as would be expected based on the data of Figure 1. However, the results of ProMax and VMGSim are closer to the Figure 1 data.

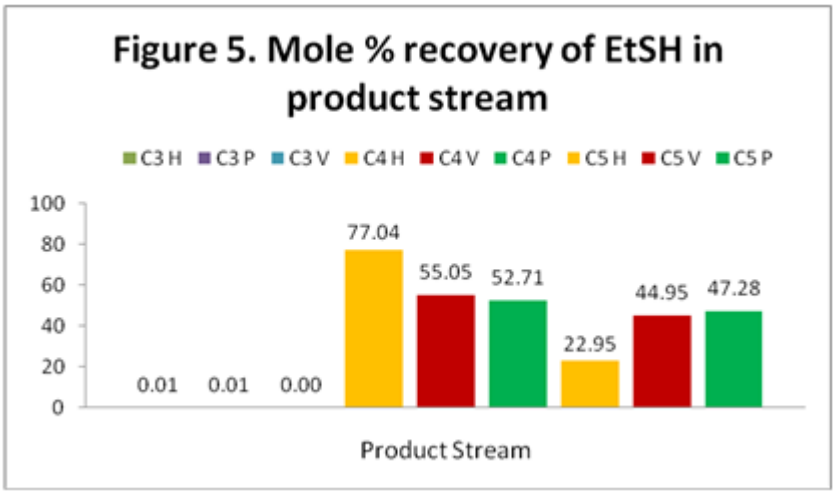

CS_2: Figure 6 shows the distribution and recovery of CS_2 in the C_4 and C_5 product streams. Contrary to the Figure 1 pure CS_2 behavior the results of HYSYS and VMGSim show that the majority of the CS_2 ends up in the C_4 stream. However, based on the ProMax results, the majority of the CS_2 ends up in the C_5 stream which is consistent with data in Figure 1.

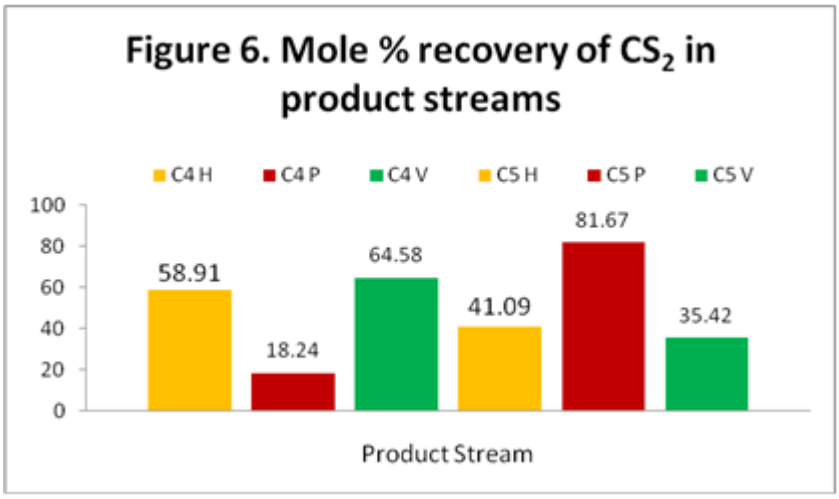

iC_3SH: Figure 7 shows the distribution and recovery of iC_3SH in the C_4, C_5 and C_{6+} product streams. As expected, iC_3SH ends up in the C_5 and C_{6+} streams. Notice that ProMax shows a higher concentration of iC_3SH in the C_5 product stream while HYSYS and VMGSim predict lower but nearly the same recovery of iC_3SH.

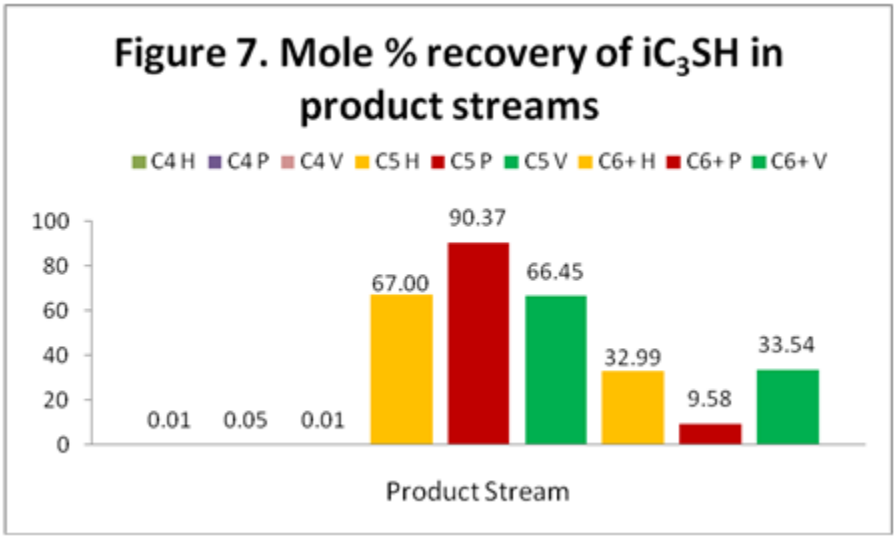

iC4SH: Figure 8 shows recovery of iC4SH in the C6+ product stream. All of the iC4SH ends up in the C6+ stream as expected when the Figure 1 data is analyzed.

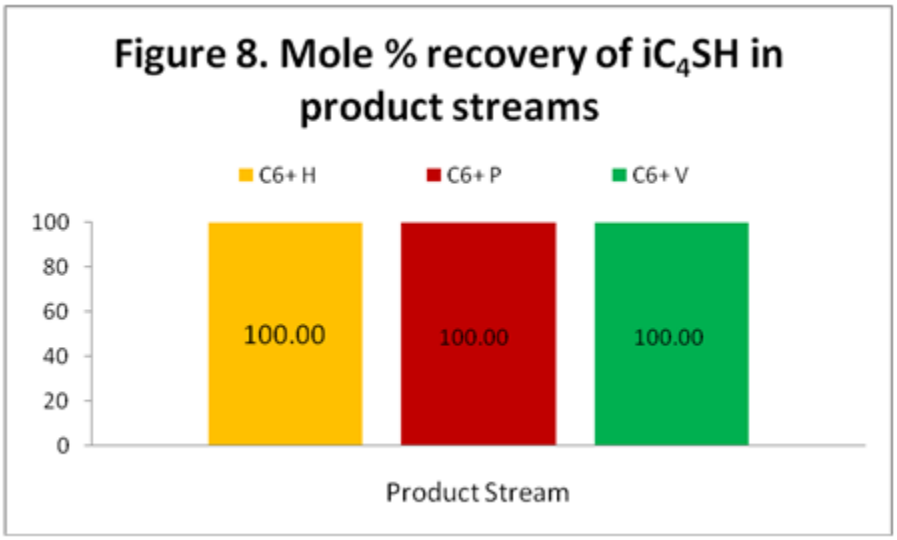

Conclusions:

The calculation results presented and discussed here are specific to the NGL fractionation plant studied here, but there are some general conclusions that can be drawn from this study.

The results indicate that the highest concentration of methyl mercaptan (MeSH) is present in the C_3 product (stream 15) based on HYSYS and VMGSim but its highest concentration is in the C_4 product (stream 20) based on the ProMax results.

The results of HYSYS indicate that the highest concentration of ethyl mercaptan (EtSH) is present in the C_4 product (stream 20) but ProMax and VMGSim results indicate that its highest concentration occurs in the C_5 Product (stream 23).

The highest concentration of carbon disulfide (CS_2) is present in C_5 Product (stream 23) according to the three simulator results.

The binary interaction parameters used in the EOS play an important role in the VLE behavior of the system under study, and affect the distribution of the sulfur-containing compounds present in the feed. Use of improper or incorrect binary interaction parameters may generate erroneous results. Care must be taken to use correct values of binary interaction parameters. In this study, the simulator library values of the binary interaction parameters were used.

The predictions by HYSYS, ProMax, and VMGSim in Figures 4 through 7 (showing the distribution of MeSH, EtSH, CS_2, and iCH_3SH respectively) contain some disagreements. The results also indicate that these compounds were not distributed among the hydrocarbon products in the same way one would expect from their volatilities and concentrations. This may be explained by the conclusion reported by Harryman and Smith [7, 8] who wrote "iC_3SH is formed during fractionation within the depropanizer and the deethanizer." Therefore, further

evaluation should be conducted to arrive at a concrete decision. *In an upcoming TOTM, we will investigate the VLE behavior of the theses systems using experimental data.* This should be a good reason to perform laboratory tests and detailed thermodynamic calculations to determine process flow rates and composition. Detailed process analysis should always be made to justify and prove correct decisions as to selection of process flow schemes.

REFERENCE

1. ASPENone, Engineering Suite, HYSYS Version 7.0, Aspen Technology, Inc., Cambridge, Massachusetts U.S.A., 2009.
2. Peng, D.,Y. and D. B. Robinson, Ind. Eng. Chem. Fundam. 15, 59-64, 1976.
3. ProMax 3.1, Bryan Research and Engineering, Inc, Bryan, Texas, 2009.
4. VMGSim 5.0.5, Virtual materials Group, Inc, Calgary, Alberta, 2010.
5. Al-Sayegh, A.R., Moshfeghian, M. Abbszadeh, M.R., Johannes, A. H. and R. N. Maddox, "Computer simulation accurately determines volatile sulfur compounds," Oil and Gas J., Oct 21, 2002.
6. Likins, W. and M. Hix, "Sulfur Distribution Prediction with Commercial Simulators," the 46th Annual Laurance Reid Gas Conditioning Conference Norman, OK 3 - 6 March, 1996.
7. Harryman, J.M. and B. Smith, "Sulfur Compounds Distribution in NGL's; Plant Test Data – GPA Section A Committee, Plant design," Proceedings 73rd GPA Annual Convention, New Orleans, Louisiana, March, 1994.
8. Harryman, J.M. and B. Smith, "Update on Sulfur Compounds Distribution in NGL's; Plant Test Data – GPA Section A Committee, Plant design," Proceedings 75th GPA Annual Convention, Denver, Colorado, March, 1996.

Process Analysis of Hydrogen Blistering in NGL Fractionation Unit

By Dr. Mahmood Moshfeghian

Hydrogen blistering is a type of hydrogen-induced failure produced when hydrogen atoms enter low-strength steels that have macroscopic defects, such as laminations. The defects in the steel (void spaces) provide places for hydrogen atoms to combine, forming gaseous molecular hydrogen (H_2) that can build enough pressure to produce blistering. Hydrogen blistering is a problem mainly in sour environments. It does not cause a brittle failure, but it can produce rupture or leakage [1]. Description and mechanisms of hydrogen blistering can be found in literature [2]. Hydrogen sulfide concentration, temperature and thickness of material affect hydrogen blistering.

In this TOTM we will consider the quantitative effect of temperature and hydrogen sulfide mole fraction causing hydrogen damage in the fractionation columns of an operating natural gasoline liquid (NGL) Plant [3]. The fractionation unit was designed to process a broad-cut of NGL, which is an off-product from crude oil production units and produces essentially propane, butane, and natural gasoline. The feed to the process is introduced into the fractionation unit where propane, butane and gasoline are separated by three distillation columns. In the first column, which is a deethanizer, ethane and lighter compounds are separated from the feed stream. In the second column, a depropanizer, propane is fractionated and sent to the amine treater for further processing to meet market specifications. The bottoms of the depropanizer are fed to the third column, a debutanizer, in which butane is distilled over and sent to a Merox unit for further treating. The bottoms of the debutanizer column, essentially gasoline, are also sent to Merox for treating. More information on NGL production technologies can be found in reference [4].

During the overhaul of this NGL Plant, the inspection team found that the deethanizer-reflux-accumulator had been damaged due to severe hydrogen blistering in the shell and bottom plate, and the vessel was rejected. Four years later, during an inspection of the Plant, the deethanizer rectifying section and depropanizer rectifying section were found to have been severely damaged by hydrogen blistering.

In order to study the effects of hydrogen sulfide and local temperature quantitatively and more closely, the three distillation columns in a fractionation unit were simulated. In this simulation, which could assist one to thoroughly understand the causes of hydrogen attack, the values of temperature and hydrogen sulfide mole fraction along each column were determined by performing tray-by-tray calculations.

Case Study:

The operating NGL Plant consists of fractionation, treating, drying, refrigeration, utility, storage and loading facilities to process approximately 57,700 barrels (9172 m^3) of broad-cut NGL per day. The charge to this plant is essentially Natural Gasoline Liquid which is condensed out of oil-field gas, and off-product from several crude oil production units. The broad-cut is

processed to produce propane, butane and light gasoline (Pentane Plus Product). The feed stream also contains some impurities such as hydrogen sulfide, carbon dioxide and mercaptan, which are removed by treating the products after fractionation.

Since hydrogen blistering occurred only in the fractionation unit, a brief description of this unit is given in the following section [3].

A schematic flow diagram for this unit is given in Figure 1. The 40-tray deethanizer tower receives raw feed from NGL recovery plants, fractionates out ethane and lighter products and delivers essentially ethane-free NGL to the depropanizer column. The feed to the deethanizer is introduced between the 27th and 28th trays at 135°F and 362 Psig (57.2 °C and 2497 kPag). Bottoms product from the deethanizer is charged to tray 22 of a 45-tray depropanizer column. The distillate product, which is essentially propane, is sent to the amine treater unit for further processing. The depropanizer bottoms are charged to tray 20 of the 40-tray debutanizer column. The debutanizer distillate product, which comprises the net butane product, is sent to the Merox plant for treating. The debutanizer bottom (pentane and heavier products essentially free of butane) is also sent to the Merox plant for further processing.

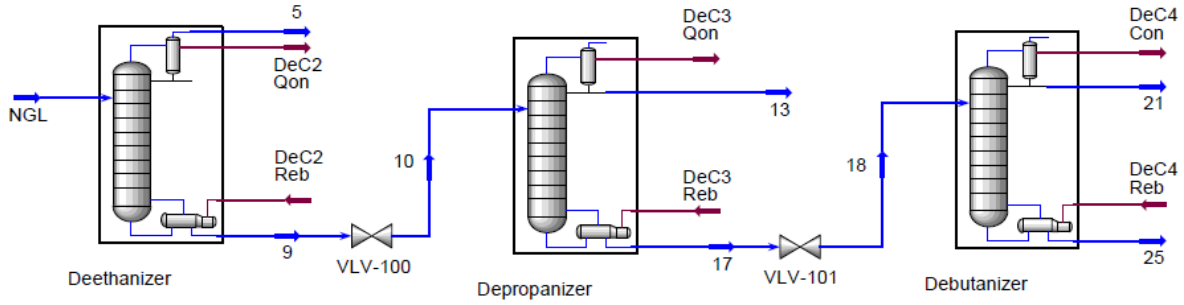

Figure 1. Flow diagram of fractionation unit

The following information was specified for simulation of the fractionation unit:

(i) Flow diagram as shown in Figure 1

(ii) Feed stream condition and composition as shown in Table 1

(iii) Column specification as presented in Table 2

Other specifications such as a desired percentage recovery of a component in any product stream, could have been used instead of the reflux ratio or bottoms product ratio. In the course of simulation, tray by tray calculations were performed to calculate temperature, pressure, vapor and liquid compositions, and vapor and liquid traffics for each tray in each column. In addition, distillate and bottoms rates, temperature, pressure, composition, reboiler and condenser duties were also calculated, as were height and diameter of the columns.

To perform the simulation, Vapor Liquid Equilibrium K-values, liquid and vapor enthalpies were computed by the Peng-Robinson equation of state [5]. In the tray-by-tray calculation it was assumed that the trays performed ideally (100 % efficiency). The simulation was carried out by UniSim simulation software [6]

Table 1. Feed stream composition and specification

Component	Mole %
CO2	1.167
H2S	0.325
Methane	5.625
Ethane	15.724
Propane	28.190
i-Butane	6.724
n-Butane	17.812
i-Pentane	5.812
n-Pentane	6.846
n-Hexane	5.998
C_{7+}	5.777
T, °F (°C)	135.0 (57.2)
P, Psig (kPag)	362.0 (2497)
Rate, lbmole/hr (kmole/h)	8619 (3909)

Table 2. Fractionation towers specifications

Column	Pressure, Psig (kPag)			No of Trays	Feed Tray from Bottom	Reflux Ratio, L/F	Bottoms Ratio, B/F	Condenser Type
	Feed	Condenser	Reboiler					
Deethanizer	362 (2497)	347 (2393)	360 (2483)	40	27	0.4438	0.7749	Partial
Depropnizer	300 (2069)	290 (2000)	300 (2069)	45	22	1.0709	0.6415	Total
Debutanizer	95 (655)	85 (586)	95 (655)	40	20	1.0082	0.4889	Total

Results and Discussion:

Performing a simulation, a great deal of information is produced. However, only information of interest in regard to hydrogen blistering is presented here. To test the validity of the simulation results,

composition and condition of the key process streams are compared with those supplied by the designer of the plant [7] and presented in Table 3. In most cases the results compare favorably. In addition, condenser and reboiler duties for each column are compared with the original design values in Table 4. This comparison of the two sets of results shows a maximum deviation of –13.3% for the depropanizer reboiler. With the exception of the deethanizer boiler, all of the design heat exchange duties are higher than those obtained in this simulation, which is, of course, a normal safeguard in plant design.

Table 3 shows hydrogen sulfide is fractionated in the first two columns and does not reach the debutanizer column. Since hydrogen blistering occurred in the first two columns, only these results were examined closely. To study the variation of hydrogen sulfide composition (in both liquid and vapor phases) along each column, its composition is plotted as a function of tray number. This is shown in Figure 2 for the deethanizer and Figure 3 for the depropanizer.

Table 3. Comparison of simulation results and design data for process streams leaving fractionation towers

Component	Stream 5		Stream 13		Stream 21		Stream 25	
	Simulation	Design	Simulation	Design	Simulation	Design	Simulation	Design
CO2	5.183	5.184	0.000	0.000	0.000	0.000	0.000	0.000
H2S	1.213	1.149	0.185	0.208	0.000	0.000	0.000	0.000
Methane	24.983	24.991	0.000	0.000	0.000	0.000	0.000	0.000
Ethane	65.138	66.171	3.812	2.994	0.000	0.000	0.000	0.000
Propane	3.483	2.505	92.460	95.808	6.779	3.987	0.000	0.000
i-Butane	0.000	0.000	3.244	0.890	22.918	25.484	0.002	0.011
n-Butane	0.000	0.000	0.298	0.100	69.276	69.542	0.529	0.477
i-Pentane	0.000	0.000	0.000	0.000	0.990	0.923	22.880	22.951
n-Pentane	0.000	0.000	0.000	0.000	0.037	0.064	28.133	28.105
n-Hexane	0.000	0.000	0.000	0.000	0.000	0.000	24.682	24.682
C_{7+}	0.000	0.000	0.000	0.000	0.000	0.000	23.773	23.774
Total	100.0	100.0	100.0	100.0	100.0	100.0	100.0	100.0
T, F	16.4	20.0	134.5	141.0	131.2	144.0	264.6	273.0
T, C	-8.7	-6.7	56.9	60.6	55.1	62.2	129.2	133.9
P, psig	347		290		85		95	
P, kPa(g)	2393		2000		586		655	
Rate, lbmole/hr	1940.4	1939.8	2394.1	2394.1	2189.6	2189.6	2094.5	2094.5
Rate, kmole/h	880.2	879.9	1086.0	1085.9	993.2	993.2	950.1	950.0

Similarly, in Figure 4, the temperature variation along these two columns is plotted as a function of tray number, and it can be seen that the temperature profiles decrease smoothly from bottom to top except in the feed zone, which is to be expected in distillation column with no side draw or inter-stage reboiler/cooler.

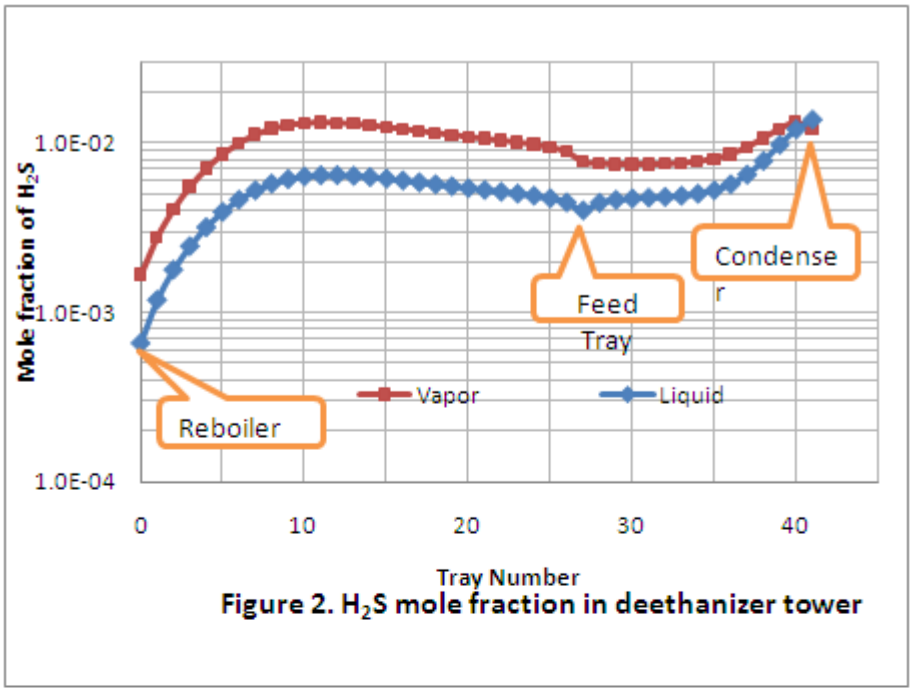

Figure 2. H_2S mole fraction in deethanizer tower

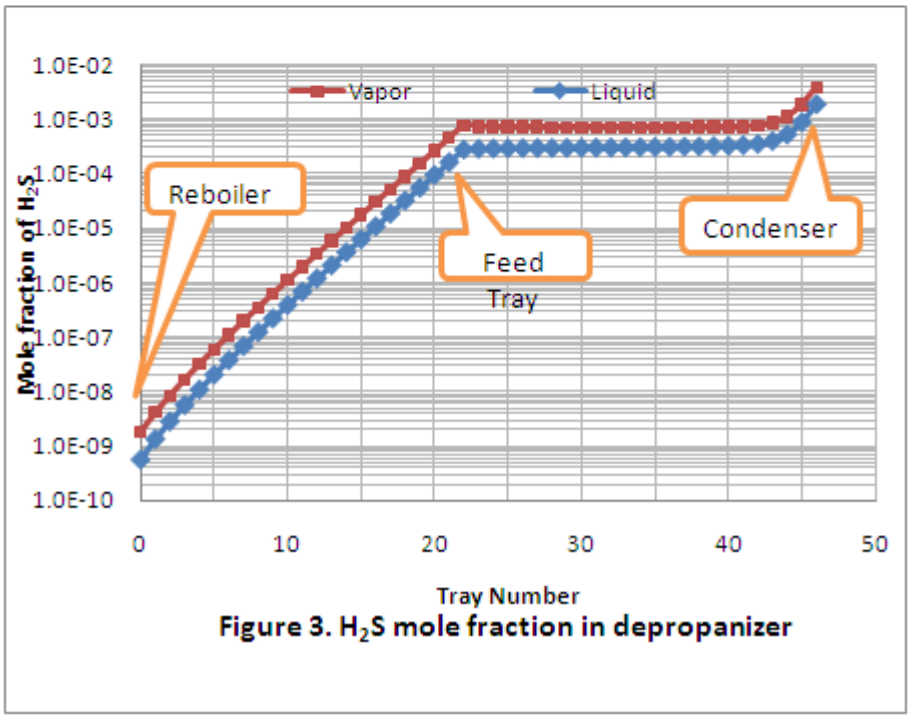

Figure 3. H_2S mole fraction in depropanizer

Figure 2 indicates that the maximum mole fraction of hydrogen sulfide occurred on tray 11 in the stripping section of the deethanizer while hydrogen blistering occurred in the rectifying section. Therefore, other factors such as temperature must be influencing the hydrogen damage. In the stripping section where no hydrogen blistering occurred, the temperature was higher than in the rectifying section where hydrogen blistering was detected. Another region where hydrogen blistering was found is the top part of the depropanizer rectifying section. In this section of the column, the hydrogen sulfide mole fraction is almost the same as in the stripping section of the deethanizer; however the temperatures for these two sections are not the same. The temperature range for the deethanizer stripping section is 142° to 240°F (61.1 to 115.6°C), and for the troubled region of the depropanizer, it is 142° to 134° F (61.1 to 56.6°C), trays 44, 45 and the condenser. Again, it can be seen how temperature influences the hydrogen blistering damage process. In this case, the hydrogen blistering was occurring at lower temperatures. Simulation results also indicate that carbon dioxide does not reach the depropanizer and debutanizer.

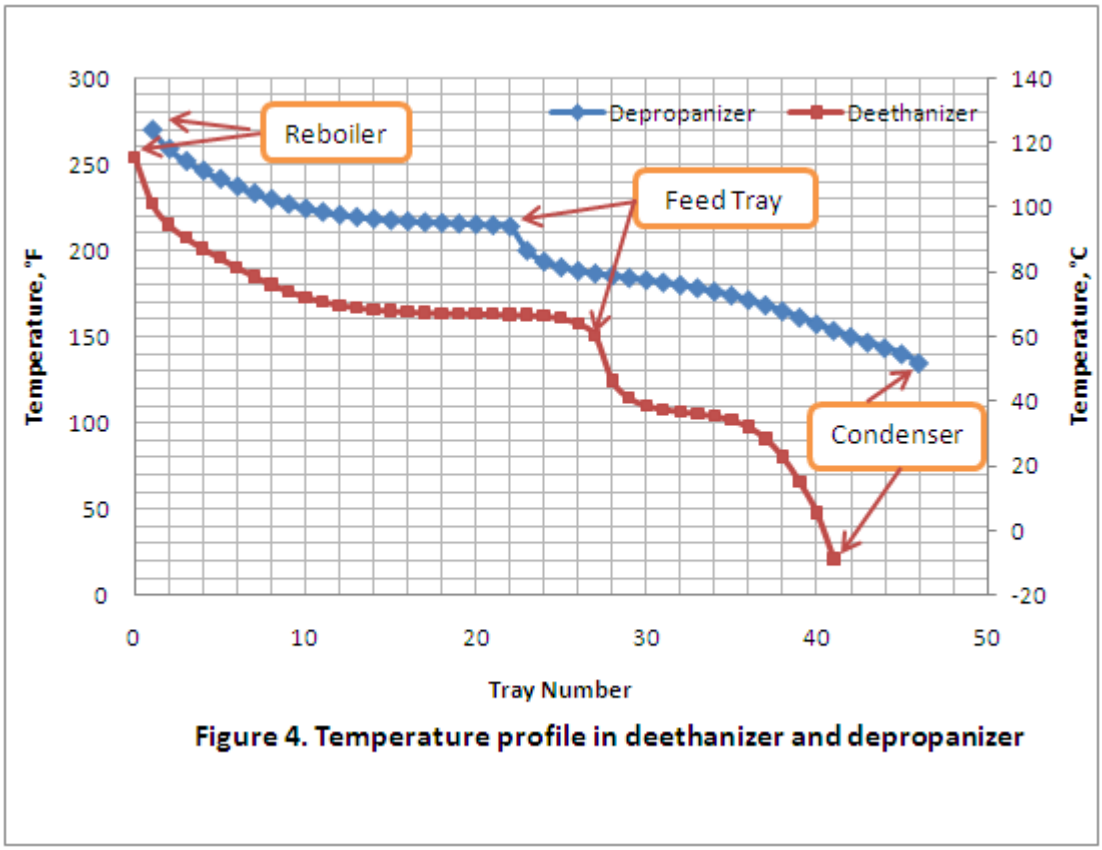

Figure 4. Temperature profile in deethanizer and depropanizer

Conclusions:

Based on the simulation results and preceding discussion, the following conclusions can be made:

1- Hydrogen blistering can occur where hydrogen sulfide is present. In the case studied a mole fraction of as low as 0.002 for hydrogen sulfide caused hydrogen damage.

2- With the presence of hydrogen sulfide, temperature is the important factor promoting hydrogen blistering. In the case studied a temperature of less than 142°F (61.1°C) caused hydrogen damage. Higher temperature drives hydrogen out of the wall to atmosphere.

There are probably other factors governing hydrogen damage such as microstructure of materials, thickness of material, presence of CO_2, etc. Even though the simulation was performed based on a dry feed, the actual feed to the plant contained some water.

The above results are consistent and the same as those reported by the author in 1985 [3]. In the original work, the simulation was carried out by a computer package named Process Analysis System (PAS) developed by Erbar and Maddox [8]. At that time, the computations were made on an IBM 370 main frame at Shiraz University Computing Center. The Soave-Redlich-Kwong [9] equation of state was used in the original work.

A heat exchanger failure at the Tesoro Anacortes refinery was determined to have experienced a form of hydrogen blistering. That failure led to the deaths of seven workers and the refinery was shut down for over six months to repair the damage. It was determined that the root cause of the failure was hydrogen blistering in the steel of the heat exchanger which resulted in rupture. These types of hydrogen attacks can be discovered during scheduled inspections. If there is a concern that conditions are conducive to hydrogen blistering, one can use a hydrogen patch probe to measure hydrogen activity within metals. If hydrogen activity is found in the metal, then additional testing can be completed to determine if any internal cracks have developed.

REFERENCES

1. http://www.glossary.oilfield.slb.com/Display.cfm?Term=hydrogen%20blistering
2. Mostert, R., and Sharp, W.R., "Low Temperature Hydrogen Damage Assessment in the Gas and Refining Industries," 3rd Middle East Nondestructive Testing Conference & Exhibition - Bahrain, Manama, 27-30 Nov 2005.
3. Moshfeghian, M., "Hydrogen damage (Blistering) case study: Mahshahr NGL Plant", Iranian J. of Science & Technology, Vol 11, No.1, 1985.
4. Campbell, J. M., "Gas Conditioning and Processing", Vol. 2, The Equipment Module, 8th Ed., Second Printing, J. M. Campbell and Company, Norman, Oklahoma, 2002
5. Peng, D. Y. and Robinson, D. B., *I. and E. C. Fund*, Vol. 15, p. 59, 1976.
6. UniSim Design R390.1, Honeywell International, Inc., Calgary, Canada, 2010.
7. Parsons, R. M., NGL Fractionation Facilities, Operation Manual Bandar Mahshahr, The Ralph M. Parsons Company U. K. Ltd.
8. Erbar, J. H., and Maddox, R. N., Process Analysis System, *Documentation*, Oklahoma State University, Stillwater OK., 1978.
9. Soave, G., *Chem. Eng. Sci.* Vol. 27, No. 6, p. 1197, 1972.

Considering the Effect of Crude Oil Viscosity on Pumping Requirements

By Dr. Mahmood Moshfeghian

In the August 2009 Tip of the Month (TOTM), it was shown that pumping power requirement varies as the crude oil °API changes. Increasing °API or line average temperature reduces the crude oil viscosity. The viscosity reduction caused higher Reynolds number, lower friction factor and in effect lowered pumping power requirements. Since the objective of the August 2009 TOTM was to study the effect °API and the line average temperature have on the pumping power requirement, the effect of crude oil viscosity on pump performance was ignored and in the course of calculation a constant pump efficiency of η =0.75 was used for all cases. In this TOTM, we will consider the crude oil viscosity effect on a selected pump performance. The Hydraulic Institute Standards [1] procedures and the guideline presented in the August 2006 TOTM written by Honeywell were applied to correct the pump efficiency.

As in the August 2009 TOTM, we will study crude oil °API and the pipeline average temperature and how these effect the pumping requirement. For a case study, we will consider a 160.9 km (100 miles) pipeline with an outside diameter of 406.4 mm (16 in) carrying crude oil with a flow rate of 0.313 m^3/s or 1,126 m^3/h (170,000 bbl/day or 4958 GPM). The pipeline design pressure is 8.963 MPa (1300 psia) with a maximum operating pressure of 8.067 MPa (1170 psia). The wall thickness was estimated to be 6.12 mm (0.24 in). The wall roughness is 51 microns (0.002 in) or a relative roughness (ε/D) of 0.00013. The procedures outlined in the March 2009 TOTM were used to calculate the line pressure drop due to friction. Then **corrected pumping efficiency was used** to calculate the required pumping power. Since the objective was to study the effect °API and the line average temperature have on the pumping power requirement, we will ignore elevation change. The change in pumping power requirements due to changes in crude oil °API and line average temperature for this case study will be demonstrated.

Viscosity Effect on Centrifugal Pump Performance

There are several papers investigating and presenting procedures for correcting centrifugal pump curves [2-3]. According to Turzo *et al.* [2], three models are available for correcting performance curves: Hydraulic Institute, Stepanoff, and Paciga. Turzo *et al.* [2] also presented a computer applications for correcting pump curves for viscosity effect. In this review, the Hydraulic Institute [1], HI, procedure was applied and is described briefly here.

HI uses a performance factor, called Parameter *B* which includes terms for viscosity, speed, flow rate and total head. The method uses a new basis for determining the correction factors C_H, C_Q, and C_n. The basic equation for Parameter *B* is given as Equation 1.

$$B = K\left[\frac{(\nu_{vis})^{0.50}(H_{BEP-W})^{0.0625}}{(Q_{BEP-W})^{0.375}(N)^{0.25}}\right] \qquad (1)$$

B = Performance factor
K = 16.5 for SI units
= 26.5 for USCS (FPS)
ν_{vis} = Viscous fluid Kinematic viscosity – cSt
H_{BEP-W} = Water head per stage at BEP – m (ft)
Q_{BEP-W} = Water flow rate at BEP – m^3/h (gpm)
N = Pump shaft speed – rpm

Correction factors are applied to capacity (C_Q), head (C_H), and efficiency (C_η). Calculation of these Correction Factors is dependent on the calculated value of Parameter *B*. For the cases considered in this study, the *B* values were less than 1; therefore, based on the HI guideline, the correction factors for head and capacity were set equal to 1 and the correction factor for efficiency, $C\eta$, was calculated by Equation 2.

$$C\eta = \frac{1-\left[(1-\eta_{BEP-W})\left(\frac{\nu_{vis}}{\nu_w}\right)\right]}{\eta_{BEP-W}} \qquad (2)$$

η_{BEP-W} = Pump efficiency at BEP
ν_w = Water kinematic viscosity – cSt

Figures 1 and 2 present the water-based pump curves used in this study. For computer calculations, these two curves were fitted to polynomials of degrees 3 and 2 for head vs. capacity and efficiency vs. capacity, respectively.

$H = 363.0439 + 0.0471Q - 3.8928\times10^{-5}Q^2 - 1.0161\times10^{-9}Q^3$ (3 SI)

$H = 1191.0714 + 0.03509Q - 6.6017\times10^{-6}Q^2 - 3.78788\times10^{-11}Q^3$ (3 FPS)

$\eta = 6.8723 + 0.08734Q - 2.4932\times10^{-3}Q^2$ (4 SI)

$\eta = 6.8752 + 0.01984Q - 1.2861\times10^{-6}Q^2$ (4 FPS)

In Equations 3 and 4, H is in m (ft) and Q is in m^3/h (GPM). For this pump:

H_{BEP-W}=323m=1060ft, Q_{BEP-W}=1726 m^3/h= 7600 GPM, N=1780 rpm, and η_{BEP-W}=83.4.

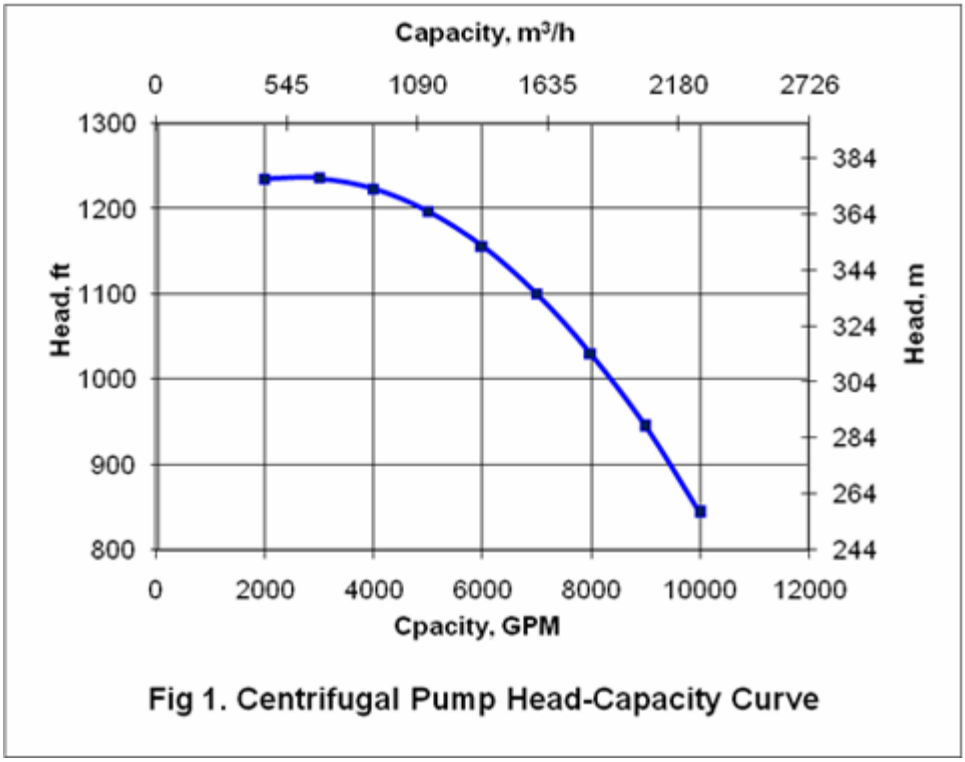

Fig 1. Centrifugal Pump Head-Capacity Curve

Case Study 1: Effect of Line Average Temperature (Seasonal Variation)

To study the effect of the line average temperature on the pumping power requirement, an in house computer program called ***OP&P*** (Oil Production and Processing) was used to perform the calculations outlined in the March 2009 TOTM. For a 35 °API crude oil in the pipeline described the required pumping power was calculated for line average temperature ranging 21.1 to 37.8 °C (70 to 100 °F). For each case, the parameter *B* was calculated by Equation 1 and since its value was less than 1, the efficiency correction factor was calculated by Equation 2. Then, the pump efficiency calculated by Equation 4 was multiplied by the correction factor for the subsequent calculations.

The corrected efficiency ranged from 0.70 to 0.72. The required pumping power was compared with an arbitrary base case (85 °F or 29.4 °C and constant η = 0.75) and the percentage change in the pumping power requirement was calculated. Figure 3 presents the percent change in power requirement as a function of line average temperature. There is about 5% change (for constant η=0.75) and more than 8% change (for corrected efficiency) in the pumping power requirement for the temperature range considered.

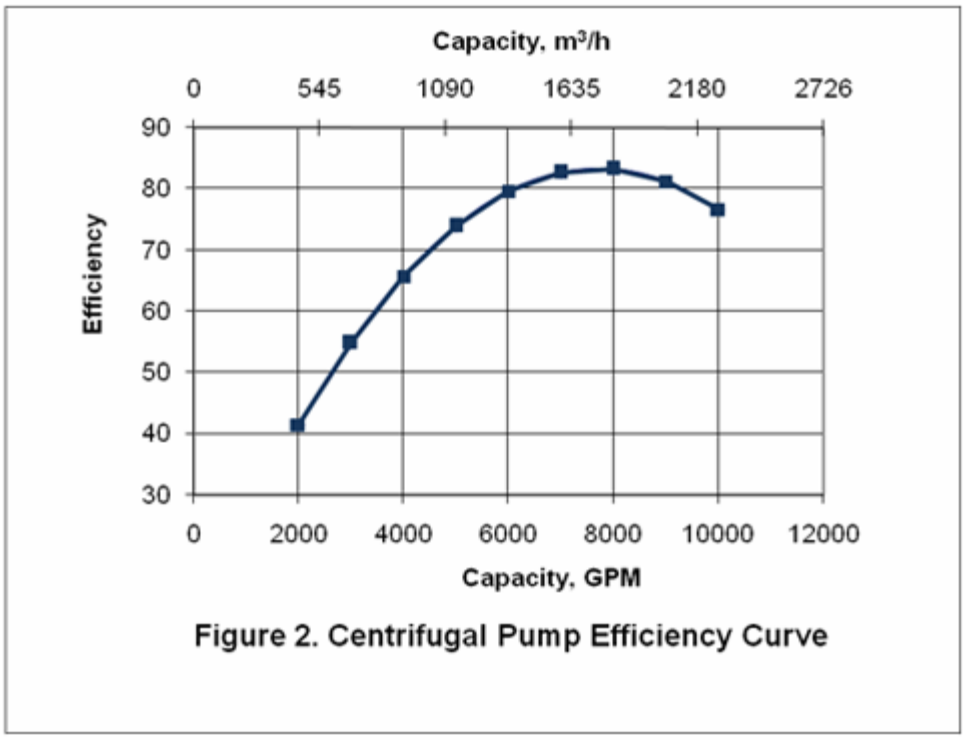

Figure 2. Centrifugal Pump Efficiency Curve

Note that as the line average temperature increases the power requirement decreases. This can be explained by referring to Figure 4 in which the oil viscosity decreases as the temperature increases. Lower viscosity results in higher Reynolds (i.e. Reynolds number $\mathrm{Re} = \frac{(V)(D)(\rho)}{\mu}$ which is the ratio of inertia force to viscous force); therefore, the friction factor decreases (refer to the Moody friction factor diagram in the March 2009 TOTM).

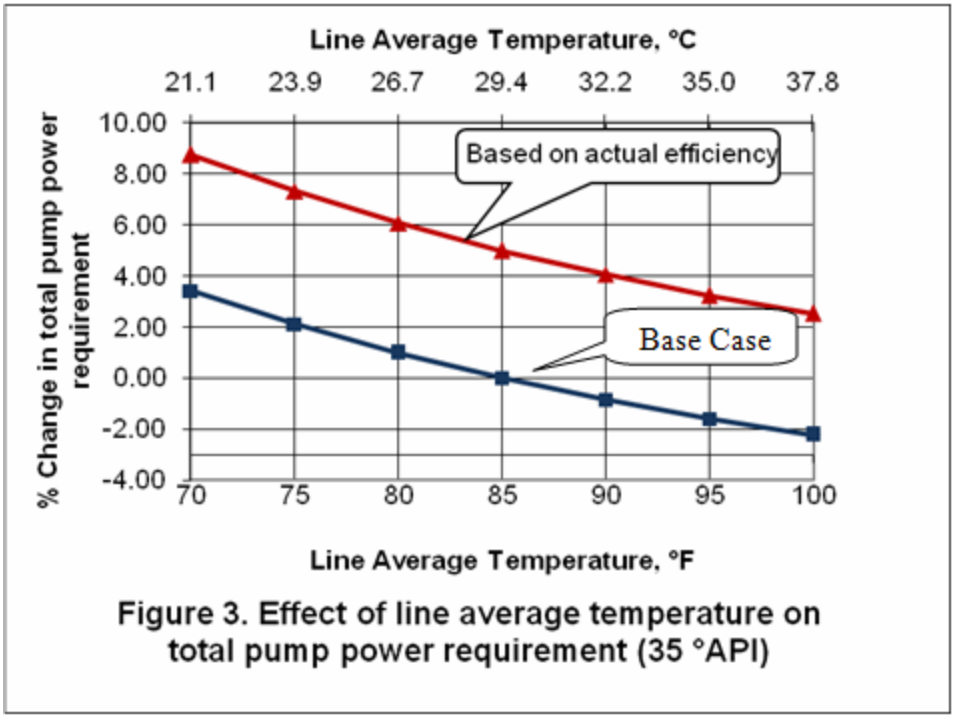

Figure 3. Effect of line average temperature on total pump power requirement (35 °API)

Case Study 2: Effect of Variation of Crude Oil °API

In this case, the effect of crude oil °API on the total pump power requirement for three different line average temperatures was studied. For each line average temperature, the crude oil °API was varied from 30 to 40 and the total pumping power requirement was calculated and compared to the base case (35 °API and average line temperature of 29.4°C=85°F).

For each case the percent change in total power requirement was calculated and is presented in Figure 5. As shown, when °API increases the total power requirement decreases. This also can be explained by referring to Figure 4 in which the crude oil viscosity decreases as ° API increases. The effect of viscosity is more pronounced at lower line average temperature (i.e. 21.1 °C or 70°F). Figure 5 also indicates that there is about 30 % change in total power requirement as °API varies from 30 to 40 °API. This is a significant variation and suggests that it should be considered during design of crude oil pipelines.

Discussion and Conclusions

The analysis of Figures 3 and 5 indicates that for the oil pipeline, the pumping power requirement varies as the crude oil °API changes. Increasing °API or line average temperature reduces the crude oil viscosity (see Figure 4). The reduction of viscosity results in a higher Reynolds number, lower friction factor and in effect lowers pumping power requirements. For the cases studied in this TOTM, the effect of crude oil viscosity on the performance of pump was considered. It was found that no correction was required for the capacity and head but a

correction factor in the range of 0.95 to 0.98 was required to adjust the pump efficiency for crude oil applications.

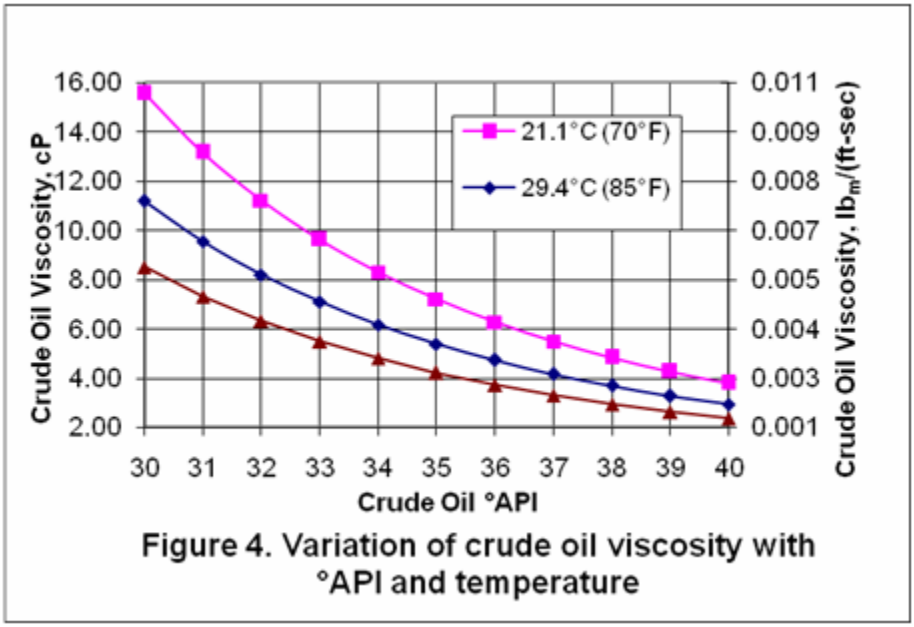

Figure 4. Variation of crude oil viscosity with °API and temperature

A sound pipeline design should consider expected variations in crude oil °API and the line average temperature. In addition, the pump performance curves should be corrected for the effect of viscosity.

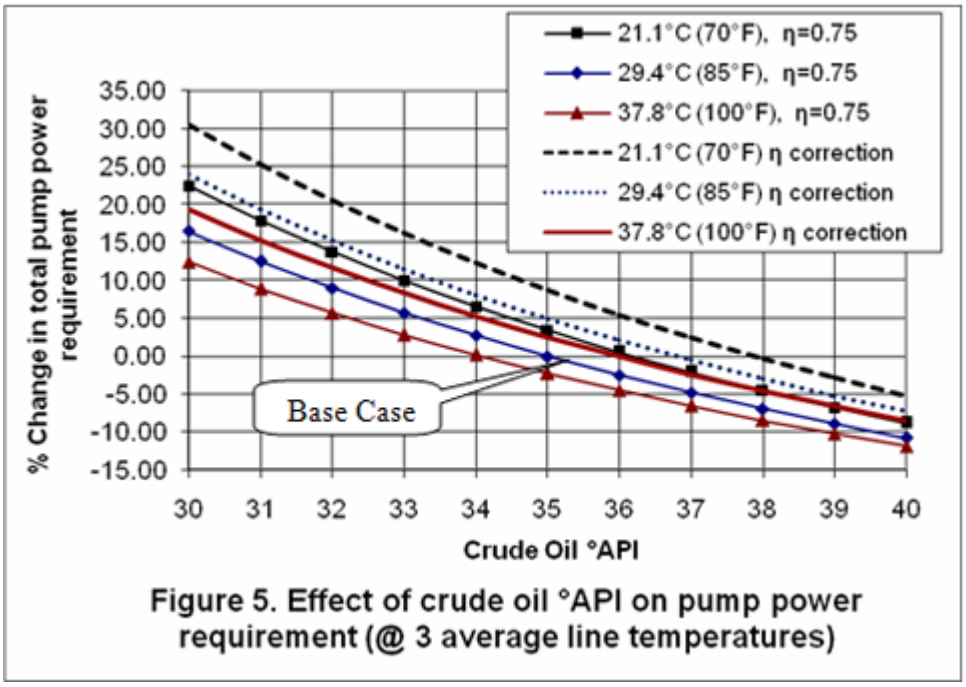

Figure 5. Effect of crude oil °API on pump power requirement (@ 3 average line temperatures)

REFERENCES

1. ANSI HI 9.6.7-2004, “Effects of Liquid Viscosity on Rotodynamic (Centrifugal and Vertical) Pump Performance”, 2004.
2. Turzo, Z.; Takacs, G. and Zsuga, J., “Equations Correct Centrifugal Pump Curves for Viscosity,” Oil & Gas J., pp. 57-61, May 2000.
3. Karassik, I.J., “Centrifugal Pumps and System Hydraulics,” Chem. Engr. J., pp.84-106, Oct. 4, 1982

How to Tune the EOS in your Process Simulation Software?

By Dr. Mahmood Moshfeghian

Process simulation computer programs are excellent tools for designing or evaluating gas processing plants, chemical plants, oil refineries or pipelines. In these simulation programs, most of the thermodynamic properties are calculated by an equation of state (EOS). The cubic equations of state can be regarded as the heart of these programs for generating the required properties. However, none of the equations of state is perfect and often some sort of tuning must be done prior to their applications. Some tuning is already done by researchers and has been embedded in the data base of these simulation programs. In dealing with non-standard or complex systems, the user should check the validity and accuracy of the selected thermodynamic package (i.e. EOS) in the simulation programs prior to attempting to run the desired simulation. Often the users find that tuning is required. This can be done by performing a series of vapor liquid equilibria (VLE) calculations such as dew point, bubble point or flash calculations and comparing the results with the field data or experimental data. If the accuracy is not within acceptable range, then the EOS should be tuned to improve its accuracy. The tuning can be done in several ways but the one most often used is adjusting/regressing the binary interaction parameters between binary pairs in the mixture using the experimental PVT or VLE data.

In this tip of the month (TOTM), we will demonstrate how the binary interaction parameters are tuned in a simulation program to improve the accuracy of a selected EOS. For this purpose, we will demonstrate how the accuracy of the bubble point pressure prediction of a ternary system of carbon dioxide, pentadecane, and hexadecane can be improved. We will use the Peng-Robinson (PR) [1] equation of state in ProMax [2] and the experimental VLE data published in the literature [3]. The same procedure can be used with any EOS in other simulation programs.

The PR EOS

The PR EOS [2] in terms of pressure (P), volume (v) and temperature (T) is defined as:

$$P = \frac{RT}{v-b} - \frac{a}{v(v+b)+b(v-b)} \quad (1)$$

The values of the parameters a and b must be determined in a special way for mixtures. Any equation, or series of equations, used to obtain mixture parameters is called a *combination rule* or *mixing rule*. The calculation, regardless of its exact form, is based on the premise that the properties of a mixture are some kind of weighted average summation of the properties of the individual molecules comprising that mixture.

The mixing rules used in cubic equations of state (i.e., Peng-Robinson, Soave-Redlich-Kwong, and van der Waals) are

$$a = \sum_i^n \sum_j^n x_i x_j a_i^{e.5} a_j^{0.5} (1 - k_{ij}) \quad (2)$$

$$b = \sum_i^n x_i b_i \quad (3)$$

Where: a and b = the interaction energy and molecular size parameters for the mixture

a_i, b_i = a and b parameters for component i in the mixture

x_i = composition (mol fraction) for component i in the mixture

k_{ij} = binary interaction parameter

n = number of component in the mixture

R = Universal gas constant

The a_i and b_i for each component in the mixture are calculated in terms of critical temperature (Tc_i), pressure (Pc_i), and acentric factor (ω_i) as presented in equations 4 and 5.

$$a_i = \left(0.45724 \frac{R^2 Tc_i^2}{Pc_i}\right)\left[\sqrt{1 + (1 - Tr_i^{0.5})(0.37464 + 1.54226\omega_i - 0.26992\omega_i^2)}\right] \quad (4)$$

$$b_i = 0.07780 \frac{RTc_i}{Pc_i} \quad (5)$$

Once a and b have been determined, the equation of state computations proceed as though a and b were for a pure component. With cubic equations of state the mixing rules sum the properties based on binary pairs.

The binary interaction parameter, k_{ij}, has no theoretical basis. It is empirical and is used to overcome deficiencies in the corresponding states theory or the basic model (equation of state). Binary interaction parameters are regressed from experimental data for a specific model and should be applied in that model only. In addition, k_{ij}'s can be determined from regression of PVT data or VLE data. This will result in different k_{ij}'s for the same binary mixture.

The Effect of k_{ij} on Bubble Point Pressure Prediction

To study the effect of the k_{ij}, the bubble point pressure for a binary mixture of CO_2 (1) and pentadecane (2) at 40 °C for a series of CO_2 mole % in the liquid phase were predicted using the PR EOS in ProMax. First, the default value of the binary interaction in the data base (DB) of ProMax in which k_{12}=0.0 was used. The predicted results were compared with the experimental values and the average absolute percent deviation (AAPD) for eight data points calculated to be 41.06%. This AAPD was reduced to 1.64% when the binary interaction parameter of k_{12}=0.112 was used. Figure 1 presents the effect of k_{12} on the predicted bubble point pressure of CO_2 and pentadecane mixture.

This figure demonstrates clearly the role of k_{ij} in improving the accuracy for bubble point pressure calculations. The improvement is substantial and the accuracy now is as good as the experimental data.

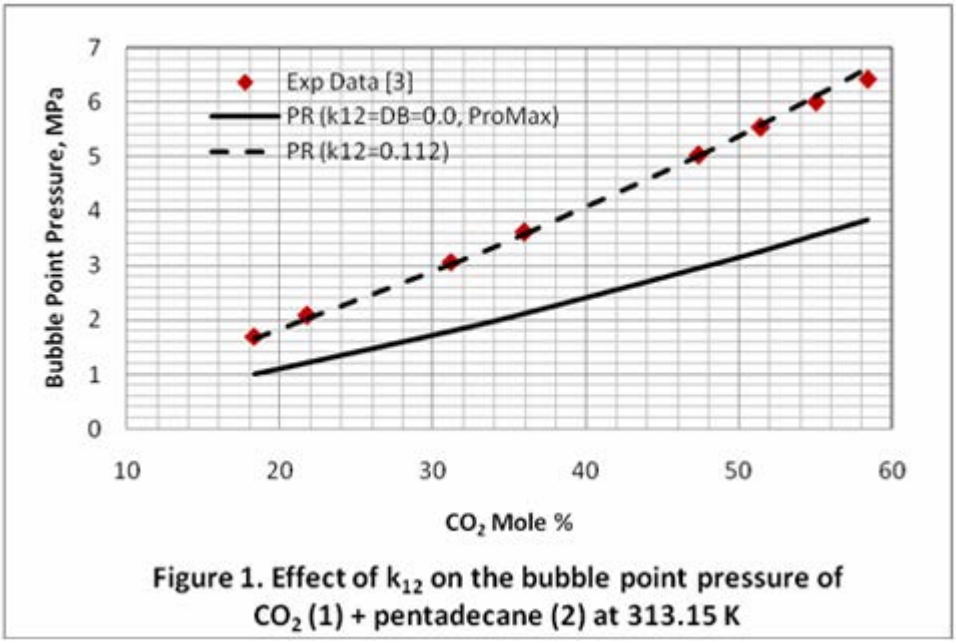

Figure 1. Effect of k_{12} on the bubble point pressure of CO_2 (1) + pentadecane (2) at 313.15 K

Similar improvement is observed when the binary interaction parameter, k_{12}, was changed from zero, and the default value in data base (k12=DB) of ProMax, to 0.112 for the binary mixture of CO_2 (1) and hexadecane (2) at 40 °C. For this case the AAPDs were 40.65%, 3.64% and 1.26% for k_{12}=0.0, k12=DB, and k_{12}=0.112; respectively.

For these two systems the liquid densities were also predicted and compared with the experimental values. For CO_2 and pentadecane binary system, the calculated AAPD for liquid densities were 6.10% and 6.36% for k_{12}=0.0 and k_{12}=0.112; respectively. Similar AAPD changes were observed for CO_2 and hexadecane binary mixture.

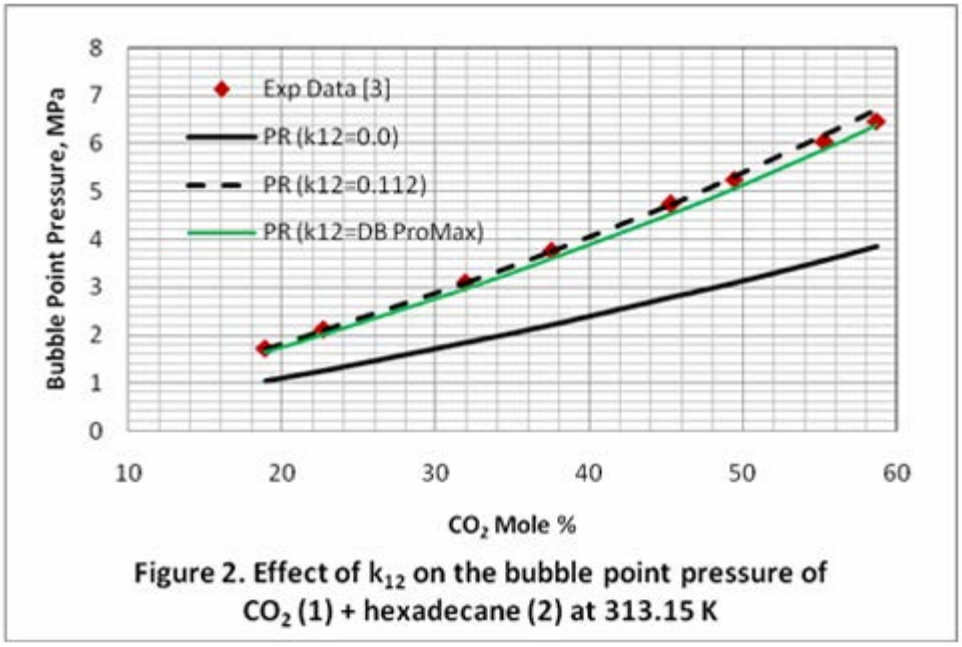

Figure 2. Effect of k_{12} on the bubble point pressure of CO_2 (1) + hexadecane (2) at 313.15 K

Normally, the binary interaction parameters obtained from regressing binary mixture VLE data work well in multicomponent systems. This is demonstrated by using the same obtained k_{ij}s in a ternary mixture. The obtained binary interaction parameters of CO_2 + pentadecane and CO_2 + hexadecane were used without any further change to predict the bubble point pressure of the ternary mixtures of CO_2 (1) + pentadecane (2) + hexadecane (3). Figure 3 indicates these binary interaction parameters obtained from the individual binary mixtures improve the accuracy of EOS considerably. Similar to the case of binary mixtures, when the binary interaction parameters, k_{12}, k_{13}, were changed from zero, and the default value of ProMax data base (k_{ij}s=DB), to 0.112 for the ternary mixture of CO_2 (1) + pentadecane (2) + hexadecane (3) at 40 °C, the AAPDs were reduced from 40.99% and 25.16% to 1.75%, respectively.

Discussion and Conclusions

It was shown that the binary interaction parameters of an EOS can be adjusted/tuned/regressed to improve the accuracy of VLE calculations considerably. It was also shown that when the regressed binary interaction parameters based on the binary experimental VLE data used without further changes in a multicomponent system considerable improvement in accuracy may be obtained. It is a sound practice to check the accuracy of a selected thermodynamic package prior to running any simulation. However, experimental or field data are required to fulfill this task.

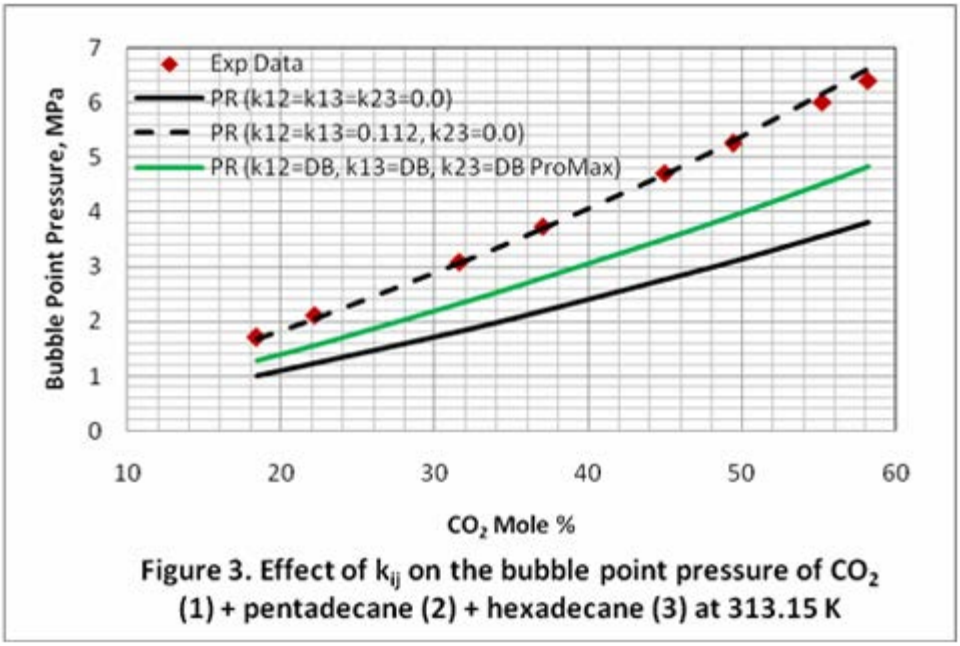

Figure 3. Effect of k_{ij} on the bubble point pressure of CO_2 (1) + pentadecane (2) + hexadecane (3) at 313.15 K

REFERENCES

1. 1. Peng, D.Y. and Robinson, D.B., "A New Two-Constant Equation of State," ***Ind. Eng. Chem., Fundam***., Vol. 15, No. 1, P. 59, 1976.
2. ProMax, V. 3.0, Bryan, Tex.: Bryan Research & Engineering Inc, 2009.
3. Tanaka, H., Yamaki, Y. and Kato, M., "Solubility of Carbon Dioxide in Pentadecane, Hexadecane, and Pentadecane + Hexadecane," ***J. Chem. Eng. Data,*** 38, 386-388, 1993.

Important Aspects of Centrifugal Compressor Testing-Part 2

by Joe Honeywell

This is the final part of a two part Tip of the Month (TOTM) series on important aspects related to centrifugal compressor performance testing. The first part dealt with the review of the testing procedure presented in ASME PTC-10 (also referred to as the Code), selection criteria for test gases and factors to consider in a performance testing. This TOTM will review the basic assumptions and performance relationships required for an accurate test. Also discussed are three important principles: volume ratio, Machine Mach Number and Machine Reynolds Number, which also influence the accuracy of the test results.

Introduction

The Code recognizes that the actual testing conditions and the specified design conditions may not be identical. Basic assumptions are made so that test results can be compared to the original design or some other baseline datum. For example, a compressor can have a different efficiency depending on where it is operating on a head-flow curve. However, if the gas composition and operating condition are not the same as the original design, then how accurate are the results? This question will be discussed below.

There are other important parameters utilized by the Code to analyze compressor performance. The first two are called flow coefficient and work coefficient. These are dimensionless parameters that are useful in the interpretation of test results, especially when comparing the test results to the original design or some other datum. Three more important parameters are called volume ratio, Machine Mach Number, and Machine Reynolds Number. These parameters assure that the aerodynamic properties of a compressor are maintained whenever test gases or alternate operating conditions are used. In addition, they establish limits on the operating range and help correct head and efficiency for friction losses. Each parameter will be briefly discussed.

Dimensionless Parameters

Most likely the actual testing conditions and specified design conditions are not identical. To compensate for the differences, the Code utilizes dimensionless parameters called flow coefficient, work coefficient and total work coefficient. The Code also makes assumptions regarding each coefficient and their equivalency at test and specified conditions. Table 1 lists the Code's principle parameters and the assumptions used to convert test data into values at specified design conditions.

Changes in compressor performance can be determined whenever the speed fluctuates by simply utilizing the affinity laws. If the compressor flow, head and efficiency characteristics are known at a given speed, then merely applying the affinity laws at an alternate speed will produce a new curve representing the compressor performance at that speed. This is the same concept behind head and flow coefficients.

In essence, the flow coefficient represents the "normalized flow rate" of the compressor at any speed. Similarly, the work coefficient and total work coefficient represents the "normalized head" of the compressor at any speed. The affinity laws also imply that the efficiency represented at the two equivalent conditions will remain the same. These properties play a major role in shop and field testing of centrifugal compressors.

Table 1

Dimensionless Parameter Assumptions

Dimensionless Parameter[1]	Description	Mathematical Description[1]
Flow coefficient	Flow coefficient of the test gas and specified gas are equal using ideal and real gas methods.	$(\phi)_{sp} = (\phi)_t$
Work input coefficient – enthalpy method	Work input coefficients of the test gas and specified gas are equal. Ideal or real gas laws apply.	$(\mu)_{sp} = (\mu)_t$
Work input coefficient – isentropic or polytropic methods	Work input coefficient of the test gas is corrected for the Machine Reynolds Number to obtain the specified work input coefficient. Ideal or real gas laws apply.	$(\mu)_{sp} = (\mu)_t \ \mathrm{Rem}_{Corr}$
Efficiency –isentropic or polytropic methods	The efficiency at the test operating condition is corrected by the Machine Reynolds Number to obtain the specified operating condition.	$(\eta)_{sp} = (\eta)_t \ \mathrm{Rem}_{Corr}$
Total work input coefficient – heat balance or shaft balance methods	The total work input coefficient is equal for test and specified gases.	$(\Omega)_{sp} = (\Omega)_t$

NOTE:
1. See ASME PTC-10 for complete mathematical description of the coefficients.

Basic Performance Relationships

The basic relationships for determining compressor flow rate, head, power and efficiency are given below. These relationships are based on known gas properties, operating conditions and compressor performance characteristics.

$$Q = m\left(\frac{T\ Z}{p}\right)\left(\frac{R_0}{MW}\right) \qquad (1)$$

$$W_{input} = h_d - h_i \qquad (2)$$

$$W_s = h_d' - h_i = \frac{n_s}{n_s - 1} f p_i v_i \left[\left(\frac{p_d}{p_i}\right)^{\frac{n_s - 1}{n_s}} - 1\right] \qquad (3)$$

$$n_s = \left[\frac{\ln \frac{p_d}{p_i}}{\ln \frac{v_i}{v_d'}}\right] \qquad (4)$$

$$W_p = \frac{n}{n-1} f p_i v_i \left[\left(\frac{p_d}{p_i} \right)^{\frac{n-1}{n}} - 1 \right] \qquad (5)$$

$$n = \left[\frac{\ln \frac{p_d}{p_i}}{\ln \frac{v_i}{v_d}} \right] \qquad (6)$$

$$W_{input} = \frac{W_s}{\eta_s} = \frac{W_p}{\eta_p} \qquad (7)$$

The Code recognizes three methods of determining compressor work (also called head). The first is the enthalpy method and is defined by Equation 2. It represents the difference in the inlet and discharge enthalpy, and results in the *actual* work supplied to the gas. The next method of determining work is by the isentropic method. This method only determines the *ideal* compressor work and may be calculated utilizing Equation 3 and 4. The last relationship for determining compressor work is the polytropic method. Only the *ideal* work is found by this method and may be calculated using Equations 5 and 6. All three methods are commonly used by compressor users and manufacturers.

Volume Ratio

The volume ratio is an important aerodynamic parameter. It maintains similar flow conditions as gas properties and operating conditions change. The best way to describe volume ratio is to consider a multi-stage compressor. The mass of gas entering the first impeller must equal the mass entering other impellers. However, the actual gas volume entering the first stage is not the same for other impellers. The gas is compressed and heated, which results in a reduction of volume. If the gas properties and operating conditions of the test gas are different from the specified gas, then the volume entering and leaving each stage will also be different. Therefore, to duplicate the aerodynamic performance of a compressor at the specified design condition it is important to simulate the equivalent flow of gas through the impellers by carefully matching the volume ratio.

A centrifugal compressor performance test is frequently performed with a gas other than the specified gas. In addition, the compressor may operate at conditions other than the original design. To assure an accurate performance test that simulates the original design, the volume ratio of the specified gas must match the volume ratio of the test gas at the respective operating conditions. Equations 1-6 can be used to determine the conditions that match the test and specified volume ratio. The Code sets limits on deviations of the test gas properties and operating conditions, which is found in Table 2 of Part 1.

Seven variables define the volume ratio relationship between a test gas and the specified gas. The variables and the influence each has to increase or decrease the volume ratio is shown in Table 2. For example, if the k-value of the test gas is greater than the specified gas, the volume ratio will decrease. Similarly, if the test gas suction temperature is less than the volume ratio will increase. Also note another important fact, and that is changes in the suction pressure of the test gas have no effect on volume ratio.

Table 2 - Variable Influence on Volume Ratio

Variable	Change	Volume Ratio	Change	Volume Ratio
Head	Increase	Increase	Decrease	Decrease
Molecular Weight	Increase	Increase	Decrease	Decrease
Suction Temperature	Increase	Decrease	Decrease	Increase
Compressibility	Increase	Decrease	Decrease	Increase
k-value	Increase	Decrease	Decrease	Increase
Speed	Increase	Increase	Decrease	Decrease
Suction pressure	Increase	No change	Decrease	No change

As previously mentioned, the volume ratio of the specified gas must match the volume ratio of the test gas. So if each of the physical properties of the test gas can change the volume ratio, what can be done so that the two volume ratios match? A common practice is to change the test speed to compensate for the mismatch of volume ratios. This practice is illustrated in Figure 1. Note how the compressor speed is decreased so that the volume ratio changes imposed by other variables add up to zero.

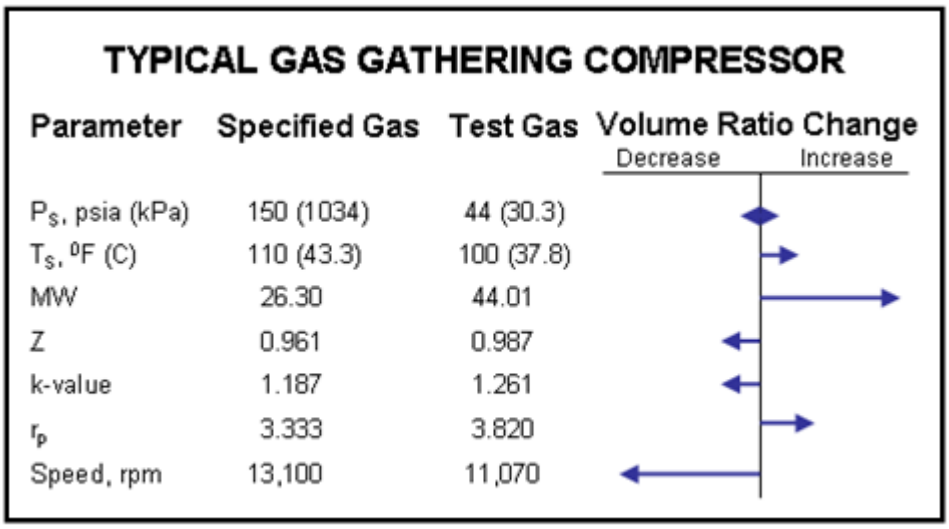

Figure 1 – Typical Volume Ratio Corrections

In summary, the operating conditions and physical properties of a performance test should be carefully examined. It is critical that the test gas volume ratio closely

match the volume ratio of the specified gas. The closer the test gas volume ratio is to the specified gas, the more accurate are the performance test results.

Mach Number

The Mach number influences the maximum amount of gas that can be compressed for a given impeller speed. The limiting flow is known as stonewall (also called choke flow) and is typically found on the compressor characteristic head-flow curve at maximum flow condition for a given speed. As the gas flow rate increases so does the velocity within the compressor's internal flow path until it approaches the fluid acoustic velocity, thus limiting the flow. Therefore, gas velocities that approach a Mach number of one indicate choke flow inside the compressor.

The Code defines a term called the Machine Mach Number which is the ratio of the outlet blade tip velocity of the first stage impeller to the acoustic velocity at inlet conditions. The Code also sets allowable limits on the deviation between the specified and test gas Machine Mach Numbers. This helps assure the accuracy of the performance test. When shop testing a compressor, the Machine Mach Number at the operating condition is calculated and compared to the difference of the specified gas and test gas. See Figure 2 for allowable deviation limits. If the value exceeds the permitted deviation the test gas operating conditions may need adjusting to comply with to these limits.

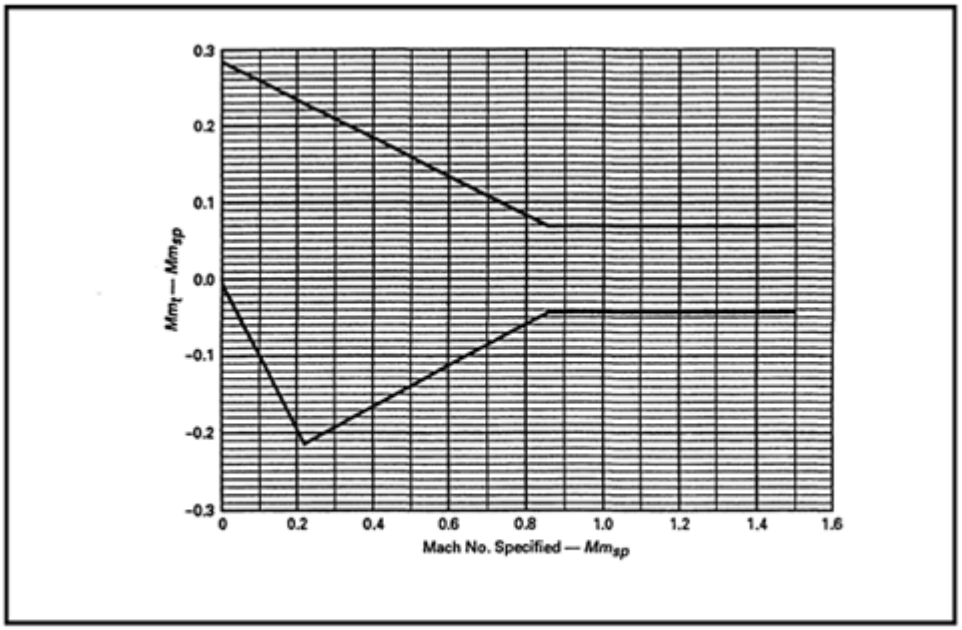

Figure 2 - Allowable Deviations for Machine Mach Number

Reynolds Number

The effect that the Reynolds Number has on a compressor is similar to the effect it has on pipes. The gas flowing through the internal passages of a compressor produce

friction and energy loss which influences the machine efficiency. For centrifugal compressors, the Code defines a term called the Machine Reynolds Number and places limits on the allowable values during a performance test and is defined by Equation 8. If the Machine Reynolds Number for the test condition and specified condition differs then a correction factor is applied to the test efficiency and head values. See Equation 9 for the correction factor.

$$\mathrm{Rem} = \frac{Ub}{\upsilon} \qquad (8)$$

$$\mathrm{Rem}_{corr} = \frac{(\mu_p)_{sp}}{(\mu_p)_t} = \frac{(\eta_p)_{sp}}{(\eta_p)_t} \qquad (9)$$

The allowable Machine Reynolds Number departure limits between the test gas and specified gas are given in Figure 3

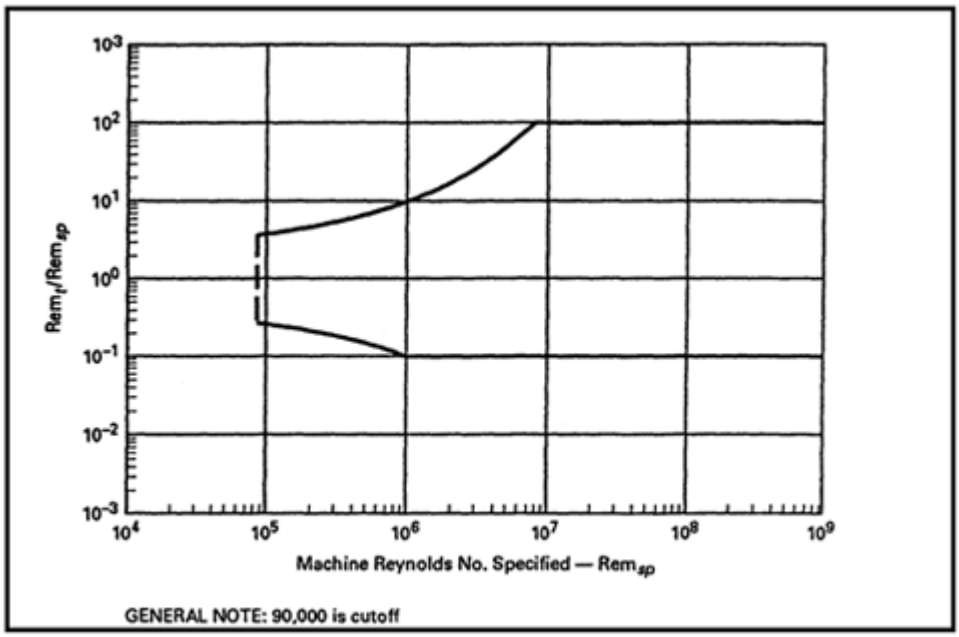

Figure 3 – Allowable Machine Reynolds Number Departures

REFERENCES

1. ASME PTC-10, "*Performance test Code on Compressors and Exhausters*", 1997
2. Short Course "*Centrifugal Compressors 201*", Colby, G.M., et al. 38th Turbomachinery Symposium, 2009.

Nomenclature

b = first stage impelle r exit width

f = polytropic or isentropic work factor

h = enthalpy

m = mass flow rate

MW = molecular weight

n = exponent

p = pressure

Q = volumetric flow rate

Rem = Machine Reynolds Number

Rem_{corr} = Machine Reynolds Number correction factor

R_0 = Universal gas constant

T = temperature

U = velocity at outer blade of first stage

v = specific volume

W_{input}= input work (actual head)

W = work (ideal head)

Z = compressibility

ϕ = flow coefficient

Ω = total work coefficient

μ = work coefficient

η = gas efficiency

ν = kinematic viscosity of the gas

subscript i = inlet conditions

subscript d = discharge conditions

subscript p = polytropic

subscript s = isentropic

subscript sp = spedified gas

subscript t = test gas

superscript '= condition at constant entropy

Effect of Nitrogen Impurities on CO2 Dense Phase Transportation

By Dr. Mahmood Moshfeghian

In the January and February 2012 tips of the month (TOTM) we discussed the isothermal and non-isothermal transportation of pure carbon dioxide (CO_2) in the dense phase region. We illustrated how thermophysical properties changed in the dense phase and studied their impacts on pressure drop calculations. The pressure drop calculation results utilizing the liquid phase and vapor phase equations were exactly the same. We showed that the effect of the overall heat transfer coefficient on the pipeline temperature is significant. In this TOTM, we will study the same case study in the presence of nitrogen impurities under non-isothermal conditions. The Joule-Thompson expansion effect and the heat transfer between pipeline and surroundings have been considered. Specifically, we will report the effect of nitrogen impurities on the pressure and temperature profiles. The Peng-Robinson equation of state (PR EOS) was utilized in this study.

For a pure compound above critical pressure and critical temperature, the system is often referred to as a "dense fluid" or "super critical fluid" to distinguish it from normal vapor and liquid (see Figure 1 for carbon dioxide in **December 2009 TOTM** [1]).

Calculation Procedure:

The same step-by-step calculation procedure described in the **February 2012 TOTM** [2] was used to determine the pressure and temperature profiles in a pipeline considering the Joule-Thompson expansion effect and heat transfer between the pipeline and surroundings.

In the following section we will illustrate the pressure drop calculations for transporting CO_2 in dense phase using the gas phase pressure drop equations. For details of pressure drop equations in the gas and liquid phases refer to the**January 2012 TOTM** [3].

Case Study:

For the purpose of illustration, we considered a case study [also described in reference 2] for transporting 160 MMSCFD (4.519×10^6 Sm^3/d) CO_2 using a 100 miles (160.9 km) long pipeline with an inside diameter of 15.551 in (395 mm). The inlet conditions were 2030 psia (14 MPa) and 104˚F (40˚C). The following assumptions were made:

a. CO_2, with nitrogen impurities of 0, 1, 5, 10, and 15 mole %.
b. Horizontal pipeline, no elevation change.
c. Inside surface relative roughness's (roughness factor), ε/D, of 0.00013.
d. The ambient/surrounding temperature,Ts, is 55 ˚F and (12.8 ˚C)
e. Overall heat transfer coefficients of 0.5 Btu/hr-ft^2-˚F (2839 W/m^2-˚C).

Properties: The dense phase behavior and properties were calculated using the Peng-Robinson equation of state (PR EOS) [4] in ProMax [5] software. ProMax was also used to determine pressure and temperature profiles along the pipeline.

Results and Discussions:

Figures 1 through 4 present the phase envelope, dry ice (CO_2 freeze out) curve, and pipeline pressure and temperature profile for 1, 5, 10, and 15 mole % N_2 impurities, respectively, the relative roughness (ε/D) of 0.00013, and the overall heat transfer coefficient (U) of 0.5 Btu/hr-˚F-ft^2 (2.839 W/m^2-˚C).

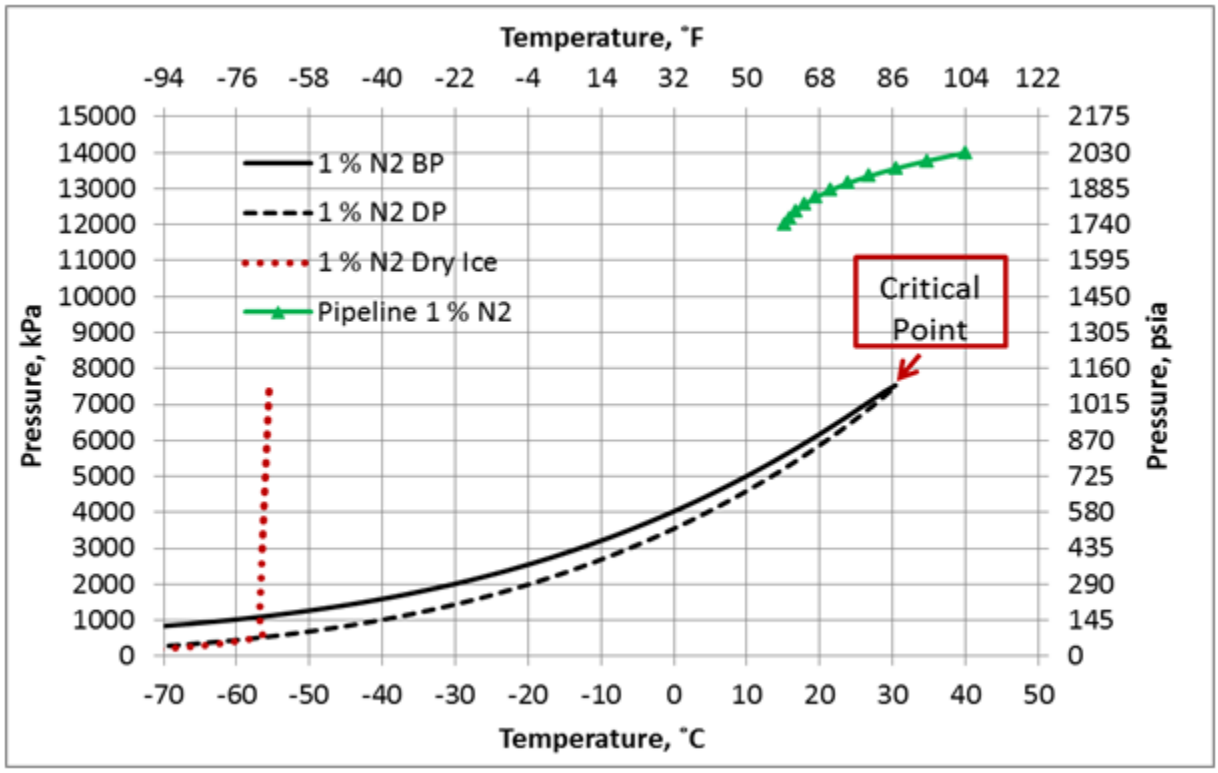

Figure 1. Phase envelop and dense phase pipeline pressure-temperature profile for 99 mole % CO_2 + 1 mole % N_2, *$\varepsilon/D=0.00013$*, and *$U=0.5$* Btu/hr-˚F-ft^2 (*2.839* W/m^2-˚C).

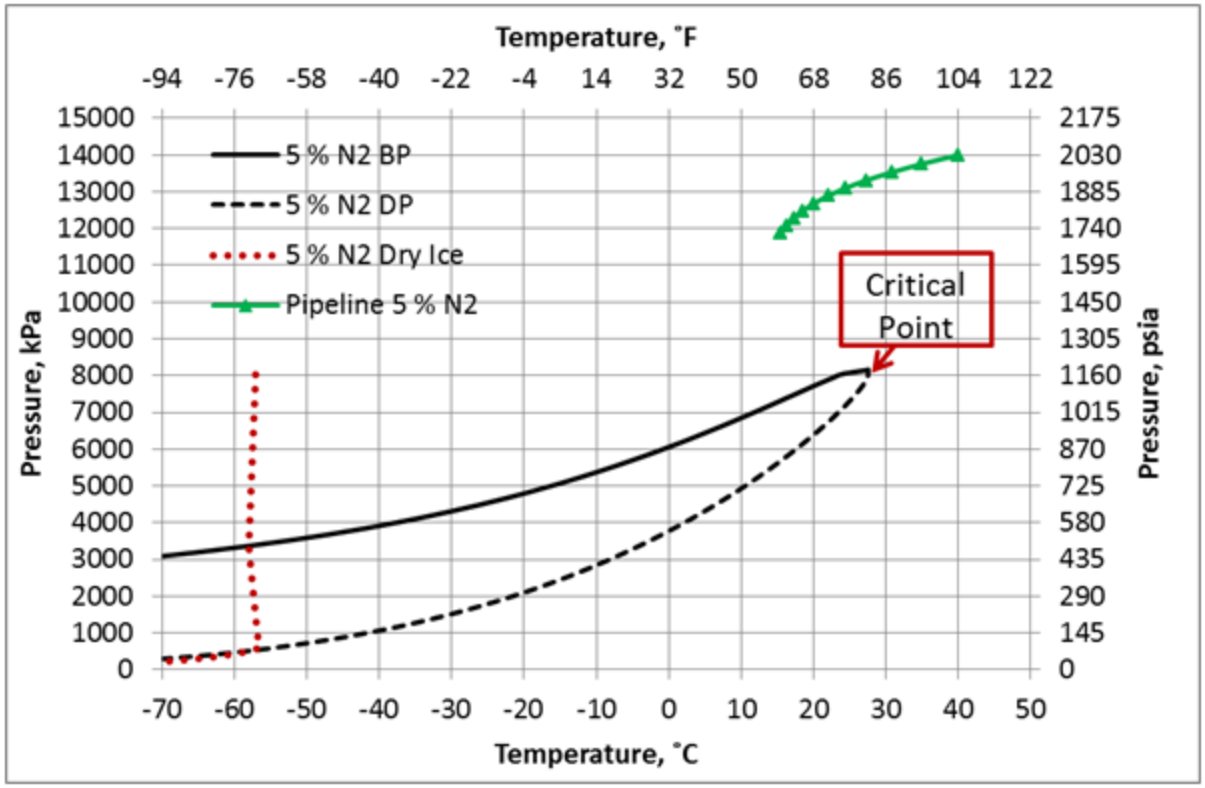

Figure 2. Phase envelop and dense phase pipeline pressure-temperature profile for 95 mole % CO_2 + 5 mole % N_2,*ε/D=0.00013*, and *U=0.5* Btu/hr-˚F-ft^2 (*2.839* W/m^2-˚C).

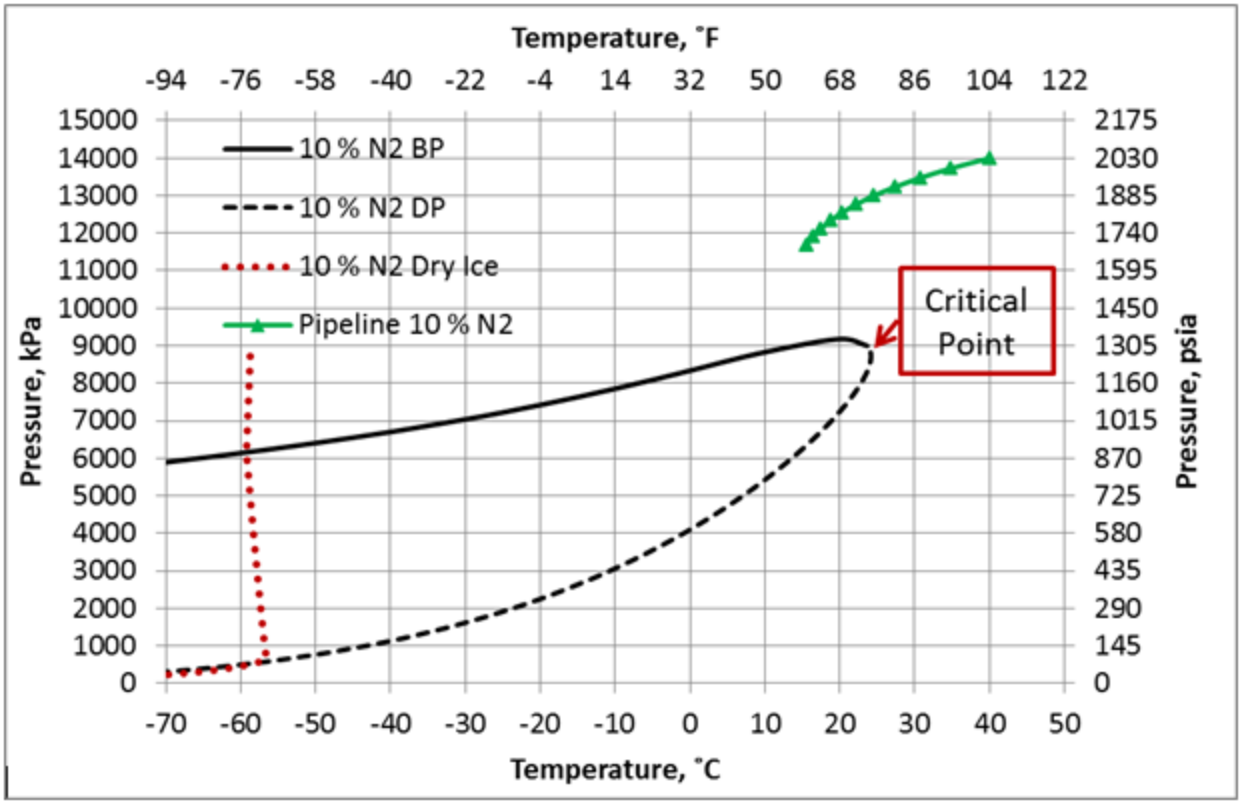

Figure 3. Phase envelop and dense phase pipeline pressure-temperature profile for 90 mole % CO_2 + 10 mole % N_2,*ε/D=0.00013*, and *U=0.5* Btu/hr-˚F-ft^2 (*2.839* W/m^2-˚C).

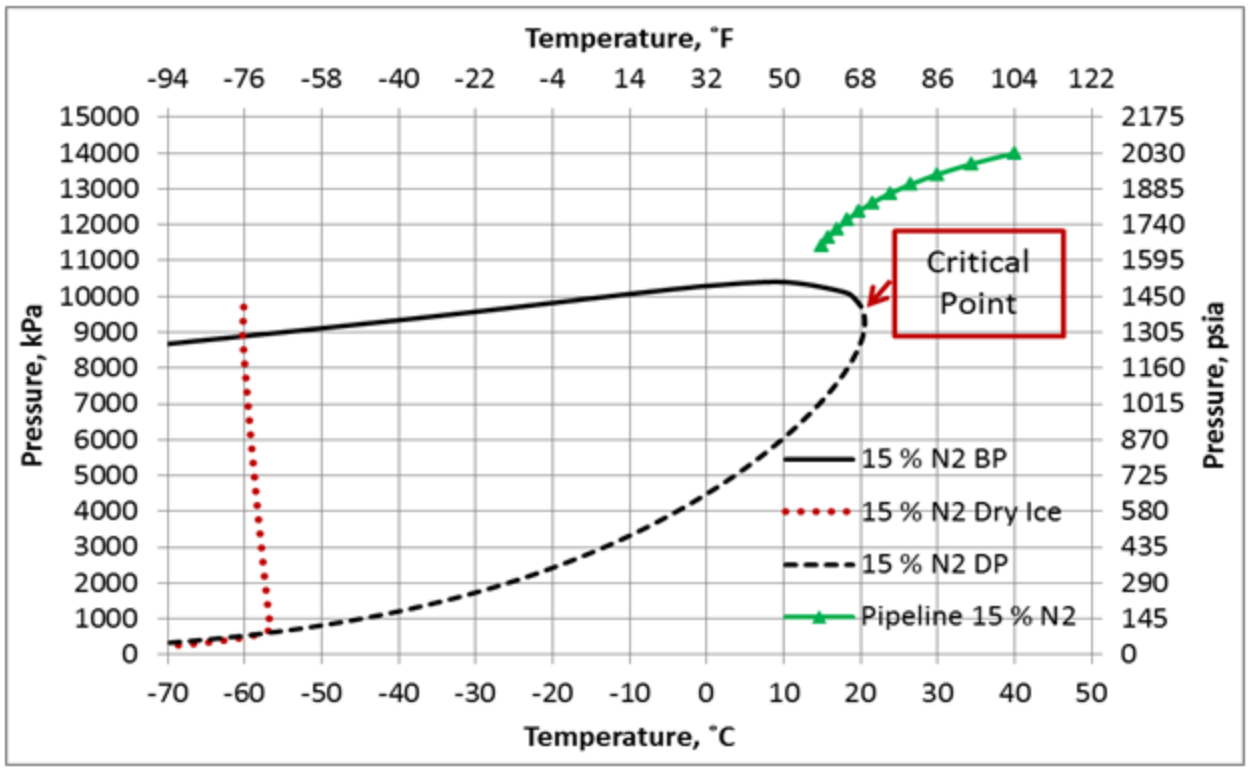

Figure 4. Phase envelop and dense phase pipeline pressure-temperature profile for 85 mole % CO_2 + 15 mole % N_2,$\varepsilon/D=0.00013$, and $U=0.5$ Btu/hr-˚F-ft^2 (2.839 W/m^2-˚C).

The effect of N_2 impurities on the line temperature profile is shown in Figure 5. This figure indicates that N_2 impurities have negligible effect on the pipeline temperature profile.

Figure 6 presents the effect of N_2 impurities on the pipeline pressure profile. This figure indicates that as the N_2impurities increases the pressure drop increases. This can be explained by the fact as the N_2 impurities increase, the mixture density decreases, consequently the velocity increases. Note the pressure drop is proportional to square of velocity and inverse of density. While viscosity decreases with increase in N_2 impurities, its effect is not as large as the density effect. Table 1 presents variation of the mixture density and viscosity as a function of N_2 mole %.

Table 1. Effect of N_2 impurities on density (ρ) and viscosity (μ) of mixture at the inlet condition of 2030 psia (14 MPa) and 104˚F (40˚C)

N_2, mole %	0	1	5	10	15
ρ, kg/m^3	726.7	708.8	634.9	542.9	462.8
ρ, lb$_m$/ft^3	45.37	44.25	39.64	33.89	28.89
μ, cP	0.0609	0.0585	0.0499	0.0411	0.0350
μ, lb$_m$/(ft-hr)	0.1472	0.1415	0.1206	0.0995	0.0847

Conclusions:

Analyzing Table 1 and Figures 1 through 6, the following conclusions can be made:

1. For the range 0 to 15 mole % N_2, the effect of the N_2 impurities on the pipeline temperature profile is negligible.
2. As the N_2 impurities increase, the pipeline pressure drop increases due to the change in thermophysical properties of mixture.
3. Care should be taken to use accurate thermophysical properties and the phase envelope should be plotted to avoid any operating problem.

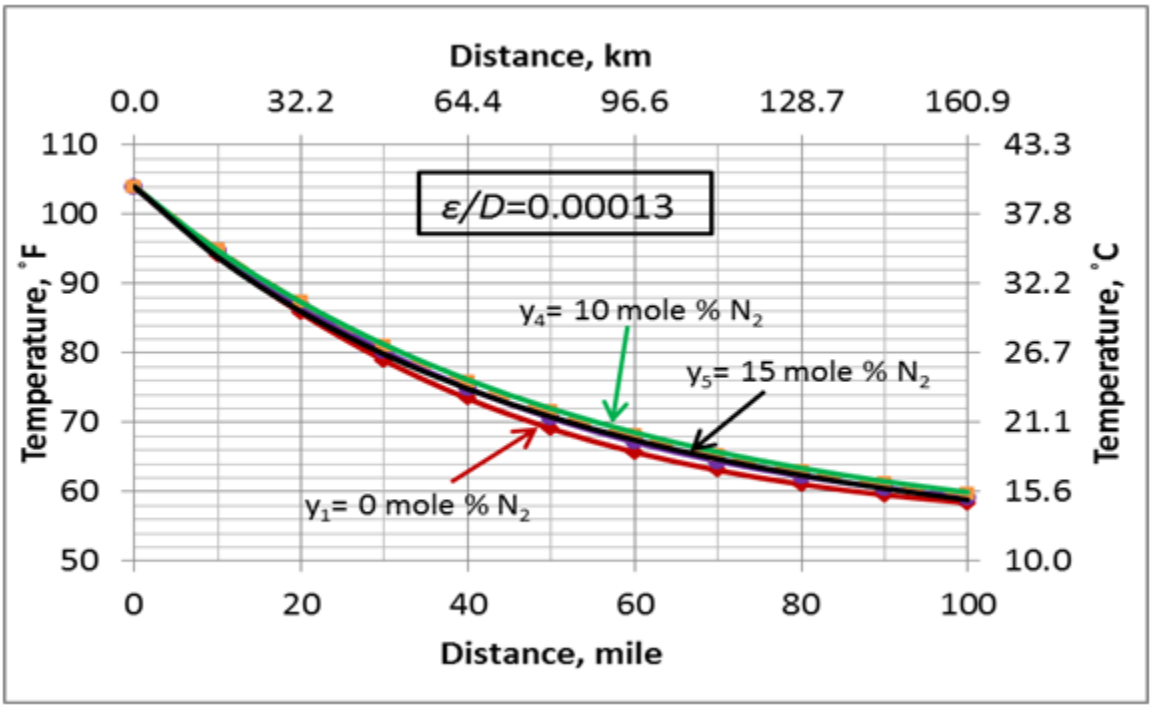

Figure 5. Variation of the pipeline temperature profile with the N_2 impurities and *U=0.5* Btu/hr-˚F-ft^2 (*2.839* W/m^2-˚C)

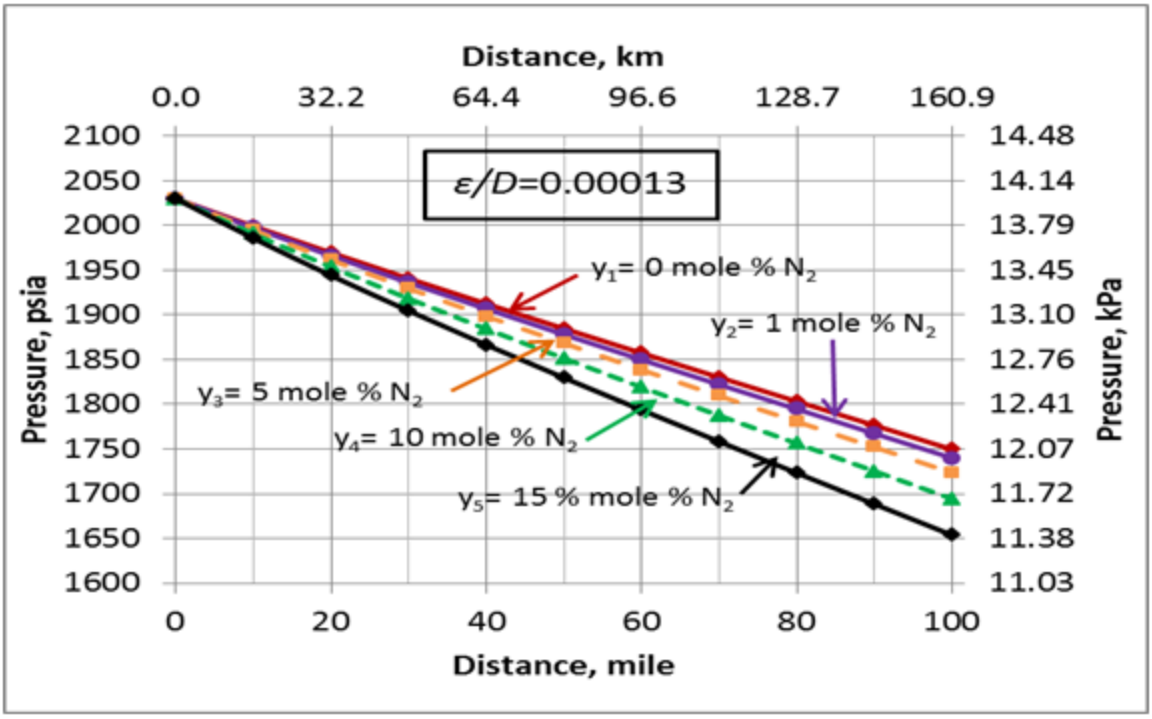

Figure 6. Variation of the pipeline pressure profile with the N_2 impurities and *U=0.5* Btu/hr-˚F-ft^2 (*2.839* W/m^2-˚C)

REFERENCE

1. Bothamley, M.E. and Moshfeghian, M., "Variation of properties in the dese phase region; Part 1 – Pure compounds," TOTM, **http://www.jmcampbell.com/tip-of-the-month/2009/12/variation-of-properties-in-the-dense-phase-region-part-1-pure-compounds/**, Dec 2009.
2. Moshfeghian, M., "Transportation of CO_2 in the Dense Phase**,"** TOTM, **http://www.jmcampbell.com/tip-of-the-month/2012/02/** , Feb 2012
3. Moshfeghian, M., "Transportation of CO_2 in the Dense Phase**,"** TOTM, **http://www.jmcampbell.com/tip-of-the-month/2012/01/**, Jan 2012
4. Peng, D. Y., and Robinson, D. B., *Ind. Eng. Chem. Fundam.*, Vol. 15, p. 59, 1976.

ProMax 3.2, Bryan Research and Engineering

About John M. Campbell & Company:

John M. Campbell & Co., an employee-owned company, is the exclusive provider of PetroSkills facilities training and one of the most distinguished providers of facilities training in the oil and gas industry. Since 1968 we have built our reputation on our “Gas Conditioning and Processing” course also known as “The Campbell Gas Course” or the “Campbell G4”. As demand for highly skilled employees in the petroleum industry grows, we have expanded our training curriculum to include the whole stream of skills needed from well-head to the finished product. For more information, please visit our website, **www.jmcampbell.com.**

For information on upcoming Public courses, please visit http://www.jmcampbell.com/public-courses.php